2015

THE SLC22 TRANSPORTER FAMILY: NOVEL INSIGHTS TO ROLES IN DRUG EFFICACY, DRUG-DRUG INTERACTIONS AND MOOD DISORDERS

Xiaolei Pan

THE SLC22 TRANSPORTER FAMILY: NOVEL INSIGHTS TO ROLES IN DRUG EFFICACY, DRUG-DRUG INTERACTIONS AND MOOD DISORDERS

A Dissertation submitted in partial fulfillment of the requirements for the degree of Doctor of Philosophy at Virginia Commonwealth University

By

Xiaolei Pan
Master of Science, Shenyang Pharmaceutical University, China, 2011

Director: Douglas H. Sweet, Ph.D.
Professor, Interim Chair
Department of Pharmaceutics, School of Pharmacy

Virginia Commonwealth University
Richmond, Virginia,
August 3rd, 2015

ACKNOWLEDGEMENTS

First and foremost, I would like to thank my advisor Dr. Douglas H. Sweet for his time, ideas and funding to support my Ph.D. studies. He is one of the smartest advisor I ever know, and the enthusiasm he has for his research was contagious and motivational for me. Dr. Sweet has been supportive and given me the freedom to pursue research with my interest in different topics, and I am grateful for his excellent guidance that help me conquer any challenges these years.

I would also like to thank my committee members Drs. Jürgen Venitz, Phillip Gerk, Malgorzata Dukat and Adam VanWert for their consistent help in my research. Dr. Venitz and Dr. Gerk have given me numerous brilliant valuable comments and suggestions in the PK/PD research group, and I have benefited tremendously from those weekly discussions. I also want to thank Dr. Dukat and Kavita Iyer for all the collaborations and suggestions in the quinazolines and guanidines project, and Dr. VanWert as a thesis reader and an inspiration in many ways. A special gratitude I give to Dr. Richard A Glennon for providing and guiding me in the synthetic cathinones project.

In addition, many thanks go to all faculties in School of Pharmacy for their help in my coursework. I would also like to thank Ms. Keyetta Tate, Ms. Laura Georgiadis and Ms. Shakim Jackson for their kindly help in arranging departmental activities, lab and office supplies, and paperwork for graduation and reimbursement.

I would like to thank my lab-mates Dr. Aditi Mulgaonkar, Dr. Christine A. Farthing, Raymond Lai and Hebing Liu for their help in my study, and all my fellow and senior Pharmaceutics graduate students for their help and advice. In addition, a special thank you to my friends and roommates in Richmond for their support and encouragement.

I would thank the VCU School of Pharmacy, Graduate School and Altria Fellowship for the financial support.

Lastly, I would like to thank my family for all their love and encouragement. My parents raised me with all their love and supported me in all my pursuits. And most of all for my loving, supportive, encouraging, and patient husband Li Wang whose faithful support through my Ph.D. is so appreciated. Thank you.

TABLE OF CONTENTS

LIST OF TABLES

LIST OF FIGURES

LIST OF ABBREVIATIONS

5-HT	serotonin
α-KG	α-ketoglutaric acid
AAPS	American Association of Pharmaceutical Scientists
ABC	ATP binding cassette
ACE	angiotensin converting enzyme
ANOVA	analysis of variance
AUC	area under the curve
BBB	blood brain barrier
BCRP	breast cancer resistance protein
BMEC	brain microvessel endothelial cell
BSEP	bile salt export pump
CA	California
C_{max}	maximum plasma concentration
CHO	Chinese hamster ovary
CP	choroid plexus
CSF	cerebrospinal fluid
D-22	decynium- 22
Da	Dalton(s)
DA	dopamine
DAT	dopamine transporter

DDI	drug-drug interaction
ED_{50}	median effective dose
EDA	2,2'-(ethylenediimino)dibutyric acid
EMB	ethambutol
ES	estrone sulfate
f_u	fraction unbound in plasma
FDA	Food and Drug Administration
GFR	glomerular filtration rate
GI	gastrointestinal
HCl	hydrochloric acid
HEK	human embryonic kidney 293
HEPEs	4-(2-hydroxyethyl)-1-piperazineethanesulfonic acid
HIV	human immunodeficiency virus
IC_{50}	half maximal inhibition concentration
K_i	inhibitory constant
K_m	Michaelis constant
MA	Massachusetts
MATE	multidrug and toxic compound extrusion transporter
MDPV	3,4- methylenedioxypyrovalerone
MDR	multidrug resistance
MDR1	multidrug resistance transporter
MO	Missouri
mRNA	messenger RNA
MPP^+	1-methyl-4-phenylpyridinium
NaOH	sodium hydroxide

NE	norepinephrine
NET	norepinephrine transporter
NSAIDs	non-steroidal anti-inflammatory drugs
NTCP	sodium-taurocholate cotransporting polypeptide
NY	New York
OA	organic anion
OAT	organic anion transporter
OATP	organic anion transporting polypeptide
OC	organic cation
OCT	organic cation transporter
PAH	para-aminohippurate
PCR	polymerase chain reaction
PDB	protein data bank
PGE2	prostaglandin E2
PiPT	Piriformospora indica high affinity phosphate transporter
QSAR	quantitative structure-activity relationship
RT-PCR	reverse transcription polymerase chain reaction
SEM	standard error of the mean
SERT	serotonin transporter
SD	standard deviation
SLC	solute carrier
SNRI	serotonin and norepinephrine reuptake inhibitor
SiRNA	small interfering RNA
SSRI	selective serotonin reuptake inhibitor
TB	tuberculosis

TM	transmembrane
TMD	transmembrane domain
TST	tail suspension test
uptake-1	high-affinity, low capacity reuptake transporters
uptake-2	low-affinity, high capacity reuptake transporters
URAT	urate transporter
VA	Virginia
VCU	Virginia Commonwealth University
WHO	World Health Organization
XDR	extensively drug-resistant strain

ABSTRACT

THE SLC22 TRANSPORTER FAMILY: NOVEL INSIGHTS TO ROLES IN DRUG EFFICACY, DRUG-DRUG INTERACTIONS AND MOOD DISORDERS

By Xiaolei Pan, M.S.

A dissertation submitted in partial fulfillment of the requirements for the degree of Doctor of Philosophy at Virginia Commonwealth University

Virginia Commonwealth University, 2015

Major Advisor: Douglas H. Sweet, Ph.D.
Professor, Interim Chair
Department of Pharmaceutics, School of Pharmacy

Numerous studies have demonstrated the impact of organic cation (OCTs; SLC22 family) and anion transporters (OATs; SLC22 family) on the efficacy and safety of clinically important therapeutics. To be specific, OCTs and OATs have been identified as determinants for uptake into and secretion from enterocytes, hepatocytes and renal proximal tubular cells, and are frequent sites of drug-drug interaction (DDI). In addition, OCTs expressed in brain are components of the low-affinity, high capacity clearance pathway (uptake-2) for biogenic monoamine neurotransmitters. As a result, OCTs may represent novel targets for mood disorders.

The inhibitory effects of several therapeutic agents, designed drugs and novel compounds were assessed on the function of OCTs/Octs and OATs/Oats. Among these compounds, the anthraquinone rhein showed significant inhibition on hOATs. While the antituberculosis drug ethambutol, the herbal products matrine and oxymatrine, synthetic cathinones, and all quinazoline and guanidine compounds produced significant inhibition on hOCT activity with most IC_{50} values in the micro- and even nanomolar ranges.

Considering the clinically relevant unbound concentrations in biofluids, significant DDI potentials were found for rhein, ethambutol, matrine, oxymatrine and several synthetic cathinones affecting enterocytes, hepatocytes and/or proximal tubules. As hOCT2 and hOCT3 may participate in modulating neurotransmitter homeostasis in the CNS, these findings also suggested that the CNS pharmacological effects of synthetic cathinones, quinazoline and guanidine compounds might be due to their inhibitory effects on OCTs; although their impact may be limited solely to clearance of these compounds. Based upon their *in vitro* OCT/Oct inhibition profiles, three lead quinazoline and guanidine compounds were chosen for *in vivo* studies. Potent antidepressant-like effects of one lead hOCT-interacting compound (KEO-099) were re-confirmed in the tail suspension test. While *in vivo* results of the two newly identified hOCT-interacting lead compounds were somewhat less clear.

Finally, homology modeling and docking studies for hOCT3 identified key amino acid residues that might be involved in interaction between hOCT3 and small molecules. Subsequent experiments confirmed a competitive mode of interaction between MPP^+ and lead compounds on hOCT3. Thus, preliminary analysis indicates our hOCT3 homology model can be used to support rational drug design and high-throughput screening of novel hOCT substrates/inhibitors.

CHAPTER 1

THE SLC22 TRANSPORTER FAMILY: NOVEL INSIGHTS TO ROLES IN DRUG EFFICACY, DRUG-DRUG INTERACTIONS AND MOOD DISORDERS

1.A OVERVIEW OF ORGANIC CATION AND ANION TRANSPORTERS

Remarkable progress has been achieved in understanding the vital role of transporters in mediating transcellular *movement* of endogenous and exogenous substances in the body [1]. Among these transporters, organic cation (OCTs) and anion transporters (OATs), belonging to the solute carrier 22 (SLC22) family, interact with hundreds of cationic, anionic and zwitterionic organic molecules [1-3]. OCTs and OATs are characterized by 12 α-helical transmembrane domains (TMDs), a large extracellular loop located between TMDs 1 and 2, a large intracellular loop between TMDs 6 and 7, and intracellular N- and C-termini [4]. OCTs and OATs utilize different mechanisms to transport organic charged molecules across the cell membranes (Figure 1.1). Uptake of organic cations into the negatively charged intracellular environment is electrochemically a downhill process, and OCTs utilize this gradient as their driving forces functioning as facilitated diffusion carriers [5]. For uptake, OATs function as tertiary active transporters that are indirectly coupled to Na^+/K^+-ATPase and Na^+/dicarboxylate cotransporter function (Figure 1.1). They utilize the stored energy of α- ketoglutarate (α-KG) gradient to drive organic anion exchange [2, 6]. The first SLC22 family member, Oct1, was cloned from rat kidney

in 1994, and Oat1 was cloned from rat kidney in 1997 [7-9]. Three major OCT subtypes (*i.e.*, OCT1, OCT2, and OCT3), and five major OAT subtypes (OAT1-4 and URAT1), as well as OCT/OAT orthologs, have been identified [2, 3]. Extensive investigations have focused on the structure, regional distribution and function of OCTs and OATs [2, 3]. The expression of OCTs and OATs have been confirmed in a number mammalian species such as human, mouse, rat and rabbit [2-4]. OAT1-3 and OCT1-3 mediate cellular entry or reuptake of small organic anions and cations, respectively [2, 3, 6]. The role of OAT4 in renal secretion and absorption is less well defined [2, 6].

While isolated from kidney, it has now been confirmed that OCT1/Oct1 exhibit a broad tissue distribution in peripheral organs. In humans, OCT1 showed strongest mRNA expression in liver compared to any other tissues [10]. A recent study using a quantitative proteomics approach showed that the protein expression of OCT1 in human liver appears to be greater than any other hepatobiliary transporters, including BCRP, BSEP, MATE1, MDR1, MRP2, MRP3, NTCP, OATP1B1, OAPT1B3 and OATP2B1 [11]. In rodents, marked mRNA and protein expression of Oct1 was found in liver, kidney and intestine [10]. OCT1/Oct1 was located in the membrane of these tissues, e.g. sinusoidal membrane of hepatocytes and basolateral membrane of enterocytes [3]. OCT1/Oct1 has a broad substrate specificity. Hundreds of clinical therapeutics, such as metformin, lamuvidine, acyclovir, ganciclovir, pentamidine and furamidine, have been identified as substrates and/or inhibitors [4].

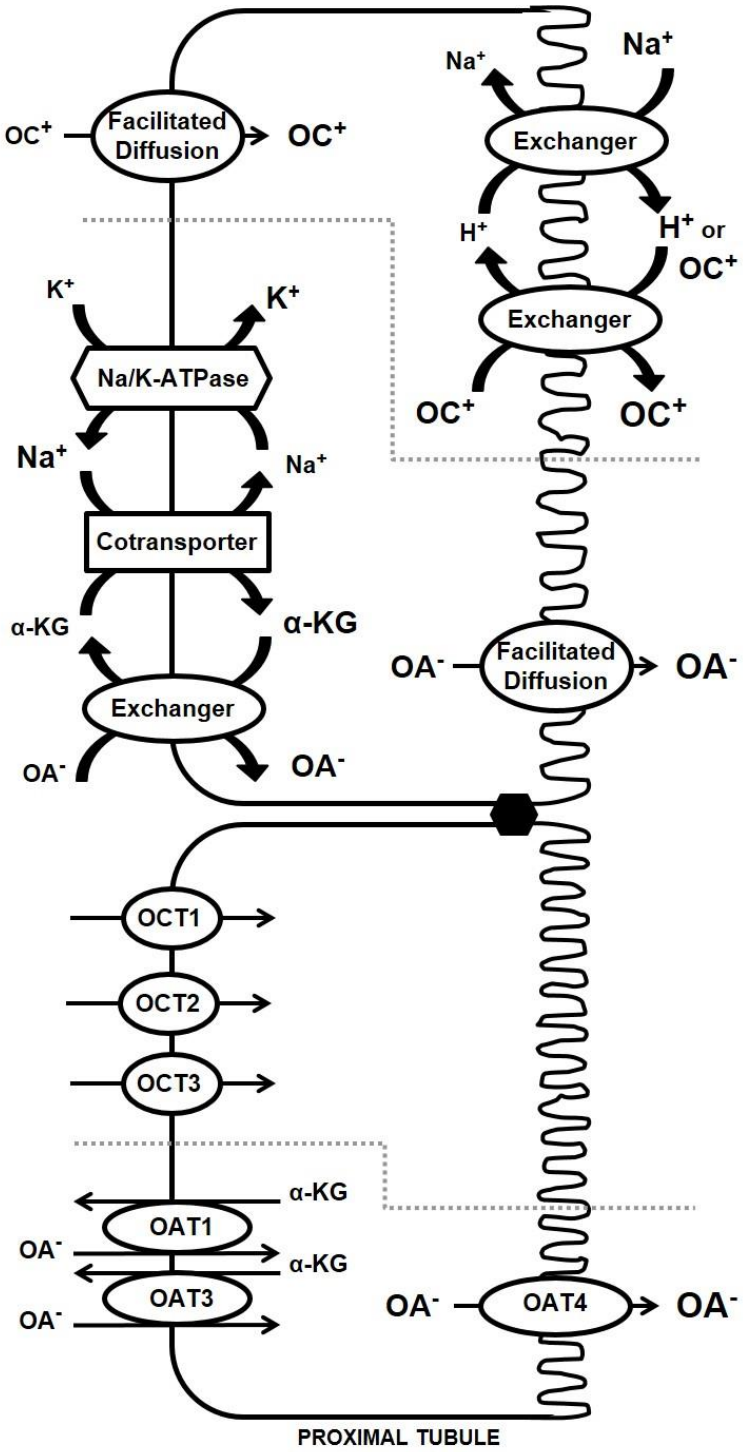

Figure 1.1 Renal cell model depicting the various driving forces for organic cation and anion transport and the SLC22 transporters studied in this work.

Upper panel: schematic model of the transport processes associated with uptake and efflux of organic cations and anions. Lower panel: SLC22 transporters expressed in the proximal tubular cells in kidney. α-KG, α-ketoglutarate; OA^-, organic anion; OC^+: organic cation; OAT: organic anion transporter; OCT: organic cation transporter.

Oct2 was cloned from rat kidney in 1996 [12]. Later, OCT2/Oct2 was identified in human, rat, mouse, rabbit and pig [13]. Unlike OCT1/Oct1, OCT2/Oct2 is mainly located in kidney, with marked expression at the basolateral membrane of proximal tubular cells. OCT2/Oct2 plays an important role in renal active secretion of cationic substances [3]. Although the expression of OCT2/Oct2 has been found in a variety of organs including kidney, small intestine, lung, skin, brain and choroid plexus, mRNA and immunohistochemical evidence suggested that OCT2/Oct2 is not expressed in human or rodent liver [3]. Evidence for overlapping substrate specificity was observed between OCT1 and OCT2. Typical substrates and inhibitors for OCT2 include endogenous substances (e.g. choline, dopamine (DA), norepinephrine (NE), epinephrine, serotonin (5-HT), and histamine H_2 receptor antagonists (e.g. cimetidine, famotidine, and ranitidine), and anti-cancer (e.g. cisplatin) and antihypertensive (e.g. debrisoquine) agents [13].

In 1998, OCT3/Oct3 was cloned from both human central nervous system (CNS) and rat placenta [14, 15]. Two years later, mouse Oct3 was cloned from kidney [16]. Compared with OCT1/Oct1 and OCT2/Oct2, OCT3/Oct3 exhibits a wider tissue expression. In addition to liver and kidney, OCT3/Oct3 was identified in heart, skeletal muscle, brain, small intestine, liver, lung, kidneys, urinary bladder, mammary gland, cornea skin, blood vessels and tumor cells [4]. OCT3 protein was localized to the basolateral membrane of the trophoblast in placenta [17], the sinusoidal membrane of hepatocytes [18], the apical membrane of enterocytes [19] and the luminal membrane of lung epithelial cells [20]. It is involved in the uptake of organic cationic molecules into these tissues. OCT3/Oct3 showed great similarity with OCT1/Oct1 and OCT2/Oct2 in terms of substrate specificity, and a broad range of endogenous and exogenous organic cations have been proved as its substrate and/or inhibitors [4].

rOat1 was cloned from rat kidney using the *Xenopus* oocyte expression system in 1997 [7, 9]. Several other Oat1 orthologs were later identified in mouse, *C. elegans*, flounder, rabbit pig and human [21-28]. Oat1 mRNA was expressed abundantly in kidney, olfactory mucosa and choroid plexus [29-31]. In addition, rOat1 was targeted to the basolateral membrane of renal tubules using an Oat1/green-fluorescent protein fusion construct [32]. Immunohistochemical studies confirmed the basolateral expression of hOAT1, rOat1 and mOat1 in the proximal tubule cells [7, 9, 25]. Interestingly, male mice expressed a higher level of mRNA for mOat1 than female mice [33]. hOAT1/mOat1 mediates transport of a broad variety of drugs and endogenous compounds including nonsteroidal anti-inflammatory drugs (ibuprofen, indomethacin and ketoprofen), antivirals (e.g., adefovir and cidofovir), histamine H2-blockers (e.g., cimetidine), and endogenous compounds (e.g., prostaglandin E2, α-KG and urate) [6].

rOat2 and hOAT2 mRNA are expressed in both liver and kidney, while mOat2 mRNA is predominantly expressed in kidney with a weaker expression in liver [34, 35]. The protein of hOAT2 was immunolocalized to the basolateral membrane of renal proximal tubules [36]. hOAT2/mOat2 function is the least studied of all the OATs, but identified substrates include glutarate, methotrexate, bumetanide and indomethacin [6].

rOat3 was isolated from rat brain in 1999 [37], and its orthologs were later identified in various tissues in mouse, rabbit, pig, and human [29, 38, 39]. The mRNA of mOat3 was abundantly expressed in kidney, eye tissues and brain [40], while rOat3 mRNA was detected in kidney, liver and brain [41]. On the contrary, a predominant expression of hOAT3 mRNA was noted in human kidney, brain and skeletal muscle, with no signal detected in liver [42]. Immunohistochemistry demonstrated that hOAT3 and rOat3 are expressed on the basolateral membrane of the renal

proximal tubule [38, 43]. OAT3/Oat3 shares a high similarity with OAT1/Oat1 and OAT2/Oat2 in terms of substrate specificity [6].

hOAT4 mRNA is only expressed in the kidney and placenta of higher primates [44-46]. It was demonstrated that hOAT4 was targeted to the apical membrane of renal proximal tubule using immunohistochemistry [44, 47]. In placenta, hOAT4 protein was localized to the basolateral membrane of the syncytiotrophoblast [42, 48]. Studies suggested that a broad variety of drugs interact with hOAT4 as substrates or inhibitors, including nonsteroidal anti-inflammatory drugs (ibuprofen and ketoprofen), furosemide, methotrexate, penicillin G and probenecid [6].

1.B EXPRESSION OF ORGANIC CATION AND ANION TRANSPORTERS IN BRAIN

The mammalian brain has its own security system, known as the blood-brain barrier (BBB) and the blood-cerebrospinal fluid (CSF) barrier to protect it from the circulating metabolites, drugs, toxins and blood-borne pathogens [49]. In brain, choroid plexuses (CPs) are localized in the ventricular system [50]. They occur in each of the four major cisternae, which are developed from the median wall of the lateral ventricles and the roof of the third and fourth ventricles [50]. As a tight epithelial barrier, they form the interface between the blood and the CSF [51]. In the CNS, CPs are the main site of secretion of the CSF [52]. They are also involved in transporting compounds into or out of brain. Previous studies have demonstrated that OCTs and OATs are expressed in the CPs [52]. The mRNA of Oat1, Oat2 and Oat3 were detected in the CPs of mice and rats [29, 31, 41, 53]. In addition, the protein expression of rOat1 and rOat3 were identified on the apical CP membranes using green fluorescent fusion proteins, Western blot analysis, and immunohistochemical staining [31, 54]. Furthermore, significantly impaired accumulation of OAT substrates such as fluorescein-methotrexate was observed in isolated choroid plexus tissues from

Oat3 knockout mice as compared with wild-type mice [29, 55]. The active transport of cationic compounds, including choline and quinacrine in rat choroid plexus cells were also observed, indicating a specific mechanism for organic cation transcellular movement as well (Table 1.1) [56, 57]. A further study confirmed that mRNA expression of Oct2 and Oct3, but not Oct1, was detected in rat CP, and Oct2 was located in the apical membrane of rat CP epithelial cells using an Oct2/green fluorescent protein fusion construct [1]. However, Choudhuri et al. reported that mRNA level of Oct1 and Oct3 was detectable in rat CP, while Oct2 expression was virtually nonexistent in CP [58]. In mouse, the mRNA expression of Oct2 has been identified in CP, while the expression of Oct1 and Oct3 were not detectable [59]. However, the mRNA of OCT1, OCT2, and OCT3 is expressed in human CP, and OCT1 was found as the most abundant transporter among the three transporters [59].

In addition to blood-CSF barrier, BBB is a highly selective barrier that separates the circulating blood from the brain extracellular fluid in the CNS. Vessel endothelial cells are connected by tight junctions producing an extremely high electrical resistivity; therefore, transporters play a vital role in regulating exchange of endogenous and exogenous substances between blood and brain [60]. The expression of Oat3 and OCTs/Octs have been identified in human and rodent, while the results are controversial (Table 1.2) [52, 61, 62]. Several studies have reported the mRNA expression of mOat3 and rOat3 in brain capillaries, and the protein expression of mOat3 and rOat3 was localized to the basolateral membrane of brain capillary endothelial cells using western blotting and immunohistochemical analysis [63-66] Lin et al. studied the cellular localization of OCT1/Oct1 and OCT2/Oct2 in isolated brain microvessel endothelial cells (BMECs) from human, rat, and mouse [61]. Both mRNA and protein expressions of OCT1/Oct1 and OCT2/Oct2 were observed in BMECs from these species, as well as in immortalized adult rat

brain endothelial cells [61, 67]. In addition, immunocytochemistry showed that these OCTs/Octs were mainly expressed on the luminal side of BMECs, which was confirmed by siRNA knockdown of OCT1/Oct1 and OCT2/Oct2 in primary BMECs [61]. In contrast, another study failed to measure Oct1 and Oct2 mRNA expression by quantitative PCR analysis in freshly isolated mouse brain capillaries, except for a negligible level of Oct3 mRNA [62]. Additionally, no capillary associated fluorescence was detected by immunocytochemistry in brain sections [62]. Several recent studies investigated the expression of OCT1, OCT2 and OCT3 in human blood brain barrier. Dickens confirmed that OCT1 and OCT3 mRNA expression was detectable in hCMEC/D3 cells, a model of the human blood brain barrier; while OCT2 mRNA expression was undetectable [68]. The protein expression of OCT1 in hCMEC/D3 cells was confirmed by immunoblotting [68]. Another study demonstrated that the mRNA for OCT3 was presented in human brain vascular smooth muscle cells, while the mRNA of OCT1 and OCT2 was absent [69]. Finally, a recent study showed that mRNAs of OCT1, OCT2 and OCT3 were detected in isolated human brain microvessels and the protein expression of OCT3 was verified by immunofluorescence staining [70]. Friedrich et al. reported that Oct1, but not Oct2 or Oct3, was expressed in the rat brain microvessel endothelial cell line RBE4 by northern blotting and RT-PCR [71]. However, another independent study showed a low mRNA level of Oct2 and Oct3, in rat brain capillary endothelial cell line TR-BBB13 [72]. In mouse brain microvessel cell line MBEC4, Oct2 but not Oct1 mRNA was identified [73]. Although these studies showed conflicting results, which appear to be dependent on experimental models (cell lines or tissues), these data support that OCTs/Octs play an active role in the CNS permeation of organic cations. Further work is necessary to validate these *in vitro* models, measure the expression of OCTs/Octs, and quantitatively evaluate their contribution in mediating brain uptake of organic cations *in vivo*.

Interestingly, a variety of studies demonstrated that OCT2/Oct2 and OCT3/Oct3 are also expressed in the neurons (Figure 1.2, Table 1.3). Busch et al. quantified OCT2 expression in human brain tissues, and they found that mRNA and protein expression of OCT2 were identified in neurons in the cerebral cortex and various subcortical nuclei [74]. Another study showed OCT3 mRNA expression in various parts of human brain, including spinal cord, medulla oblongata, caudate nucleus, cerebral cortex, hippocampus, substantia nigra, medulla oblongata, cerebellum, nucleus accumbens and Pons [75]. A recent study also reported that mRNA expression of OCT2 and OCT3 was quantifiable in a human astrocytoma-derived cell line, 1321N1 [76]. As rodents are widely used animal models for neurological study, extensive investigations have been conducted to exhibit the distribution of Oct2 and Oct3 in mouse and rat brain.

In mouse brain, the mRNA and protein of Oct1 were found in brain stratum and cerebral cortex (Table 1.4) [67]. A high level of protein expression of Oct2 was found in the frontal cortex, hippocampus and amygdale [67, 77], which was consistent with a previous study shown that Oct2 mRNA expression was observed in the cerebellum and hippocampus (Table 1.4) [78]. Oct2 protein expression was also detected in some aminergic neuron-containing areas including the locus coeruleus (most noradrenergic neurons) and dorsal raphe (some serotonergic neurons) [77]. However, Oct2 expression was not observed in substantia nigra or ventral tegmental area [77]. A recent study confirmed Oct2 expression in mouse brain (infralimbic cortices, hippocampus, amygdala, dorsomedial and arcuate nuclei of hypothalamus) [79]. In addition to Oct1 and Oct2, Oct3 was widely distributed in mouse brain. In 2004, Vialou et al. reported that OCT3 was distributed throughout the brain and highly expressed in circumventricular organs such as area postrema and subfornical organ [80]. Another study showed Oct3 mRNA expression in raphe nuclei, striatum and thalamus, implicating monoaminergic pathways [78]. Further studies

focused on expression of mOct3 in neurons and astrocytes [80, 81]. According to Vialou et al., Oct3 protein expression was identified in dopaminergic neurons of substantia nigra compacta, non-aminergic neurons of the ventral tegmental area, substantia nigra reticulata, locus coeruleus, hippocampus and cortex, as well as the astrocytes in the substantia nigra reticulata, hippocampus and hypothalamic nuclei [80]. However, Cui et al. claimed that Oct3 was expressed in the nigrostriatal astrocytes, but not in the astrocytes from regions such as cerebellum, hippocampus, and cortex [81]. Additionally, no Oct3 expression was observed in dopaminergic structures from ventral midbrain and striatum [81].

In 1998, Oct3 mRNA expression was identified from rat brain tissue, especially in cerebellum, hippocampus, pontine nuclei and cortex (Table 1.4) [82]. Ten years later, several groups confirmed that Oct3 protein expression was throughout the rat brain, with the highest level observed in the superior and inferior colliculi, islands of Calleja, subiculum, lateral septum, lateral and dorsomedial hypothalamic nuclei, granule cell layers of the main and accessory olfactory bulbs, the cerebellum, the retrosplenial granular cortex, circumventricular organs, and the linings of all cerebral ventricles [83, 84]. A further study from Gasser's group showed that Oct3 was expressed in most neurons of the intercalated cell groups of the amygdala of rat brain, and it shows co-distributed with the areas of dense D1 receptor expression [85]. Oct2 was found to be localized in cholinergic nerve terminals (C-terminals) and endplates that correspond to the presynaptic terminals of cholinergic motoneurons of the anterior horn [86]. In addition, Oct2 might also exist on synaptic vesicles at presynaptic terminals, based on the results from immunoelectron microscopy [86].

In summary, both Oct2 and Oct3 were expressed in the main aminergic projection regions in rodent brain, including the cortex, hippocampus, thalamus, hypothalamus, amygdala and

hindbrain [74, 77, 80, 83]. They also showed marked expression in aminergic nuclei, raphe, locus coeruleus and the tuberomammillary nucleus [74, 77, 80, 83]. However, OCT2/Oct2 and OCT3/Oct3 showed differences in distribution (subregions and nuclei) and relative expression levels. OCT3 showed relatively higher expression in circumventricular organs [80, 87] and Oct3 might be the only OCT isoform expressed in dopaminergic nuclei substantia nigra [83]. In addition, the expression of Oct3 in the astrocytes in the dorsomedial hypothalamus nucleus and substantia nigra indicated that OCT3/Oct3, rather than Oct2, might be involved in mediating extracellular 5-HT level [80, 81, 88].

Table 1.1 Expression of OCTs/Octs in choroid plexus.

	Species	Level	Expression	Localization	Techniques	References
OCT1/Oct1	Mouse	mRNA	—		RT-PCR	[59]
	Rat	mRNA	?		RT-PCR	[1, 58]
	Human	mRNA	+		RT-PCR	[59]
OCT2/Oct2	Mouse	mRNA	+		RT-PCR	[59, 67]
	Rat	mRNA	?		RT-PCR	[1, 58, 78]
		Protein	+	Apical Membrane of CP epithelial cells	Green Fluorescent Protein Fusion	[1]
	Human	mRNA	+		RT-PCR	[59]
OCT3/Oct3	Mouse	mRNA	—		RT-PCR	[59, 67]
	Rat	mRNA and protein	+		RT-PCR and Immunohistochemistry	[1, 58, 78, 89]
	Human	mRNA	+		RT-PCR	[59]

$^{+}$: indicates transporter expression;

$^{-}$: indicates no expression detected.

$^{?}$: controversial study results.

Table 1.2 Expression of OCTs/Octs in blood brain barrier.

	Species	Level	Expression	Localization	Techniques	References
OCT1/*Oct1*	Mouse	mRNA	?		RT-PCR	[62, 67, 73]
		Protein	+	Luminal and abluminal side of BMECs[a]	Confocal microscopy, western blot and immunohistochemistry	[61, 67]
	Rat	mRNA	+		Northern blotting and RT-PCR	[71, 72]
		Protein	+	Luminal and abluminal side of BMECs	Confocal microscopy and western blot	[61]
	Human	mRNA	+		RT-PCR	[68, 70]
		Protein	+	Luminal and abluminal side of BMECs	Confocal microscopy and western blot	[61]
OCT2/*Oct2*	Mouse	mRNA	?		RT-PCR	[62, 73]
		Protein	+	Luminal and abluminal side of BMECs	Confocal microscopy, western blot and immunofluorescence	[61, 67]
	Rat	mRNA	?		Northern blotting and RT-PCR	[71, 72]
		Protein	+	Luminal and abluminal side of BMECs	Confocal microscopy and western blot	[61]
	Human	mRNA	?		RT-PCR	[68, 70]
		Protein	+	Luminal and abluminal side of BMECs	Confocal microscopy and western blot	[61]
OCT3/*Oct3*	Mouse	mRNA	+		RT-PCR	[62]
	Rat	mRNA	?		Northern blotting and RT-PCR	[71, 72]
	Human	mRNA	+		RT-PCR	[68-70]
		protein	+		Immunofluorescence staining	[70]

[a]: BMECs, brain microvascular endothelial cells;
[b]: IHC, immunohistochemistry;
[+]: indicates transporter expression;
[−]: indicates no expression detected;
[?]: controversial study results.

Table 1.3 Expression of OCTs/Octs in neuron and glia cells.

	Species	Localization	Expression	Level	Techniques	References
OCT1/*Oct1*	Mouse		+	mRNA and protein	RT-PCR and Immunohistochemistry	[67]
	Rat		+	mRNA	In situ hybridization	[78]
	Human		—	mRNA	Northern blot	[74]
OCT2/*Oct2*	Mouse	Neurons	+	Protein	Immunofluorescent histochemistry	[77]
		Astrocytes	—	Protein	Immunofluorescent histochemistry	[77]
	Rat	Neurons	+	Protein	Immunohistochemistry	[86]
	Human	Neurons	+	mRNA and protein	Northern blot, in situ hybridization and Western blot	[74, 76]
OCT3/Oct3	Mouse	Neurons	?	Protein	Immunohistochemistry	[80, 81]
		Glial cells	+	Protein	Immunohistochemistry	[80, 81]
	Rat	Neurons	+	mRNA and protein	In situ hybridization and immunohistochemistry	[82, 85, 89]
		Glial cells	?	Protein	Immunohistochemistry	[88, 89]
		Pinealocyte	+	Protein	Immunohistochemistry	[89]
	Human	Neurons	+	Protein	Immunohistochemistry	[81]
		Astrocytes	+	mRNA and protein	RT-PCR and immunohistochemistry	[76, 81]

$^{+}$: indicates transporter expression; $^{-}$: indicates no expression detected.
$^{?}$: controversial study results.

Table 1.4 Expression of OCTs/Octs in different brain regions.

	Species	Localization	Expression	Level	Techniques	References
OCT1/*Oct1*	Mouse	Cerebral cortex	+	mRNA and protein	RT-PCR and immunohistochemistry	[67]
		Brain striatum	+	Protein	Immunohistochemistry	[67]
	Rat	Cerebellum	+	mRNA	In situ hybridization	[78]
		Corpus callosum (white matter)	+	mRNA	In situ hybridization	[78]
	Human		—	mRNA	Northern blotting	[74]
OCT2/*Oct2*	Mouse	Amygdala	+	Protein	Immunofluorescent histochemistry	[77]
		Brain striatum	+	Protein	Immunohistochemistry	[67]
		Cerebral cortex	+	mRNA and protein	RT-PCR and immunofluorescent histochemistry	[67]
		Dorsal raphe	+	Protein	Immunofluorescent histochemistry	[77]
		Frontal cortex	+	Protein	Immunofluorescent histochemistry	[77]
		Hippocampus	+	Protein	Immunofluorescent histochemistry	[77]
		Locus coeruleus	+	Protein	Immunofluorescent histochemistry	[77]
	Rat	Cerebellum	+	mRNA	In situ hybridization	[78]
		The third ventricle layer boarding	+	mRNA	In situ hybridization	[78]
		Hippocampus	+	mRNA	In situ hybridization	[78]

	Species	Localization	Expression	Level	Techniques	References
	Human	Amygdaloideus nucleus	+	mRNA	Northern blot	[74]
		Caudatus nucleus	+	mRNA	Northern blot	[74]
		Cerebral cortex	+	mRNA	In situ hybridization	[74]
		Hippocampus	+	mRNA and protein	Northern blot, in situ hybridization and western blot	[74]
		Subthalamicus nucleus	+	mRNA	Northern blot	[74]
		Substantia nigra	+	mRNA	Northern blot	[74]
		Thalamus	+	mRNA	Northern blot	[74]
OCT3/*Oct3*	Mouse	Cerebral cortex	+	mRNA	RT-PCR	[67]
		Dentate gyrus	+	Protein	Immunohistochemistry	[80]
		Dorsal raphe	+	Protein	Immunohistochemistry	[80]
		Frontal cortex	+	Protein	Immunohistochemistry	[80]
		Hippocampus	+	Protein	Immunohistochemistry	[80]
		Striatum	+	Protein	Immunohistochemistry	[81]
		Subfornical organ	+	Protein	Immunohistochemistry	[89]
		Substantia nigra	+	Protein	Immunohistochemistry	[80, 81]
		Ventral tegmental area	+	Protein	Immunohistochemistry	[80]

Species	Localization	Expression	Level	Techniques	References
Rat	Amygdala	+	Protein	Western blot and immunohistochemistry	[83, 85]
	Area postrema	+	Protein	Immunohistochemistry	[83, 89]
	Brainstem	+	Protein	Western blotting	[83]
	Cerebellum	+	mRNA and protein	In situ hybridization and immunohistochemistry	[82, 83, 88, 89]
	Cerebral cortex	+	mRNA	In situ hybridization	[78, 82]
	Dorsal raphe	+	mRNA and protein	In situ hybridization and immunohistochemistry	[78, 83, 88, 89]
	Frontal cortex	+	Protein	Immunohistochemistry	[83, 84, 89]
	Hypothalamic nuclei	+	mRNA and protein	In situ hybridization and immunohistochemistry	[78, 83, 88, 89]
	Hippocampus	+	mRNA and protein	RT-PCR, in situ hybridization, Western blot and immunohistochemistry	[78, 82-84, 89]
	Lateral geniculate nucleus	+	mRNA	In situ hybridization	[78]
	Lateral septum	+	mRNA	In situ hybridization	[78]
	Locus coeruleus	+	Protein	Immunohistochemistry	[83, 89]
	Medial preoptic nuclei	+	Protein	Immunohistochemistry	[89]

Species	Localization	Expression	Level	Techniques	References
	Olfactory bulbs	+	Protein	Immunohistochemistry	[83]
	Pontine nucleus	+	mRNA	In situ hybridization	[82]
	Pineal gland	+	Protein	Immunohistochemistry	[89]
	Striatum	+	mRNA	In situ hybridization	[78, 83, 84]
	Septal complex	+	Protein	Western blot	[83]
	Subcommissural organ	+	Protein	Immunohistochemistry	[83, 89]
	Subfornical organ	+	mRNA and protein	In situ hybridization and immunohistochemistry	[78, 83, 89]
	Substantia nigra	+	Protein	Immunohistochemistry	[83, 89]
	Supraoptic nuclei	+	Protein	Immunohistochemistry	[83, 89]
	Thalamus	+	mRNA	In situ hybridization	[78]
	White matter	+	Protein	Western blot	[83]
Human	Caudate Nucleus	+	mRNA	RT-PCR	[75]
	Cerebellum	+	mRNA	RT-PCR	[75]
	Cerebral Cortex	+	mRNA	RT-PCR	[75]
	Medulla Oblongata	+	mRNA	RT-PCR	[75]
	Nucleus accumbens	+	mRNA	RT-PCR	[75]
	Hippocampus	+	mRNA	RT-PCR	[75]

Species	Localization	Expression	Level	Techniques	References
	Substantia nigra	+	mRNA	RT-PCR	[75]
	Pons	+	mRNA	RT-PCR	[75]

+: indicates transporter expression;
−: indicates no expression detected.

1.C. CURRENT EVIDENCE ON ORGANIC CATION TRANSPORTER-MEDIATED NEUROTRANSMITTER DISPOSTION IN BRAIN

Depressive disorders is one of the most burdensome psychiatric disorders in the world. People who suffer from depression showed poor worker productivity and loss of interest in activities or hobbies. In addition, depression carries a high risk of suicide. Previous studies have demonstrated that the level of neurotransmitter 5-HT is decreased in the patients with depressive disorders [90]. As a consequence, understanding the mechanism of 5-HT clearance in brain is critical for designing and developing antidepressant drugs. There are two distinguishable mechanisms of aminergic neurotransmitter clearance from the synapse: uptake-1 (high-affinity, low capacity reuptake) and uptake-2 (low-affinity, high capacity reuptake) [91, 92]. Uptake-1 comprised the serotonin transporter (SERT; SLC6A4), norepinephrine transporter (NET; SLC6A2), and dopamine transporter (DAT; SLC6A3) (Figure 1.2) [91, 92]. Uptake-2 is proposed to play a backup role in monoamine neurotransmitter clearance [14]. The uptake-1 has been well characterized and a variety of antidepressant drugs, known as serotonin transporter reuptake inhibitors (SSRIs, e.g., fluoxetine and sertraline) and serotonin and norepinephrine transporter reuptake inhibitors (SNRIs, e.g., venlafaxine), have been developed to block SERT- and/or NET-mediated neurotransmitter uptake from the extracellular space. Uptake-2 has been gradually gaining attention as a new therapeutic target for antidepressant drugs. Over the last decade, much evidence has suggested that uptake 2 transporters are, at least partially, OCTs, specifically OCT2/Oct2 and OCT3/Oct3 (Figure 1.2). Compared with OCT1/Oct1, OCT2/Oct2 and OCT3/Oct3 are widely distributed throughout brain [80, 81, 83, 87-89]. Several neurotransmitters, including 5-HT, NE and DA, are known substrates of OCTs [93]. in 1996, Busch et al measured the

transport of monoamine neurotransmitters mediated by rOct1, and it was found that rOct1 showed low affinity (high K_m) but high capacity (maximum uptake rate) for 5-HT compared with SERT [74]. Further studies have been conducted to explore the impact of OCTs in depression, using OCT inhibitors or knockout mice. In 2005, Feng and co-workers observed a dose-dependent increase of 5-HT when perfusing decynium-22 (D-22), an inhibitor of OCTs, via a dialysis probe, that correlated with increased grooming, indicating that Octs might be an important regulatory element in adaptive neurophysiological and behavioral responses [94]. Interestingly, the magnitude of extracellular 5-HT concentration increased (~2-6 fold increase) by OCT inhibition was comparable to another study in which a 4 fold increase of extracellular 5-HT concentration was observed after SERT blockade by fluoxetine [94, 95]. Similarly, perfusing corticosterone (OCT inhibitor) into the medial hypothalamus potentiated the effect of fenfluramine on blocking the uptake of extracellular 5-HT [94]. Administration of another OCT inhibitor, normetanephrine, in mice also increased extracellular NE in brain and produced enhanced antidepressant-like effects [96].

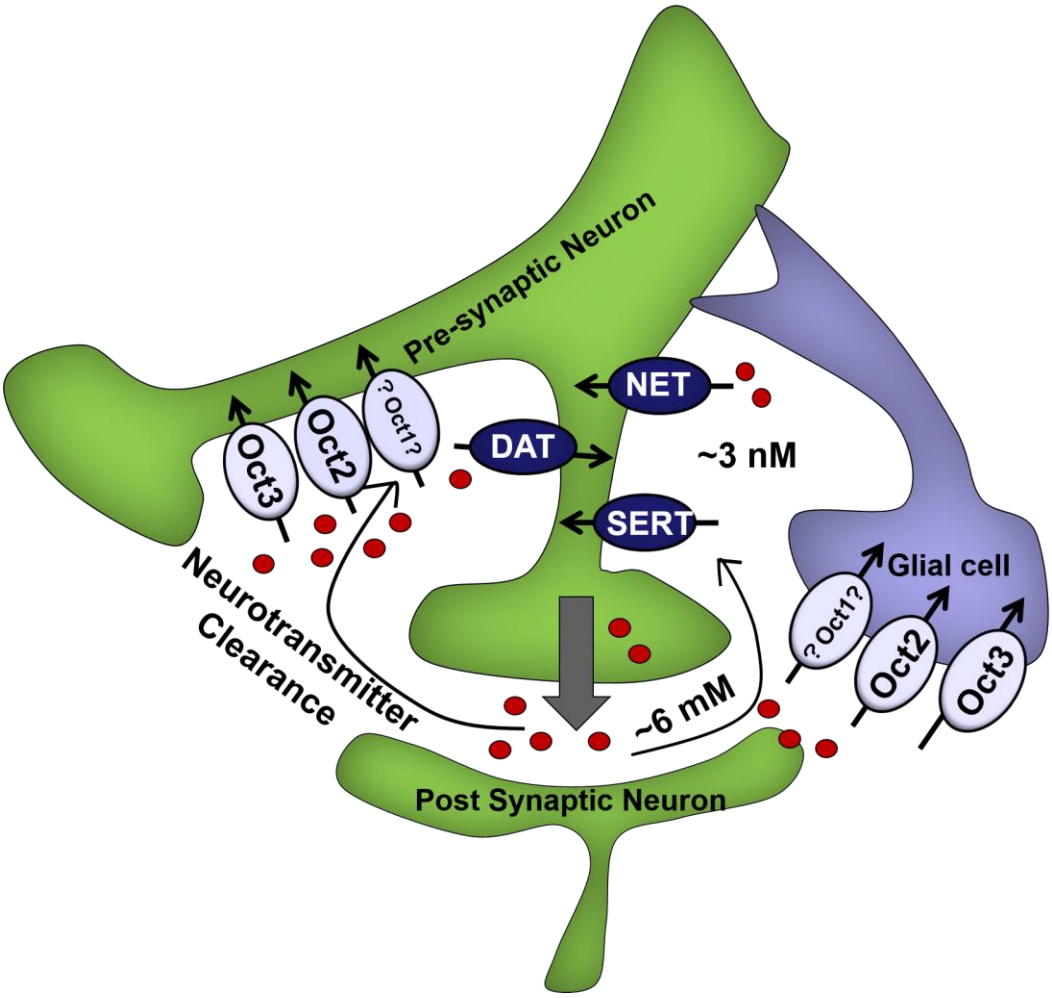

Figure 1.2 Expression of the examined OCTs (SLC22 family) in the neurons and glial cells in the CNS.

OCT: organic cation transporter; SERT: serotonin transporter; DAT: dopamine transporter; NET: norepinephrine transporter; concentrations indicated are for serotonin [97, 98].

Several studies have been conducted to investigate Oct expression in SERT knockout mice [99-101]. Notably, Oct3 mRNA expression in SERT knockout mice was significantly increased in hippocampus, but not in the cortex, striatum, cerebellum or brainstem, while Oct1 mRNA expression remained unchanged [100, 101]. Oct3 protein expression, measured by immunohistochemistry in the hippocampus was increased by 28% in SERT knockout mice [101]. Indeed, antidepressant-like effects (reflected in tail suspension test) in SERT mutant mice were observed when D-22 was administrated [101]. Similarly, another study demonstrated that Oct3 expression was decreased by ~30% after seven day infusion of antisense mOct3 oligonucleotides in the third ventricle of adult mice brain [102]. And the mice also exhibited antidepressant-like effect correlated with loss of Oct3 activity, including enhanced locomotor response to methamphetamine, decreased immobility during the forced swim test, and a potentiated antidepressant response to imipramine [102]. These data indicated that OCT3/Oct3 might serve as a compensatory mechanism in response to dysfunctional 5-HT clearance.

In a recent study, Horton et al. investigated the effect of D-22 on 5-HT clearance in the synapse and associated antidepressant-like activity in mice, when coadministered with fluvoxamine [103]. Clearly, D-22 coadministered with fluvoxamine increased the concentration of 5-HT in brain and caused increased antidepressant-like activity compared to those using fluvoxamine alone, indicating that Oct3 might be a novel target for antidepressant drugs [103]. The role of Oct2 in 5-HT clearance was investigated in Oct2 knockout mice [77]. A marked reduction in brain concentrations of NE and 5-HT, and in ex vivo uptake of both these neurotransmitters, were observed in Oct2 knockout mice in the presence of venlafaxine (an SNRI) [77]. As a consequence, markedly increased immobility time was observed in both forced swim and tail suspension tests, indicating an increased depressive-like phenotype [77]. In addition,

compared with wild-type mice, Oct2 knockout mice showed increased sensitivity to the acute administration of antidepressants [77]. Collectively, these data indicated an active role of OCT2/Oct2 in mediating NE and 5-HT clearance in brain. Thus, both *in vitro* and *in vivo* studies indicated that OCTs might be an important determinant of CNS monoamine neurotransmitter balance, and therefore play an important role in mood-related behaviors, elevating their potential as novel pharmacological targets for mood disorder therapy.

1.D ORGANIC CATION AND ANION TRANSPORTER-MEDIATED DRUG INTERACTION

Drug transporters are widely involved in drug absorption, distribution and elimination [104]. OCT1 has been recognized as a major transporter dominating the hepatic uptake of metformin, and genetic variation in OCT1 showed significant impact on metformin pharmacokinetics [105]. Several OATs, including OAT1, OAT3 and OAT4, are expressed in renal proximal tubular cells and manipulate active renal secretion and reabsorption [2]. As drug transporters influence the pharmacokinetics of a broad variety of therapeutics, it is expected that drug pharmacokinetic properties (e.g. AUC, clearance, and tissue distribution) and pharmacodynamic response might be altered due to concomitant administration of drugs that are substrates or inhibitors of the same transporter during situations of polypharmacy. This phenomenon is called drug-drug interactions (DDI), in which patients may experience unexpected side effects, such as loss of efficacy or toxicity. For instance, a clinical study demonstrated that systemic and peak exposure of rosuvastatin was significantly increased in transplant recipients using cyclosporine, with AUC and C_{max} increased by ~7 fold and ~11 fold compared with those using rosuvastatin [106]. Such DDIs might be caused by cyclosporine inhibition of OATP1B1-mediated rosuvastatin hepatic uptake, and increased systemic exposure of rosvustatin showed high

risk of rosvustatin-related toxicity. Therefore, the United States Food and Drug Administration and the European Medicines Agency has issued guidance documents regarding circumstances under which drug interactions with specified transporters need to be investigated (http://www.fda.gov/downloads/Drugs/GuidanceComplianceRegulatoryInformation/Guidances/UCM292362.pdf and http://www.ema.europa.eu/ema/index.jsp?curl=pages/includes/document/document_detail.jsp?webContentId=WC500090112&murl=menus/document_library/document_library.jsp&mid=WC0b01ac058009a3dc&jsenabled=true) for drug safety and efficacy.

As mentioned in section 1.B, OCTs and OATs are widely expressed in many organs and *in vivo* mediate the absorption, distribution, and disposition of a broad variety of charged endogenous and exogenous organic substances [2, 3, 6]. Currently, hundreds of important clinical therapeutics have been identified as substrates and/or inhibitors of OCTs and OATs[16, 20]. For example, methotrexate, a commonly used drug for the treatment of cancer and rheumatic diseases, was identified as an OAT3/Oat3 substrate [107]. In Oat3 knockout mice, increase plasma concentration of methotrexate and methotrexate-to-inulin clearance were observed as compared to those in wildtype mice, indicating a role of Oat3 in the renal elimination of methotrexate [107]. Some fluoroquinolone antimicrobials, such as ciprofloxacin, gatifloxacin, and norfloxacin, showed significant inhibition on hOCT1, indicating that hOCT1 may play a role in the hepatic and renal disposition of these antimicrobial agents [108]. The antiviral lamivudine was identified as a substrate of hOCT2 [109]. As lamivudine is cleared predominantly by the kidney via renal tubular secretion, concomitant administration of drugs that inhibit hOCT2 could decrease its renal clearance. The antiplatelet drug clopidogrel and its major metabolite clopidogrel carboxylate showed potent inhibition of hOCT1 (IC_{50} values: 0.307–14.0 μM) [110]. Ethambutol, an anti-tuberculosis drug, showed significant inhibitory effect on hOCT1, hOCT2, and hOCT3 [111].

Considering the clinically unbound plasma concentration of ethambutol, tuberculosis patients with coexisting HIV or diabetes may experience DDIs with coadministration of ethambutol and drugs known to be hOCT1/hOCT3 substrates (e.g. lamivudine or metformin) [111]. Interestingly, some research groups have been starting to investigate the interaction of natural products and OCTs. Pan et al. reported that the alkaloids matrine and oxymatrine, which are widely used in China as herbal medicine for the treatment of cancer, viral, and cardiac diseases, showed inhibitory effects on hOCTs [112]. Additionally, berberine, known as an active constituent of many medicinal herbal extracts was identified as a potent inhibitor of hOCT2 and hOCT3, with IC_{50} values in the low micromolar range (0.1-1 μM) [113]. Such increased understanding of the vital roles SLC22 transporters play in the absorption, distribution, elimination and reabsorption of drugs and endogenous compounds will serve to facilitate the development of drugs with increased specificity, safety and favorable pharmacokinetic profiles, as well as broaden our understanding of their roles in various pathophysiologies.

CHAPTER 2

RESEARCH OBJECTIVES AND SPECIFIC AIMS

2.A RESEARCH OBJECTIVES

2.A.1 Many components in clinical therapeutics, herbal products, and drugs of abuse are charged at physiological pH and therefore represent unidentified substrates/inhibitors of organic cation (OCTs) or anion transporters (OATs).

2.A.2 OCTs/OATs are sites of drug-drug interaction (DDI) during situations of polypharmacy and the DDI index, estimated based on the affinity (K_i and IC_{50}) and clinical unbound plasma concentrations, can be used to predict clinically relevant DDIs potentially mediated by compounds confirmed to interact with SLC22 transporters in SA1.

2.A.3. OCTs, as an important component of the low-affinity, high capacity clearance pathway (uptake-2) for biogenic monoamine neurotransmitters, represent novel targets for psychostimulant drugs of abuse and antidepressants.

2.A.4. Construction of a hOCT3 homology model based upon the solved structure of the *Piriformospora indica* phosphate transporter (PiPT, PDB id 4J05) will allow identification of key transporter structural features required for substrate/inhibitor interactions.

2.B SPECIFIC AIMS TO ADDRESS THE ABOVE HYPOTHESES

SPECIFIC AIM 1:

To quantify the inhibitory effects on OCTs/Octs (hOCT1-3 and mOct1-3) or OATs (hOAT1, hOAT3 and hOAT4) of 5 constituents from therapeutic agents/herbal products, 5 drugs of abuse and 13 novel synthesized compounds having been identified as possessing physicochemical properties similar to known SLC22 family substrates and inhibitors.

SPECIFIC AIM 2:

To quantify IC_{50} or K_i values for lead compounds identified in SA1 as producing significant OCT or OAT inhibition based upon predefined conditions and to use this information to calculate DDI indices to determine the potential for clinically relevant DDIs mediated by OCTs/OATs based on "Guidance for Industry: Drug Interaction Studies" issued by the FDA.

SPECIFIC AIM 3:

To conduct *in vivo* dose response studies in mice to quantify (*i.e.,* ED_{50} assessment) the antidepressant-like effects of lead quinazoline and/or guanidine compounds identified in SA1 and SA2 as having significant interaction potential on SLC22 transporters.

SPECIFIC AIM 4:

To construct a 3-D homology model for hOCT3 and dock known substrates and lead quinazoline and/or guanidine compounds identified in SA1 and SA2 in order to identify key amino acid residues that might be involved in interaction between hOCT3 and small molecules (done in collaboration with Dr. Dukat's laboratory and Kavita Iyer). To determine the mode of inhibition of docked compounds to support modeling and docking study conclusions.

CHAPTER 3

THE ANTHRAQUINONE DRUG RHEIN POTENTLY INTERFERES WITH ORGANIC ANION TRANSPORTER-MEDIATED RENAL ELIMINATION

Drawn from manuscript published in *Biochemical Pharmacology.* 2013, 86: 991–996.

3.A INTRODUCTION

Great insight has been gained from *in vitro* and *in vivo* studies on drug transporters regarding their role in physiology and biopharmaceutics [104]. These drug transporters are expressed in barrier organs and involved in the interchange (e.g. uptake or removal) of endogenous and exogenous substances between cells and biofluids. Among these transporters, organic anion transporters (OATs), which belong to the SLC22 family, interact with anionic compounds [2, 6]. Three human (h) OAT paralogs, hOAT1, hOAT3, and hOAT4 have been identified as determinants for tubular secretion and reabsorption [2, 6]. Human OAT1 and hOAT3, immunolocalized to the basolateral side of proximal tubules, mediate cellular uptake of negatively charged organic molecules from the blood [2, 6]. Human OAT4, which is expressed on the apical side of proximal tubules, appears to mediate reabsorption of organic anions from tubular fluid [2,

6]. Such OAT-mediated organic solute flux is vital for maintaining systemic homeostasis and normal renal elimination.

Numerous first-line therapeutics (*e.g.*, antibiotics, ACE inhibitors and NSAIDs) and components of herbal medicines have been identified as substrates and/or inhibitors for OATs [2, 6]. These findings demonstrate the impact of OATs on the pharmacokinetic properties of these drugs and provide efficacy and safety information for their clinical application. Interestingly, Oat3 function has been linked to the regulation of blood pressure in mice. Oat3 knockout mice, and wild-type mice treated with potent Oat3 inhibitors, exhibited significantly reduced blood pressure compared to untreated wild-type animals [114]. For diabetic patients, blood pressure is a major determinant of the risk of developing nephropathy [115]. Thus, impairment of OAT function (either through genetics or pharmacology) may influence normal physiological status and result in unexpected drug-drug interactions (DDIs).

The anthraquinone compound rhein is a major component of the medicinal herb *Rheum sp*., which is widely used for its antidotal, anti-inflammatory, antipyretic and laxative properties in Asian countries including China, Korea, and Japan. This medicinal herb is also used to treat diabetic nephropathy [116]. Further, rhein was identified as a major metabolite of diacerein, a prodrug used in the treatment of osteoarthritis [117]. *In vivo,* diacerein is completely converted to rhein before *entering the systemic circulation* [118, 119]. Rhein is highly protein bound in human plasma (99%) and, after oral administration, the majority of rhein is eliminated in urine as glucuronide conjugates (60%), followed by unchanged form (20%) and sulfate conjugates (20%) [118]. In clinical practice diacerein is utilized in polypharmacy therapies, *e.g.,* a fixed dose of diacerein (50 mg) and aceclofenac (100 mg) has been approved in India to treat osteoarthritis [120]. Recently, a phase II clinical trial was initiated in Thailand to investigate the safety and efficacy of

the combined therapy of diacerein and methotrexate to treat early rheumatoid arthritis (http://clinicaltrials.gov/ct2/show/NCT01264211). As methotrexate and a number of NSAIDs are known inhibitors and substrates of OATs [2, 6], the interaction of rhein with OAT family members needs to be investigated in order to meaningfully assess the potential for transporter-mediated adverse events.

Based on its chemical structure, rhein, which bears a carboxylic group, has the potential to be a substrate and/or inhibitor for OATs. Because OATs have broad substrate specificity, rhein may cause DDIs with co-administered therapeutics that are OAT substrates. This information may also be useful to elucidate the beneficial effects of *Rheum sp*. on diabetic nephropathy. In the present study, inhibition of hOAT1-mediated *p*-aminohippuric acid (PAH) transport and hOAT3- and hOAT4-mediated estrone sulfate (ES) transport by rhein was explored using stably transfected cell lines. Further kinetic studies were conducted to estimate the half maximal inhibitory concentration **(**IC_{50}**)** and inhibitory constant (K_i). In order to investigate potential species differences IC_{50} and K_i estimates also were determined in murine (m) Oat1 and mOat3 expressing cells. The results showed that rhein was a potent inhibitor for hOAT1, hOAT3, and hOAT4. The IC_{50} values for rhein on hOAT1 and hOAT3 were estimated as 77.1 ± 5.5 nM and 8.4 ± 2.5 nM, respectively. However, rhein failed to produce > 50% inhibition on hOAT4 transport activity at 100 µM, indicating that the IC_{50} value on hOAT4 was higher than 100 µM. Comparison of estimated IC_{50} values with clinical unbound plasma concentrations indicated the potential for clinically relevant DDIs on hOAT1 and hOAT3 in the kidney. In addition, marked species differences appeared to exist in inhibitory potency, with hOAT1 and hOAT3 exhibiting 3- and 28-fold higher affinity with rhein as compared to their murine orthologs, respectively. Together, these findings suggested that rhein could interfere with hOAT1- and hOAT3-mediated renal elimination

in vivo, leading to unintended changes in pharmacokinetics, pharmacodynamics, toxicity and the therapeutic effects of *Rheum sp*.

3.B Materials and Methods

3.B.1 Chemicals

Rhein (≥ 98% purity) was purchased from Santa Cruz Biotechnology, Inc. (Santa Cruz, CA). Tritiated *p*-aminohippuric acid ([^{3}H]PAH) and estrone sulfate ([^{3}H]ES) were purchased from PerkinElmer Life and Analytical Sciences (Waltham, MA) and unlabeled PAH, ES, and probenecid were purchased from Sigma-Aldrich (St. Louis, MO).

3.B.2 Tissue culture

Derivation of stably transfected Chinese hamster ovary (CHO) cells expressing hOAT1 (CHO-hOAT1), hOAT4 (CHO-hOAT4), mOat1 (CHO-mOat1), and mOat3 (CHO-mOat3) as well as stably transfected human embryonic kidney 293 (HEK) cells expressing hOAT3 (HEK-hOAT3), and their corresponding empty vector transfected background control cell lines, has been described previously [107, 121, 122]. All cells lines were maintained at 37°C with 5% CO_2 in medium containing 10% FBS and 1% Pen/Strep. CHO-hOAT1 cells were cultured in phenol red-free RPMI 1640 media (Gibco-Invitrogen, Grand Island, NY) containing 1 mg/mL G418. CHO-hOAT4 cells were cultured in EMEM Alpha Modification media (Sigma-Aldrich (St. Louis, MO) containing 0.5 mg/mL G418. CHO-mOat1 and CHO-mOat3 cells were cultured in DMEM F-12 media (Mediatech, Inc., Herndon, VA) containing 125 μg/mL hygromycin B. HEK cell lines were cultured in DMEM high glucose media (Mediatech, Inc., Herndon, VA) containing 125 μg/ml hygromycin B.

3.B.3 Cellular uptake assay

The procedure for the cellular uptake assay was adapted from that previously published [123]. Two days before cellular uptake experiment, 2×10^5 cells/well were seeded in 24-well tissue culture plates and grown in the absence of antibiotics. On the day of the experiment, cells were equilibrated in transport buffer at room temperature (22-25°C) for 10 min [500 µL of Hanks' balanced salt solution containing 10 mM HEPES, pH 7.4]. After equilibration, this solution was replaced with 500 µL of fresh transport buffer containing 1 µM [^{3}H]PAH (0.5 µCi/mL) or [^{3}H]ES (0.25 µCi/mL) with or without inhibitors. At the end of incubation, cells were quickly rinsed three times with ice-cold transport buffer. Then cells were lysed with 1N NaOH, neutralized with 1N HCl, and analyzed via liquid scintillation counting. The intracellular accumulation of tritiated substrates was reported as picomoles of substrate per milligram total protein. All uptake data were corrected for background accumulation in corresponding empty vector transfected control cells. Substrate concentrations and accumulation times used for kinetic analysis of hOAT1, hOAT3, mOat1, and mOat3 were determined previously [107, 121, 123, 124]. Kinetic calculations were performed using GraphPad Prism Software version 5.0 (GraphPad Software Inc., San Diego, CA). The half maximal inhibitory concentrations (IC_{50}) and inhibitory constants (K_i) were calculated using nonlinear regression. Results were confirmed by repeating all experiments at least three times with triplicate wells for each data point in every experiment.

3.B.4 Statistics

Data are reported as mean ± SD or mean ± SEM as indicated. Raw cell line accumulation data are reported as mean ± SEM. Statistical differences were assessed using one-way ANOVA followed by post-hoc analysis with Dunnett's t-test ($\alpha = 0.05$) except for statistical differences

between murine and human transporter K_i values which were assessed by two-tailed Student's unpaired t-test.

3.C Results

3.C.1 Inhibitory effects of rhein on hOAT1-, hOAT3-, and hOAT4-mediated substrate uptake

Markedly increased cellular accumulation of PAH (7.9 ± 0.1 pmol mg protein^{-1} 10 min^{-1}) was observed in CHO-hOAT1 cells compared to that in the empty vector transfected background control cells (0.3 ± 0.1 pmol mg protein^{-1} 10 min^{-1}), and this hOAT1-mediated cellular uptake was inhibited by probenecid at 1 mM (Figure 3.1A). Rhein was assessed for inhibitory effects on CHO-hOAT1 transport activity at 100 µM (Figure 3.1A). Under this condition, rhein completely blocked PAH accumulation (> 99% inhibition) in CHO-hOAT1 cells. Dose-response studies, applying increasing concentrations of rhein (10^{-9} to 10^{-5} M), were performed to determine the IC_{50} value (Figure 3.1B and Table 3.1). The IC_{50} value for rhein on hOAT1 was estimated as 77.1 ± 5.5 nM. Previous studies demonstrated that the mode of inhibition of most identified OAT inhibitors was competitive [107, 124-128]. Thus, assuming competitive inhibition, the inhibition constant (K_i) was estimated as 71.5 ± 5.2 nM (Table 3.1).

CHO-hOAT3 cells exhibited significantly increased accumulation of ES (6.5 ± 0.2 pmol mg protein^{-1} 10 min^{-1}) compared to that in the empty vector transfected background control cells (2.2 ± 0.3 pmol mg protein^{-1} 10 min^{-1}). Similar to probenecid (1 mM), rhein showed virtually complete inhibition of hOAT3-mediated ES uptake at 100 µM (Figure 3.2A). Accordingly, dose-response studies (10^{-9} to 10^{-4} M) were conducted to estimate affinity of rhein for hOAT3. Rhein showed much higher affinity for hOAT3 than for hOAT1, with an IC_{50} value of 8.4 ± 2.5 nM

(Figure 3.2B and Table 3.1). Assuming competitive inhibition, the K_i was estimated as 7.7 ± 2.4 nM (Table 3.1).

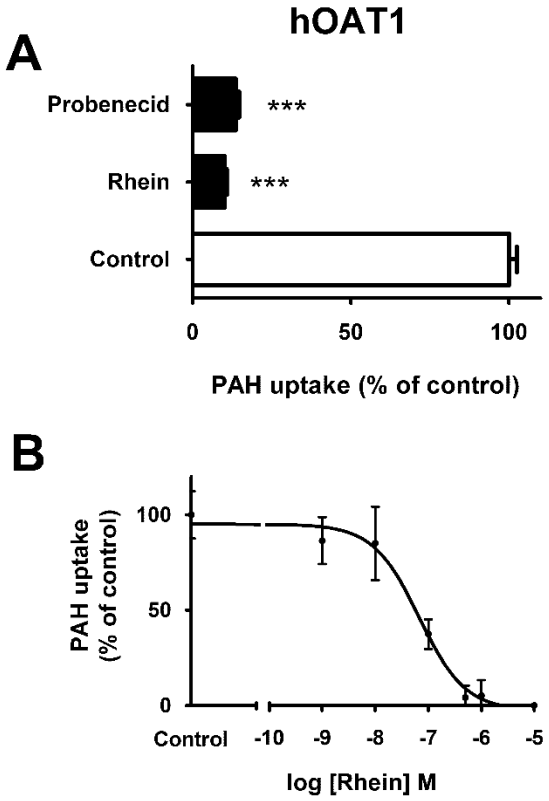

Figure 3.1 Inhibition of hOAT1 by rhein.

A: Inhibition of hOAT1-mediated PAH (1 µM) uptake by rhein (100 µM) was assessed at 10 min. Values are mean ± SD of triplicate samples. ***denotes $p < 0.001$ as determined by one-way ANOVA followed by Dunnett's t-test. B: Dose-response curve for rhein on hOAT1. One minute uptake of PAH (1 µM) was measured in CHO-hOAT1 cells in the presence of increasing concentrations of rhein (10^{-9} to 10^{-5} M). The IC_{50} was estimated using non-linear regression and the "log(inhibitor) vs. response" model (GraphPad Prism). All data were corrected for non-specific background measured in control cells.

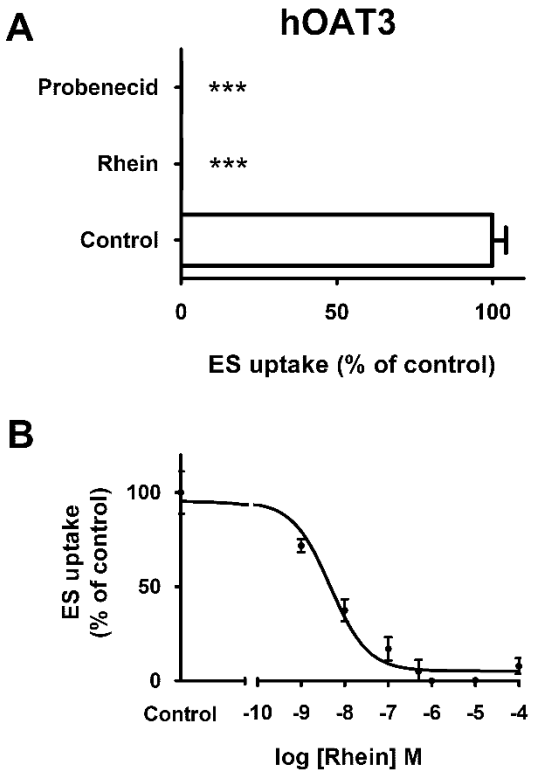

Figure 3.2 Inhibition of hOAT3 by rhein.

A: Inhibition of hOAT3-mediated ES (1 µM) uptake by rhein (100 µM) was assessed at 10 min. Values are mean ± SD of triplicate samples. ***denotes $p < 0.001$ as determined by one-way ANOVA followed by Dunnett's t-test. B: Dose-response curve for rhein on hOAT3. One minute uptake of ES (1 µM) was measured in HEK-hOAT3 cells in the presence of increasing concentrations of rhein (10^{-9} to 10^{-4} M). The IC_{50} was estimated using non-linear regression and the "log(inhibitor) vs. response" model (GraphPad Prism). All data were corrected for non-specific background measured in control cells.

Stably transfected hOAT4-expressing (CHO-hOAT4) cells showed higher accumulation of ES (~24 fold) relative to empty vector transfected background control cells (26.9 ± 3.5 vs. 1.1 ± 0.1 pmol/mg protein/10 min, respectively; Figure 3.3). This active transport underwent self-inhibition (> 99% inhibition) by ES (1 mM). Rhein, however, showed modest inhibition (~29%) on hOAT4 transport activity at 100 µM. As this indicated that the IC_{50} value of rhein on hOAT4 should be higher than 100 µM, no further kinetic studies were performed.

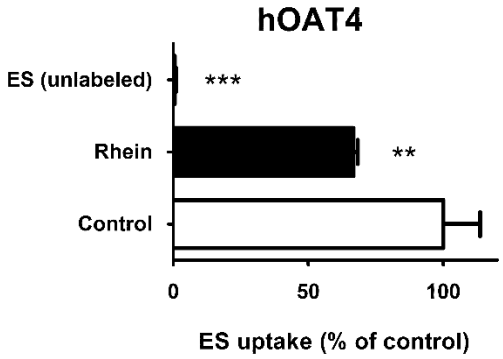

Figure 3.3 Inhibition of hOAT4 by rhein.

A: Inhibition of hOAT4-mediated ES (1 µM) uptake by rhein (100 µM) was assessed at 10 min. Values are mean ± SD of triplicate samples. **denotes $p < 0.01$ and ***denotes $p < 0.001$ as determined by one-way ANOVA followed by Dunnett's t-test.

3.C.2 Inhibitory effects of rhein on mOat1- and mOat3-mediated substrate uptake

CHO-mOat1 and CHO-mOat3 cells showed > 10-fold increased substrate uptake compared to that in the empty vector transfected background control cells. The intracellular accumulation of PAH was measured as 8.0 ± 0.3 pmol mg protein^{-1} 10 min^{-1} and 0.8 ± 0.2 pmol mg protein^{-1} 10 min^{-1} in CHO-mOat1 and background control cells, respectively. Accumulation of ES was measured as 171 ± 12 pmol mg protein^{-1} 10 min^{-1} and 5.7 ± 1.5 pmol mg protein^{-1} 10 min^{-1} in CHO-mOat3 and background control cells, respectively. As shown in Figures 3.4A and 3.5A, probenecid (1 mM) achieved complete inhibition (> 99% inhibition) of mOat1- and mOat3-mediated substrate uptake. At 100 µM, rhein exhibited potent inhibition, completely blocking mOat1 and mOat3 transport activity (Figures 3.4A and 3.5A). Further dose-response studies (10^{-8} to 5×10^{-4} M) were performed to determine the IC_{50} values in order to evaluate potential species differences between human and murine OATs (Figures 3.4B and 3.5B and Table 3.1). The IC_{50} values were estimated as 215 ± 29 nM and 235 ± 74 nM for mOat1 and mOat3, respectively. Assuming that rhein was a competitive inhibitor, K_i values were estimated as 198 ± 26 nM and 216 ± 68 nM, respectively (Table 3.1).

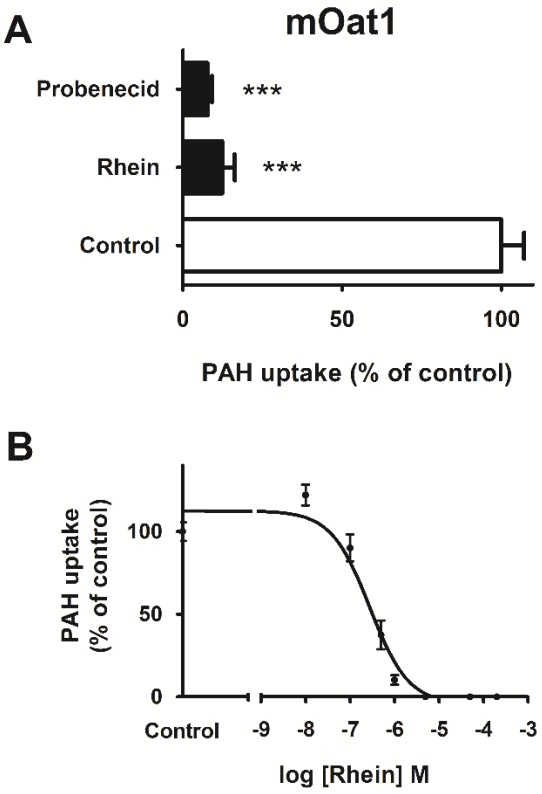

Figure 3.4 Inhibition of mOat1 by rhein.

A: Inhibition of mOat1-mediated PAH (1 µM) uptake by rhein (100 µM) was assessed at 10 min. Values are mean ± SD of triplicate samples. ***denotes $p < 0.001$ as determined by one-way ANOVA followed by Dunnett's t-test. B: Dose-response curve for rhein on mOat1. One minute uptake of PAH (1 µM) was measured in CHO-mOat1 cells in the presence of increasing concentrations of rhein (10^{-8} to 5×10^{-4} M). The IC_{50} was estimated using non-linear regression and the "log(inhibitor) vs. response" model (GraphPad Prism). All data were corrected for non-specific background measured in control cells.

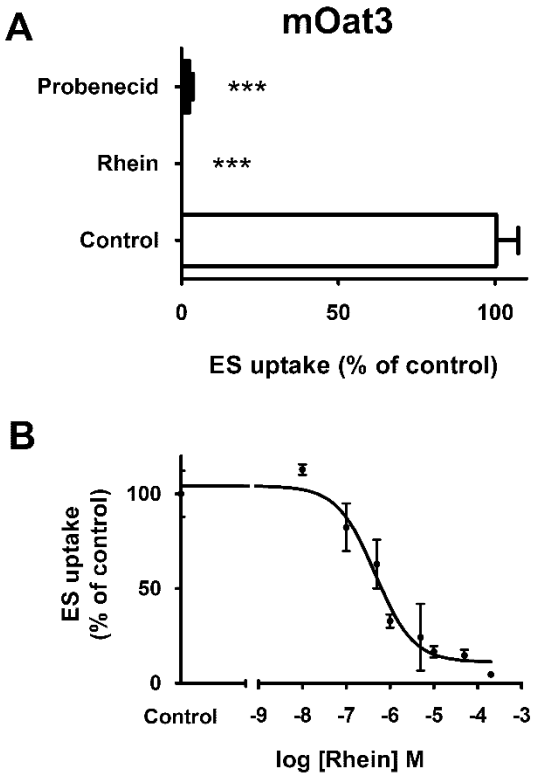

Figure 3.5 Inhibition of mOat3 by rhein.

A: Inhibition of mOat3-mediated ES (1 µM) uptake by rhein (100 µM) was assessed at 10 min. Values are mean ± SD of triplicate samples. ***denotes $p < 0.001$ as determined by one-way ANOVA followed by Dunnett's t-test. B: Dose-response curve for rhein on mOat3. One minute uptake of ES (1 µM) was measured in CHO-mOat3 cells in the presence of increasing concentrations of rhein (10^{-8} to 5×10^{-4} M). The IC_{50} was estimated using non-linear regression and the "log(inhibitor) vs. response" model (GraphPad Prism). All data were corrected for non-specific background measured in control cells.

Table 3.1 Estimated kinetic constants (IC_{50}, K_i) and DDI indices for rhein on OATs.

Transporter	IC_{50} (nM)	K_i (nM)[a]	Unbound C_{max} (nM)[b]	DDI index	K_i ratio (murine/human)
hOAT1	77.1 ± 5.5	71.5 ± 5.2	67-387	**5.0**	
hOAT3	8.4 ± 2.5	7.7 ± 2.4	67-387	**46**	
hOAT4	> 100, 000	> 100, 000			
mOat1	215 ± 29	198 ± 26			2.8**
mOat3	235 ± 74	216 ± 68			28**

Values are reported as mean ± SEM.
[a] K_i values were estimated assuming competitive inhibition based on literature.
[b] Clinical C_{max} values were reported from literature.
**denotes significant difference between murine and human K_i values $p < 0.01$ as determined by two-tailed Student's unpaired t-test.

3.D Discussion

With increasing clinical evidence supporting drug transporter-mediated DDIs, it is necessary to identify potential substrates and inhibitors from both existing and new candidate drugs [104]. Hundreds of endogenous and exogenous compounds have been identified as substrates and/or inhibitors for OATs, including clinically important therapeutics such as antibiotics (benzylpenicillin, cephaloridine, cefdinir and cefotiam), antivirals (adefovir, cidofovir, and ganciclovir), anticancer agents (methotrexate), cholesterol-lowering agents (pravastatin), and angiotensin-converting enzyme inhibitors (quinapril) [2, 6]. Such broad substrate specificity markedly increases the risk of DDIs, especially during combination therapies. In addition, recent investigations demonstrated potential interaction between OATs and natural products, including phenolic acids, flavonoids, and other anionic compounds [123, 124]. While these natural products are major components of herbal medicines and nutritional supplements, information on the proper use and safety of these compounds is limited compared to "traditional" western drugs. Rhein is

both a major metabolite of the prodrug diacerein and a major constituent of the medicinal herb *Rheum sp*.

In the present study, the inhibitory effects of rhein on three human OATs (hOAT1, hOAT3, and hOAT4) and two murine OAT orthologs (mOat1 and mOat3) were assessed. Rhein showed significant inhibition on substrate uptake mediated by hOAT1, hOAT3 and hOAT4 at 100 µM. Kinetic studies demonstrated that the estimated IC_{50} values for hOAT1 and hOAT3 were in the low nanomolar range (IC_{50} = 77.1 ± 5.5 nM and 8.4 ± 2.5 nM for hOAT1 and hOAT3, respectively), while hOAT4 showed poor affinity with rhein (IC_{50} > 100 µM). The estimated IC_{50} values for mOat1 and mOat3 were somewhat higher (IC_{50} = 215 ± 29 nM and 235 ± 74 nM for mOat1 and mOat3, respectively), indicating that human OATs exhibited higher affinity for rhein compared to their murine orthologs. In addition, rhein exhibited ~9-fold higher affinity (lower K_i value) for hOAT3 than for hOAT1, while no significant difference between mOat1 and mOat3 was observed (Table 3.1).

For most identified OAT inhibitors, K_i values are in the micromolar range, with some compounds exhibiting much poorer affinity (K_i values > 1 mM) [2, 6]. Very few compounds have shown extremely high affinity (nM) for OATs, *e.g.*, some cephalosporin antibiotics, ochratoxin A, prostaglandin E_2 and prostaglandin $F_{2\alpha}$. In this study, the estimated IC_{50} and K_i values for hOAT1 and hOAT3 were less than 100 nM, making rhein one of the most potent inhibitors yet identified for hOAT1 and hOAT3. Such high affinity indicates that rhein has the potential to interfere with hOAT1- and hOAT3-mediated renal elimination of endogenous, as well as xenobiotic, substances. The Food and Drug Administration guidance for industry, "Drug Interaction Studies — Study Design, Data Analysis, Implications for Dosing, and Labeling Recommendations" recommends that DDI potency be estimated using the DDI index, calculated as the [unbound] C_{max}/K_i (or IC_{50})

ratio [129]. A DDI index value greater than 0.1 indicates that the test compound has the potential to perpetrate *in vivo* DDIs. Based on clinical reports, the range of C_{max} of rhein was from 8.8 to 14.8 μM after administration of a typical dose of diacerein (50 mg) [119, 120, 130], and the C_{max} of rhein in patients administered *Rheum sp*. ranged from 6.7 to 38.7 μM [131-133], indicating similar peak exposure level. Although most rhein molecules in human plasma exist as the bound form (99%), the unbound C_{max} (67-387 nM) of rhein is close to or higher than the IC_{50} values determined in this study. The maximum DDI index was calculated as 5.0 and 46 for hOAT1 and hOAT3, respectively. These results indicated significant inhibition potential on hOAT1 (83%) and hOAT3 (98%) transport activity, resulting in reduced hOAT1- and hOAT3-mediated renal tubular secretion of co-administered therapeutics that are OAT substrates. As mentioned earlier, diacerein is combined with NSAIDs or methotrexate in clinical applications for the treatment of osteoarthritis or rheumatoid arthritis. However, for herbal medicines containing *Rheum sp*. (rhein) there is no official warning regarding potential herb-drug interactions. Therefore, further *in vivo* pharmacokinetic studies are necessary to explore potential DDIs involving rhein.

Animal models are commonly employed to demonstrate DDI potential *in vivo*. However, if notable species differences between the animal model and humans appear to exist, the utility of results from animal studies may be lacking. Currently, limited work has been done to demonstrate species differences in inhibitory potency on OATs. Some compounds (*e.g.,* diclofenac and sulindac) showed preferential affinity with rodent OATs compared to human orthologs, while other substances (*e.g.*, adefovir, cefoperazone, cephalothin, cidofovir and methotrexate) exhibited lower K_i or K_m values for human OATs [6]. Previous work showed that hOAT1 exhibited 3.4-16 fold higher affinity for three Danshen (a traditional Chinese herbal medicine) components, rosmarinic acid, salvianolic acid B and tanshinol, as compared to mOat1, and five Danshen

compounds (lithospermic acid, rosmarinic acid, salvianolic acid A, salvianolic acid B and tanshinol) exhibited much higher affinity (by 1-2 orders of magnitude) for hOAT3 over mOat3 [124]. In the current study, rhein also exhibited higher affinity for hOAT1 and hOAT3, with 3- and 28-fold lower K_i values than those for mOat1 and mOat3. These differences raised the issue that DDI potency observed in mice at clinically relevant doses may underestimate the *in vivo* DDI potential for humans. Thus, the dose would need to be adjusted in order to balance the discrepancy in affinities between species. This highlights the significance of *in vitro* work to delineate species differences in affinity with OATs before using animal models to conduct pharmacokinetic studies and extrapolating the results to humans. Other animal models (*e.g.*, dog or monkey) should be investigated more thoroughly with respect to OATs to determine if they represent a more appropriate animal model.

Progression of diabetes mellitus sometimes results in diabetic nephropathy and renal failure [115]. Although the mechanism underlying the therapeutic effect of antihypertensive drugs is not well understood, clinically they are used to slow the onset of diabetic nephropathy and lower blood pressure [115]. In 2008, Vallon *et al.* reported that reduced blood pressure was observed in Oat3 knockout mice and wild-type mice treated with potent Oat3 inhibitors [114]. These data suggested that hOAT3 might represent a novel target to ameliorate diabetic nephropathy. Similarly, the Danshen component, lithospermic acid, was demonstrated to significantly reduce blood pressure and to exert nephroprotective effects in diabetic rats [134, 135]. Though other mechanisms for attenuated diabetic nephropathy may exist, the potential contribution of reduction in blood pressure via inhibition of OAT3/Oat3 function by Danshen components such as lithospermic acid can not be ruled out [124]. A clinical investigation demonstrated that rhei rhizoma (the dried root and rhizome of *Rheum sp.*) also exhibited beneficial effects for diabetic nephropathy [116]. Thus, it is

possible that rhein might exert positive effects on diabetic nephropathy through inhibition of hOAT3 transport activity and subsequent downregulation of blood pressure.

In summary, the anthraquinone drug rhein showed marked inhibition on hOAT1- and hOAT3-mediated substrate uptake at clinically relevant concentrations. Notable species differences were observed between human and murine OAT orthologs, with human OATs exhibiting preferential affinity. The DDI indices for rhein on hOAT1 and hOAT3 indicated a strong potential for OAT-mediated DDIs in patients involved in combination therapy of rhein and drugs that are known hOAT1 and/or hOAT3 substrates. Moreover, the nanomolar affinities of rhein for hOAT1 and hOAT3 mirror known OAT affinities for endogenous compounds, *e.g.*, hormones, raising the possibility of significant drug-endogenous molecule interactions as well. Such a mechanism might explain the effects of rhein and lithospermic acid on blood pressure, *i.e.*, via inhibiting the uptake of an endogenous hOAT3 substrate involved in regulation of blood pressure.

CHAPTER 4

INTERACTION OF ETHAMBUTOL WITH HUMAN ORGANIC CATION TRANSPORTERS (SLC22 FAMILY) INDICATES POTENTIAL FOR DRUG-DRUG INTERACTIONS DURING ANTITUBERCULOSIS THERAPY

Drawn from manuscript published in *Antimicrob. Agents Chemother*. 2013. 57(10): 5053-5059.

4.A INTRODUCTION

Ethambutol dihydrochloride (EMB) (Figure 4.1) is a potent antimycobacterial agent employed in the treatment of tuberculosis (TB) and Mycobacterium avium complex infections. The main pharmacological effect of EMB is to inhibit arabinosyl transferase, preventing the synthesis of arabinogalactan, which is a vital component of the mycobacterial cell wall. EMB, pyrazinamide, isoniazid, and rifampin comprise the four first-line antituberculosis drugs recommended by the World Health Organization (WHO) [136]. EMB is used in the treatment of multidrug-resistant tuberculosis to prevent the emergence of isoniazid- or rifampin-resistant mycobacteria [137]. In clinical practice, EMB use is associated with many adverse effects, including optic neuritis (reported in 1% to 5% of patients) [138] and reduced renal clearance of urate (reported in about 66% of patients) [139], the incidence of which is higher when EMB is concomitantly administered with pyrazinamide [140]. The *in vivo* pharmacokinetic properties of EMB have been well defined [141-143]. In humans, EMB showed high bioavailability (80%) and low plasma protein binding (20 to 30%) [144]. A peak serum concentration (C_{max}) of 4.5g/ml was

reported after oral dosing of 25 mg/kg [141]. Only a small portion of EMB (8% to 15%) is metabolized in the liver to form the final dicarboxylic metabolite, 2,2'-(ethylenediimino)dibutyric acid (EDA) (Figure 4.1) [145]. Renal elimination is the major clearance mechanism for EMB, with 70 to 84% of an intravenous dose being excreted in the urine as the unchanged parent compound [144]. The renal clearance rate (417 ml/min) indicates that active net tubular secretion, as well as glomerular filtration (120 ml/min), is involved [141]. While EMB has been identified as a substrate of P-glycoprotein [146], based upon their chemical structures (Figure 4.1) and physicochemical properties, EMB and EDA have the potential to be a substrate and/or inhibitor of OCTs and/or OATs.

The organic cation/anion/zwitterion transporters belong to the solute carrier 22 (SLC22) family and *in vivo* mediate the absorption, distribution, and elimination of a broad variety of charged endogenous and exogenous organic substances [2, 3, 6]. OATs and OCTs are widely expressed in many barrier organs, such as the intestine, kidney, liver, and brain [2, 3, 6]. In the intestine (Figure 4.2), human OCT1 (hOCT1) (SLC22A1) is expressed in the basolateral membrane and hOCT3 (SLC22A3) is targeted to the brush border membrane of enterocytes, where they mediate the cellular entry of cationic compounds [3]. hOCT1 and hOCT3 are both expressed in the sinusoidal membrane (blood side) of hepatocytes (Figure 4.2) and represent the first step in the hepatic excretion of many substances [3, 147]. In the kidney (Figure 4.2), hOCT2 (SLC22A2), hOCT3, hOAT1 (SLC22A6), and hOAT3 (SLC22A8) are each expressed on the basolateral sides of proximal tubule cells and extract drugs from the blood. hOCT1 mRNA has been detected; however, the protein has not been immunolocalized [2, 3]. Hundreds of important clinical therapeutics are known substrates and/or inhibitors of OATs and OCTs, such as chemotherapeutics (e.g., cisplatin and paclitaxel), analgesics (e.g., morphine), cholesterol-lowering drugs (e.g.,

atorvastatin and pravastatin), antivirals (e.g., cidofovir and lamivudine), and antidiabetic agents (e.g., metformin) [2, 3, 6].

Recently, it was reported that TB infection is closely linked to both human immunodeficiency virus (HIV) and diabetes. According to the WHO, 10% of TB patients also suffer from diabetes and 13% of the 9 million TB patients newly diagnosed in 2011 were coinfected with HIV [136]. Thus, the complexity of these disease treatment regimens (TB, TB-diabetes, or TB-HIV), in terms of polypharmacy, raises concerns regarding the potential for drug-drug interactions (DDIs) involving OCTs and/or OATs. The aim of the present study was to explore the inhibitory effects of EMB and its metabolite EDA on hOCT1, hOCT2, hOCT3, hOAT1, and hOAT3. Potent inhibition was further characterized by kinetic investigations to estimate IC50s, which were used to quantitatively evaluate the clinical DDI potential on these transporters during antituberculosis therapy.

4.B MATERIALS AND METHODS

4.B.1 Chemicals

Tritiated p-aminohippuric acid ([^{3}H]PAH), estrone sulfate ([^{3}H]ES), and 1-methyl-4-phenylpyridinium ([^{3}H]MPP$^+$) were purchased from PerkinElmer Life and Analytical Science (Waltham, MA). Unlabeled ES, MPP$^+$, PAH, probenecid, and ethambutol dihydrochloride (EMB, 95% purity) were obtained from Sigma-Aldrich (St. Louis, MO). Quinine monohydrochloride dihydrate was purchased from Acros Organics (Fair Lawn, NJ). 2,2’-(Ethylenediimino)dibutyric acid (EDA; 99% purity) was purchased from Santa Cruz Biotechnology, Inc. (Santa Cruz, CA).

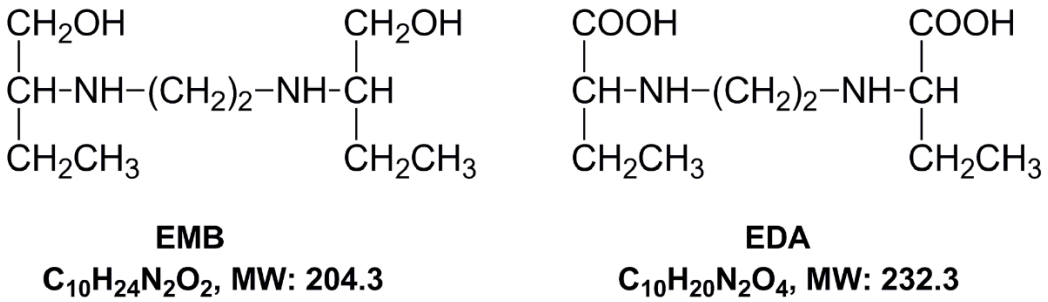

Figure 4.1. Chemical structures of ethambutol (EMB) and its dicarboxylic metabolite 2,2'-(ethylenediimino)dibutyric acid (EDA).

MW, molecular mass.

4.B.2 Tissue culture

Derivation of stably transfected Chinese hamster ovary (CHO) cell lines expressing hOAT1 (CHO-hOAT1) and stably transfected human embryonic kidney 293 (HEK) cells expressing hOAT3 (HEK-hOAT3), hOCT1 (HEK-hOCT1), hOCT2 (HEK-hOCT2), or hOCT3 (HEK-hOCT3), as well as their corresponding empty vector-transfected background control cell lines, has been described previously [14, 107, 121, 148]. CHO-hOAT1 cells were maintained at 37°C with 5% CO_2 in phenol red-free RPMI 1640 medium (Gibco-Invitrogen, Grand Island, NY) containing 10% serum, 1% penicillin/streptomycin, and 1 mg/ml G418. HEK-hOAT3 cells were maintained at 37°C with 5% CO_2 in high glucose Dulbecco's modified Eagle medium (DMEM; Mediatech, Inc., Herndon, VA) containing 10% serum, 1% penicillin/streptomycin, and 125 µg/ml hygromycin B. The HEK-hOCT1, HEK-hOCT2, and HEK-hOCT3 cell lines were maintained at

37°C with 5% CO_2 in high-glucose DMEM containing 10% serum, 1% penicillin/streptomycin, and 600 μg/ml G418.

4.B.3 Cell accumulation assays

The procedure for the cell accumulation assay has been described previously [123, 124]. Briefly, cells were seeded into 24-well tissue culture plates at a density of 2×10^5 cells/well (without antibiotics) for 48 h. On the day of the cell transport experiment, the cells were equilibrated to serum-free conditions with transport buffer for 10 min (500 μL of Hanks' balanced salt solution containing 10 mM HEPES, pH 7.4). Equilibration buffer was replaced with 500 μL of fresh transport buffer containing 1 μM unlabeled substrate spiked with [^{3}H]PAH (0.5 μCi/ml), [^{3}H]ES (0.25 μCi/ml), or [^{3}H]MPP^+ (0.25 μCi/ml) in the presence or absence of test compounds. At the end of the incubation, the cells were quickly rinsed three times with ice-cold transport buffer and lysed. The radioactivity of cell lysate was quantified by liquid scintillation counting, and the uptake profile was normalized by the total protein content determined by the Bradford method. The intracellular accumulation of substrates was reported as picomoles of substrate per milligram total protein. All uptake data were corrected for background accumulation in corresponding empty vector-transfected control cells. Substrate concentration and accumulation time used for kinetic analyses were determined previously [3, 124]. Kinetic calculations were performed using GraphPad Prism software version 5.0 (GraphPad Software Inc., San Diego, CA). The half-maximal inhibitory concentrations (IC_{50}s) were calculated using nonlinear regression with the appropriate model. Results were confirmed by repeating all experiments at least three times with triplicate wells for each data point in every experiment.

4.B.4 Drug-drug interaction (DDI) index calculation

The DDI index [104] was estimated as the ratio of the maximal unbound EMB concentration in biofluid (unbound C_{max}) after therapeutic dosing of EMB divided by transporter-specific IC_{50}s estimated by *in vitro* assay. A cutoff value of ≥ 0.1 is thought to indicate the need for a prospective *in vivo* pharmacokinetic study [104]. Specifically, the predicted intestinal lumen concentration of EMB after oral dosing (25-mg/kg dose, 70-kg patient body weight, 250 ml volume) was used to estimate the DDI index for hOCT3 located in the apical (luminal) membranes of enterocytes, while the portal venous plasma concentration (presystemic circulation) of EMB was used to estimate DDI index values for hOCTs in the basolateral membranes of hepatocytes (hOCT1 and hOCT3) and/or enterocytes (hOCT1 and hOCT2), and the plasma concentration (systemic circulation) of EMB was used to estimate DDI index values for hOCT1, hOCT2, and hOCT3 in the basolateral membranes of renal proximal tubule cells (Figure 4.2). The concentration of EMB in the intestinal lumen was estimated to be ~34 mM, assuming that patients (70 kg) take EMB with 250 ml of water. From clinical reports, after oral dosing (25 mg/kg) the plasma C_{max} of EMB was 22.02 μM, with about 20% being protein bound [141, 144, 149]. Accordingly, the method of Ito et al. can be used to estimate drug concentrations in the portal vein [150]: $C_{port,vn} = C_{max} + (k_a \times D)/(Q_h \times F_a)$, where $C_{port,vn}$, k_a, D, Q_h, and F_a represent concentration in the portal vein, absorption rate constant, dose, hepatic blood flow rate (~1,200 ml/min), and fraction absorbed, respectively. For EMB, k_a and F_a were reported as 0.48 h^{-1} and 80% [144, 149]. Using an average patient body weight of 70 kg, the predicted portal venous blood concentration for EMB was ~67 μM.

4.B.5 Statistical analysis

The data in the figures and the raw uptake scores are expressed as means ± standard deviations (SD), while IC_{50} estimates are means ± standard errors of the means (SEM). Statistical differences were assessed using one-way analysis of variance (ANOVA) followed by post hoc analysis with Dunnett's t test ($\alpha = 0.05$).

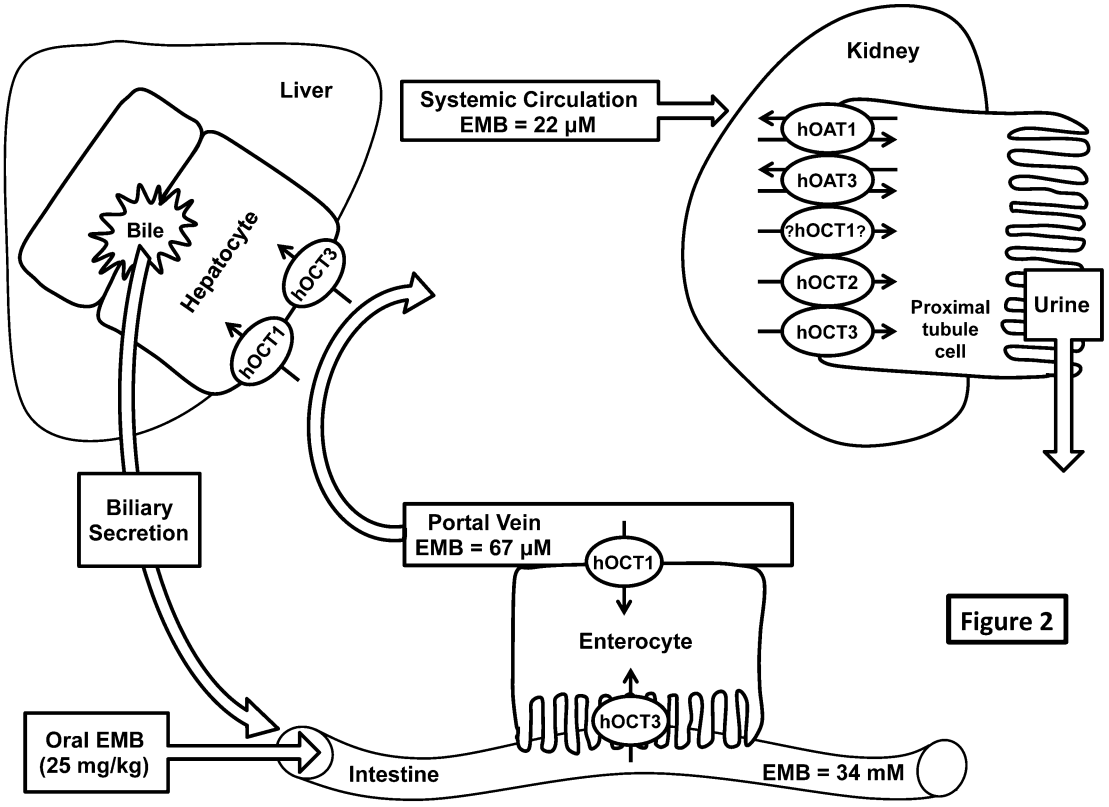

Figure 4.2 Illustration relating expression of the examined human OCTs and OATs (SLC22 family) in the intestine, liver and kidney.

Predicted (GI lumen and portal circulation) and clinically determined (systemic circulation) concentrations of EMB are indicated. Renal expression and targeting of hOCT1 remains controversial, with conflicting reports about its location in the literature, however, the rat Oct1 ortholog has been immunolocalized to the basolateral membrane of proximal tubule cells.

4.C RESULTS

4.C.1 Inhibitory effects of EMB on hOCT1-, hOCT2-, and hOCT3-mediated MPP^+ uptake

The inhibitory effects of EMB were examined on three OCT paralogs, hOCT1, hOCT2, and hOCT3, using MPP^+ as a prototypical substrate. Significant accumulation of MPP^+ (~33-fold) was observed in stably transfected hOCT1-expressing cells relative to empty-vector-transfected background control cells (132.6 ± 9.9 versus 4.0 ± 0.2 pmol/mg protein/10 min, respectively). The known hOCT inhibitor, quinine (200 μM), showed virtually complete inhibition of hOCT1-mediated MPP^+ uptake (>90% inhibition) (Figure 4.3A). Significant inhibition (66%) of hOCT1-mediated MPP^+ transport by EMB (at 100 μM versus 1 μM MPP^+) was observed (Figure 4.3A). Subsequent dose-response (10^{-7} to 10^{-3} M EMB) studies were performed to derive the IC_{50} for EMB on hOCT1 (Figure 4.4, top). The IC_{50} of EMB for hOCT1 was estimated as 92.6 ± 10.9 μM. Therefore, the DDI indices were calculated to gauge DDI potency in enterocytes, hepatocytes, and proximal tubule cells, using the EMB concentration in gastrointestinal (GI) biofluid, portal venous blood, or the systemic circulation, as appropriate (Figure 4.2 and Table 4.1).

We next examined the inhibitory effect of EMB on hOCT2-mediated transport. HEK-hOCT2 cells exhibited marked accumulation of MPP^+ (93.0 ± 5.2 pmol/mg protein/10 min) compared to background control cells (4.0 ± 0.2 pmol/mg protein/10 min). Quinine (200 μM) completely blocked (>99%) hOCT2-mediated MPP^+ uptake (Figure 4.3B). The cell accumulation assay demonstrated that EMB at 100 μM significantly inhibited hOCT2-mediated MPP^+ uptake (21%), and complete inhibition of hOCT2 transport activity (96%) was observed at 1 mM EMB. Kinetic studies were conducted to estimate the IC_{50} for EMB on hOCT2. Using EMB concentrations ranging from 10^{-6} to 10^{-3} M, the IC_{50} was estimated as 253.8 ± 90.8 μM (Figure 4.4,

middle). As shown in Table 4.1, the DDI index for hOCT2 expressed in kidney was estimated as 0.1.

Stably transfected hOCT3-expressing (HEK-hOCT3) cells also showed marked accumulation of MPP^+ (~30-fold) compared to empty vector-transfected background control cells (80.3 ± 11.3 versus 2.7 ± 0.1 pmol/mg protein/10 min). Such active transport was completely (99%) blocked by quinine at 200 μM (Figure 4.3C). Though EMB failed to show significant inhibition on hOCT3 transport activity at 100 μM, marked inhibition was observed with increasing concentrations (Figure 4.3C). EMB showed ~50% and ~80% inhibition at 1 and 10 mM, respectively. Further dose-response (10^{-3} to 10^{-1} M EMB) studies yielded an estimated IC_{50} of 4.1 ± 1.6mM (Figure 4.4, middle). Due to low EMB concentration in the presystemic (portal) and systemic circulation, DDI indices for hOCT3 in liver and kidney were negligible compared to the 0.1 threshold value (Table 4.1). However, the high concentration of EMB in the GI biofluid yielded an estimated DDI index around 8.3.

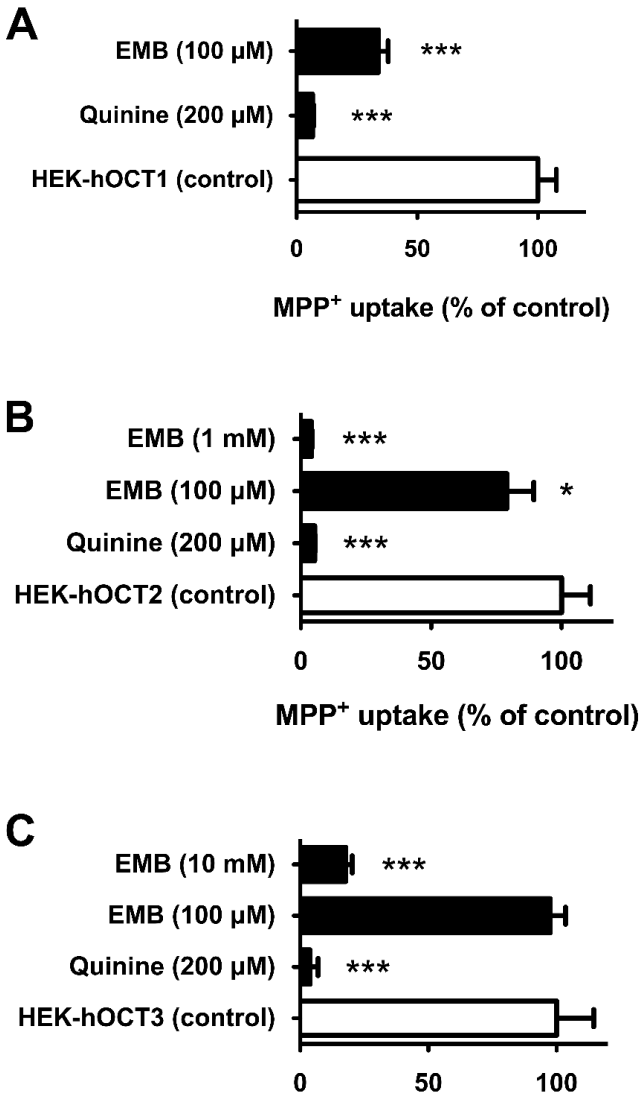

Figure 4.3. Inhibition profiles of EMB on hOCT1, hOCT2 and hOCT3.

A: Inhibition of hOCT1-mediated MPP^+ uptake by EMB and quinine (200 µM). B: Inhibition of hOCT2-mediated MPP^+ uptake by EMB and quinine (200 µM). C: Inhibition of hOCT3-mediated MPP^+ uptake by EMB and quinine (200 µM). The concentration of MPP+ was 1 µM, incubation time was 10 min, and data shown were corrected for non-specific background. Values are mean ± SD of triplicate values. *** denotes $p < 0.001$ as determined by one-way ANOVA followed by Dunnett's t-test.

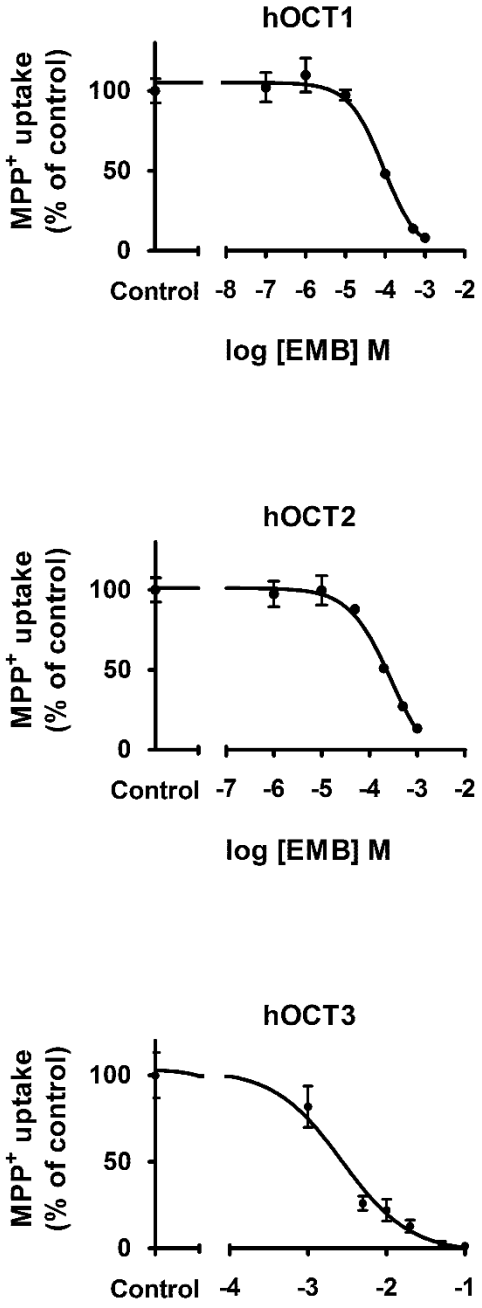

Figure 4.4. Dose-response curves for EMB on hOCT1, hOCT2 and hOCT3.

Representative data showing 1 min uptake of MPP^+ (1 μM) measured in HEK-hOCT1, HEK-hOCT2, and HEK-hOCT3 cells in the presence of increasing concentrations of EMB (10^{-7} to 10^{-1} M) are shown. Data were corrected for nonspecific background measured in the empty vector control cells and are means ± SD of triplicate values. IC_{50}s were determined with nonlinear regression and the "log(inhibitor) versus response" model using GraphPad Prism software.

4.C.2 Inhibitory effects of EDA on hOAT (hOAT1andhOAT3) and hOCT (hOCT1, hOCT2, and hOCT3) transport activity

The zwitterionic dicarboxylic acid metabolite of EMB, EDA, was examined for interactions with hOAT1, hOAT3, hOCT1, hOCT2, and hOCT3 (Figure 4.5). The standard substrate used for hOAT1 was PAH, and that for hOAT3 was ES. Stably transfected hOAT1-expressing (CHO-hOAT1) and hOAT3-expressing (HEKhOAT3) cells showed 5-fold- and 3-fold-greater substrate accumulation than empty-vector-transfected background control cells, respectively (7.5 ± 1.6 versus 1.6 ± 0.2 pmol/mg protein/10 min for hOAT1 and 4.1 ± 0.2 versus 1.6 ± 0.1 pmol/mg protein/ 10 min for hOAT3). The known OAT inhibitor probenecid completely blocked (>99%) hOAT1- and hOAT3-mediated substrate uptake (Figure 4.5). With the exception of hOAT3 (~17% inhibition), EDA (100 μM) failed to produce any significant inhibitory effects. Despite the modest inhibition of hOAT3, for all tested transporters IC_{50}s of EDA were expected to be greater than 100 μM, which greatly exceeds the EDA concentration in the systemic circulation, and further kinetic analysis was not performed.

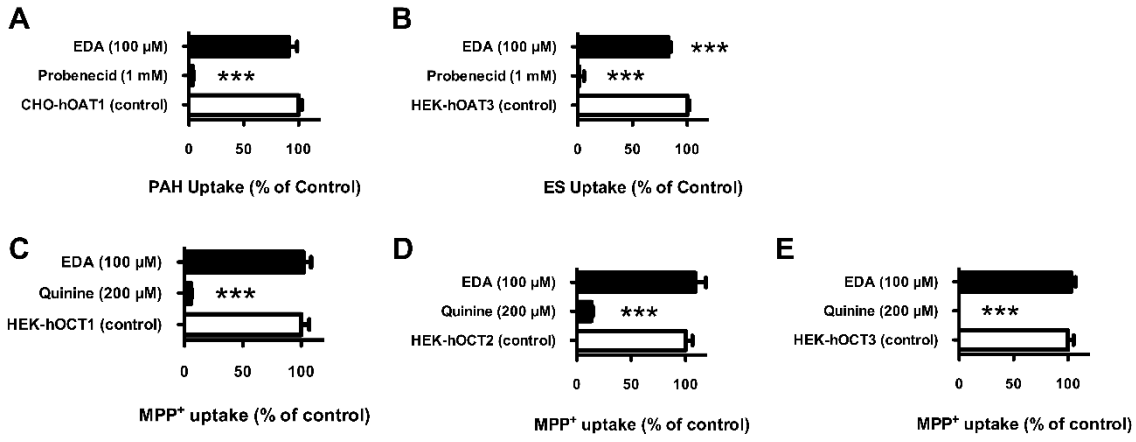

Figure 4.5 Inhibition profile of EDA on hOATs and hOCTs.

(A) Inhibition of hOAT1-mediated PAH uptake by EDA (100 μM) and probenecid (1,000 μM). (B) Inhibition of hOAT3-mediated ES uptake by EDA (100 μM) and probenecid (1,000 μM). (C) Inhibition of hOCT1-mediated MPP^+ uptake by EDA (100 μM) and quinine (200 μM). (D) Inhibition of hOCT2-mediated MPP^+ uptake by EDA (100 μM) and quinine (200 μM). (E) Inhibition of hOCT3-mediated MPP^+ uptake by EDA (100 μM) and quinine (200 μM). The concentration of substrates was 1 μM, incubation time was 15 min, and data were corrected for nonspecific background. Values are means ± SD of triplicate values. ***, $P < 0.001$, determined by one-way ANOVA followed by Dunnett's t test.

Table 4.1 Estimated DDI index values for EMB on hOCT-mediated transport after an oral dose of 25 mg/kg.

	Drug-drug interaction index[a]		
hOCT	GI tract	Liver	Kidney
hOCT1	0.6	0.6	0.2[b]
hOCT2	NE[c]	NE	0.1
hOCT3	8.3	< 0.1	< 0.1

[a] Drug-drug interaction index is defined as the unbound concentration of drug divided by the drug IC_{50} for the transporter of interest. A DDI index value of >0.1 is thought to indicate the potential for clinically relevant DDIs.
[b] Assuming basolateral targeting for hOCT1.
[c] NE, transporter not expressed in this tissue.

4.D DISCUSSION

Although numerous antitubercular drugs have been developed since the 1940s, TB is still a prevalent disease and a common cause of death worldwide. Recently, the spread of multidrug-resistant TB strains (MDR-TB; estimated to account for 3.7% of new cases and 20% of previously treated cases) and the emergence of an extensively drug-resistant strain (XDR-TB; ~9% of MDR-TB cases) that has proven virtually impossible to successfully treat have become new challenges to disease management [136, 151]. The appearance of XDR-TB has been reported in 84 countries, and the threat of its spread is viewed as a significant enough health issue that the United Kingdom has enacted regulations obligating people traveling from regions where TB is prevalent to have a current chest X-ray in their possession upon arrival in order to be issued a visa [152]. Isolation and therapy may be required for up to 2 years and can cost upwards of one million U.S. dollars per patient [152].

A further complication in TB therapy arises from the increasing clinical association of TB with diabetes and HIV, with TB becoming one of the leading causes of mortality among HIV infected patients [153, 154]. Indeed, of the ~9 million new TB patients diagnosed in 2011, 13% were reported to be coinfected with HIV, and of the 1.4 million TB deaths, 430,000 were HIV associated [136]. As a result, more TB patients need to be prescribed combination therapies to treat comorbidities or to minimize the development of drug resistance, making therapy management and compliance extremely complex and increasing the risk of patients' experiencing unintended drug-drug interactions. Indeed, there are a number of case reports regarding adverse events, including nephrotoxicity, associated with EMB use during antituberculosis therapy [155-158]. In these patients, discontinuation of EMB resulted in improvement in renal function.

Competition for binding to membrane transporters is one mechanism resulting in DDIs, and while there is currently insufficient clinical data to conclusively determine transporter-mediated DDI involvement, it is possible that hOCT-mediated DDIs explain some of these cases. As such, potential interactions between antituberculosis agents and drug transporters have received increased attention. For example, rifampin was identified as an inhibitor of P-glycoprotein (ABCB1), OATP1B1 (SLCO1B1), and OAPT1B3 (SLCO1B3), whereas pyrazinamide was demonstrated to inhibit hURAT1 (SLC22A12) [159-161]. EMB also was reported as a substrate for P-glycoprotein [146]; however, information regarding potential interactions with other drug transporters, especially drug uptake transporters, is virtually nonexistent. Additionally, many anti-diabetic (metformin) and anti-HIV (lamivudine, raltegravir, tenofovir, and zalcitabine) agents have been identified as substrates and/or inhibitors of OCTs and OATs [2, 3, 6, 162-164]. Therefore, in order to more effectively and safely manage the longterm therapies of these complicated patient populations, improved understanding of the interactions of these drugs with the transporters responsible for their absorption, distribution, and elimination is needed.

A number of preclinical and clinical studies have demonstrated the role of hOCT1, -2, and -3 in the disposition and efficacy of metformin, a hypoglycemic agent widely used for the treatment of type 2 diabetes mellitus [105, 164-166]. In humans, subjects carrying a mutated form of hOCT1 with reduced function exhibited significantly altered pharmacokinetic properties of metformin that manifested as increased area under the plasma concentration-time curve, increased C_{max}, and reduced oral volume of distribution, as well as reduced glucose-lowering effects, i.e., loss of efficacy [105, 166]. Given the predicted EMB portal vein concentration of 67 μM after oral dosing [141, 144, 149, 150], the rank order of DDI potencies for hOCT1 was enterocytes (0.6) = hepatocytes (0.6) ≥ proximal tubule cells (0.2); all the DDI indexes are above the 0.1 threshold

value (Figure 4.2 and Table 4.1). These results indicated that 38% of hOCT1 transport activity might be inhibited in enterocytes and hepatocytes during routine EMB therapy, suggesting a strong potential for EMB-metformin interactions in TB-diabetes patients. The IC_{50} for hOCT3 was higher (4.1 ± 1.6 mM) than those for hOCT1 and hOCT2 (Figure 4.4, bottom). However, given the expected high luminal GI tract concentration of EMB after oral dosing (~34 mM after a 1,750-mg dose [25 mg/kg in a 70-kg patient] diluted in 250 ml GI fluid), hOCT3 may represent an important pathway for GI absorption of EMB due to its apical membrane localization in enterocytes (Figure 4.2). Furthermore, the estimated DDI index of 8.3 (Figure 4.4, bottom, and Table 4.1) is 83-fold higher than the DDI threshold value and is indicative of a marked potential for EMB to interfere (89% inhibition) with intestinal absorption of coadministered drugs that are hOCT3 substrates, including metformin.

As many anti-HIV agents are also hOCT substrates, the same DDI potential exists for polypharmacy in TB-HIV patients. Recently, expression of hOCT1 and hOCT2 mRNA was detected in CD4 cells isolated from patients with HIV [167]. Therefore, EMB present in the systemic circulation also might reduce accumulation of anti-HIV agents in CD4 target cells that serve as a viral reservoir, resulting in loss of antiviral efficacy via inhibition of hOCT1 and/or hOCT2 function. Similarly, systemic EMB might impact hOCT1-mediated (DDI index = 0.2; ~20% inhibition) and/or hOCT2-mediated (DDI index = 0.1; ~9% inhibition) renal secretion.

hOCTs are also involved in the pharmacological action of platinum antineoplastics (e.g., cisplatin and oxaliplatin), raising the possibility for significant DDIs during chemotherapy in TB patients [168-171]. Patients receiving cisplatin therapy frequently experience cumulative dose-dependent nephrotoxicity involving the proximal tubule [172-174]. Moreover, treatment with inhibitors of hOCTs (e.g., tetraethylammonium and cimetidine) prevented accumulation of

cisplatin in renal proximal tubule cells, and subsequently, cisplatin was identified as a competitive inhibitor of rat Oct2 [168, 175-178]. Thus, coadministration of EMB and cisplatin or oxaliplatin might alter associated hepatic and renal accumulation and toxicity.

In summary, our findings demonstrate the inhibitory effect of EMB on hOCT1, hOCT2, and hOCT3, while its zwitterionic dicarboxylic metabolite EDA failed to produce significant inhibition of hOCT1, -2, and -3, hOAT1, or hOAT3. EMB concentrations in the GI tract and portal vein after oral administration indicate the potential for marked DDIs *in vivo* for hOCT1 expressed in hepatocytes, enterocytes, and potentially renal proximal tubule cells. Human OCT3 in enterocytes exhibited the highest DDI index, suggesting that EMB might significantly alter cationic drug/nutrient absorption. Renal hOCT2 has a slight possibility of EMB DDIs. Future investigations encompassing *in vivo* DDI studies between EMB and known substrates for hOCT1, hOCT2, and hOCT3 appear to be necessary in order to optimize clinical safety and efficacy in these complex patient populations.

CHAPTER 5

INHIBITION OF HUMAN ORGANIC CATION TRANSPORTERS BY THE ALKALOIDS MATRINE AND OXYMATRINE

Drawn from manuscript published in *Fitoterapia.* 2014, 92: 206–210.

5.A INTRODUCTION

Matrine and oxymatrine are the major quinolizidine alkaloids derived from several traditional Chinese medicinal herbs including *Sophora alopecuroides* (kudouzi), *Sophora flavescens* (kushen) and *Sophora subprostrata* [179-181]. *In vivo*, oxymatrine can be metabolized to form matrine in the GI tract and liver [180, 181]. Pharmacological studies have demonstrated that these compounds exhibit anti-arrhythmic, anti-viral, anti-immunodeficiency and anti-cancer activities [179, 180, 182]. The China State Food and Drug Administration database of drug manufacturing certificates currently lists 306 commercial matrine and oxymatrine preparations (http://www.sda.gov.cn/WS01/CL0001/). These pharmaceutical products, including granule, capsule, suppository and injectable dosage forms have been used in China for the treatment of viral hepatitis, cancer, and cardiac disease [183-186].

The analysis of their chemical structures indicated that matrine (pKa = 7.8) and oxymatrine (pKa = 6.0-6.7) might be positively charged at physiological pH [187, 188]. As a result, they have the potential to interact with organic cation transporters (OCTs) belonging to the Solute Carrier 22

(SLC22) family. OCTs mediate the absorption, distribution, and elimination of a broad array of positively charged endogenous and exogenous organic substances. Hundreds of clinically important therapeutics are known OCT substrates and/or inhibitors, including many antineoplastic (e.g., cisplatin, oxaliplatin and paclitaxel), antidiabetic (e.g. metformin) and antiviral (e.g., acyclovir and ganciclovir) agents [6, 163, 168, 189, 190]. OCTs are widely expressed in many organs including intestine, liver, kidney and brain [3, 6, 163]. Thus, OCT expression and function can be a major determinant of drug absorption across the GI tract, preferential tissue distribution, or active hepatic and renal drug excretion, which also leads to these transporters being frequent sites of drug-drug interaction (DDI). Indeed, numerous studies have demonstrated OCT-mediated DDIs between therapeutics [191]. Therefore, it is necessary to investigate potential OCT-mediated DDIs in order to establish informed safety and efficacy profiles for therapeutic products that contain OCT substrates and inhibitors.

In the present study, inhibition of hOCT1-, hOCT2- and hOCT3-mediated 1-methyl-4-phenylpyridinium (MPP^+) transport by the alkaloids matrine and oxymatrine was explored. Potent inhibition was further quantified with kinetic studies to estimate the inhibitory constant (IC_{50}). Inhibitory constant estimates were then used to aid evaluation of the potential for clinical DDIs on hOCTs.

5.B MATERIALS AND METHODS

5.B.1 Chemicals

Tritiated 1-methyl-4-phenylpyridinium ([^{3}H]MPP$^+$) was purchased from PerkinElmer Life and Analytical Science (Waltham, MA) and unlabeled MPP$^+$ was obtained from Sigma-Aldrich (Saint Louis, MO). Matrine and oxymatrine were purchased from Fisher Scientific (Portland, OR). The chemical structures of matrine and oxymatrine are shown in Figure 5.1. Quinine monohydrochloride dihydrate was purchased from Acros Organics (Fair Lawn, NJ).

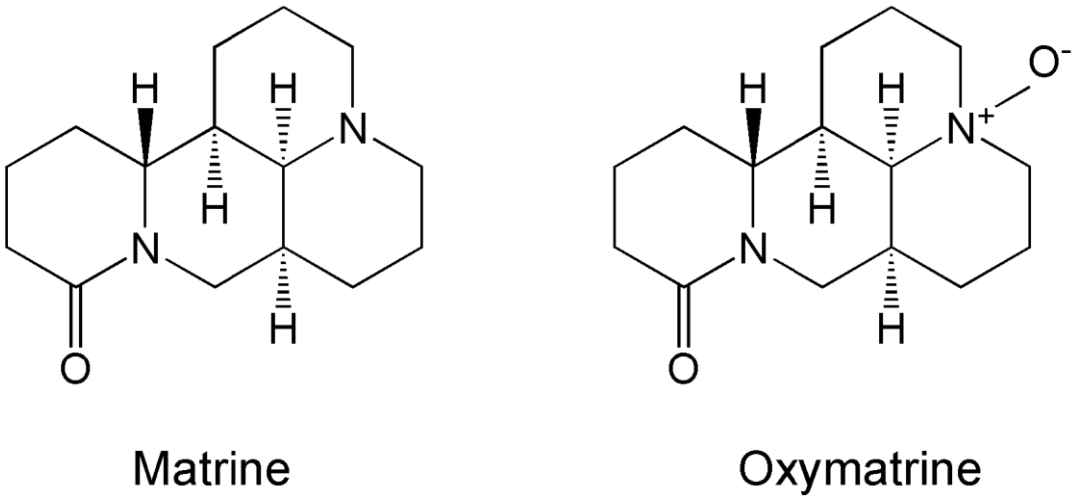

Figure 5.1 Chemical structures of matrine and oxymatrine.

5.B.2 Tissue culture

Derivation of the human embryonic kidney 293 (HEK) cells stably transfected with hOCT1 (HEK-hOCT1), hOCT2 (HEK-hOCT2), hOCT3 (HEK-hOCT3), or the corresponding empty vector (background control), has been described previously [14, 107, 121, 148]. The HEK cell lines were maintained at 37°C with 5% CO_2 in DMEM high glucose media containing 10% serum, 1% Pen/Strep and 600 µg/mL G418.

5.B.3 Cell accumulation assay

The procedure for cell accumulation assay was described previously with minor modification [123]. Briefly, cells were seeded into 24-well tissue culture plates at a density of 2×10^5 cells/well in antibiotics-free medium. After 2 days, the cells were initially equilibrated with transport buffer for 10 min (500 µL of Hanks' balanced salt solution containing 10 mM HEPES, pH 7.4). The cells were then treated with 500 µL of fresh transport buffer containing 1 µM unlabeled substrate spiked with [^{3}H]MPP^+ (0.25 µCi/mL) in the presence or absence of test compounds. At the end of the incubation, the cells were quickly rinsed three times with ice-cold transport buffer and lysed with 1M NaOH. The radioactivity of cell lysate was quantified by liquid scintillation counting, and the uptake profile was normalized by the total protein content determined by the Bradford method. The cellular uptake of substrates was shown as picomoles of substrate per milligram total protein. All uptake data were corrected for background accumulation in corresponding empty vector transfected control cells. Kinetic calculations were performed using GraphPad Prism Software version 5.0 (GraphPad Software Inc., San Diego, CA). The half maximal inhibitory concentration (IC_{50}) was calculated using nonlinear regression with the appropriate model. All experiments were repeated at least three times with triplicate wells for each data point.

5.B.4 Statistical analysis

Data in figures and reported raw uptake scores are expressed as mean ± SD, while IC_{50} estimates are mean ± SEM. Statistical differences were analyzed using one-way ANOVA followed by Dunnett's post-hoc t-test (α=0.05).

5.C RESULTS

5.C.1 Inhibitory effects of matrine and oxymatrine on hOCT1-mediated MPP^+ uptake

Stably transfected hOCT1-expressing (HEK-hOCT1) cells showed marked accumulation of MPP^+ (~42 fold) compared to empty vector transfected background control cells (300 ± 53 vs. 7.1 ± 0.4 pmol/mg protein/15 min, respectively). The known OCT inhibitor, quinine, showed virtually complete inhibition of hOCT1-mediated MPP^+ uptake at 200 µM (>90% inhibition; Figure 5.2A). Matrine and oxymatrine produced 26% and 35% inhibition of hOCT1 transport activity at 100 µM (Figure 5.2A). Subsequently, a dose-response study (1 to 5000 µM) was performed on hOCT1 to derive the IC_{50} value for oxymatrine, which showed a much higher plasma level in patients (68 µM) compared to matrine (8.1 µM) [192, 193]. The IC_{50} value was estimated as 513 ± 132 µM (Figure 5.2B).

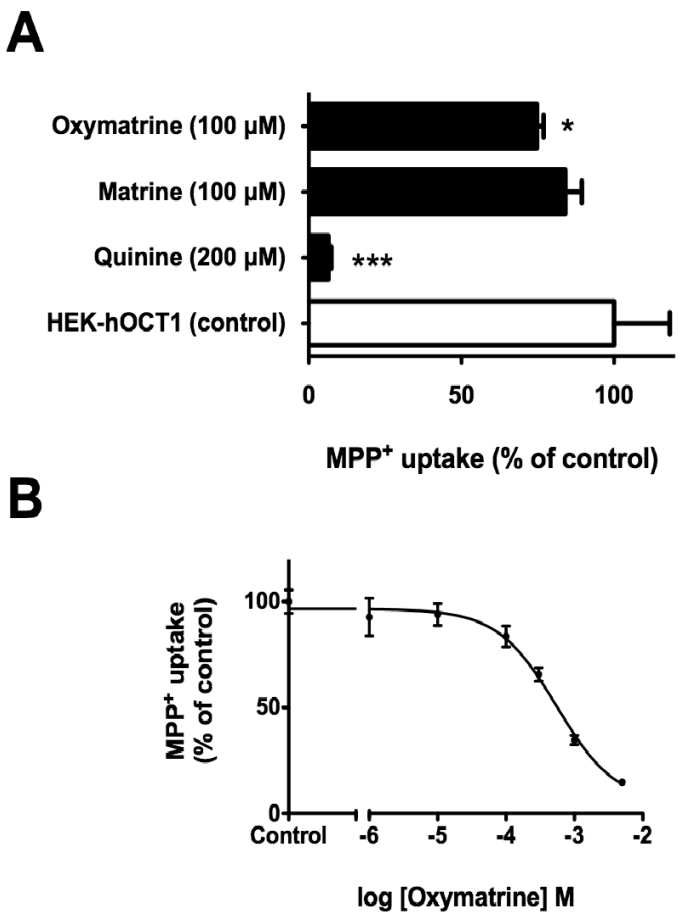

Figure 5.2 Inhibition of hOCT1 by matrine and oxymatrine.

A: Inhibition of hOCT1-mediated MPP^+ (1 µM) uptake by matrine (100 µM), oxymatrine (100 µM) and quinine (200 µM) was assessed at 15 min. Values are mean ± SD of triplicate samples. *** denotes $p < 0.001$ as determined by one-way ANOVA followed by Dunnett's t-test. B: Dose-response curve for oxymatrine on hOCT1. One minute uptake of MPP^+ (1 µM) was measured in HEK-hOCT1 cells in the presence of increasing concentrations of oxymatrine (1×10^{-6} to 5×10^{-3} M). The IC_{50} was estimated using non-linear regression and the "log(inhibitor) vs. response" model (GraphPad Prism). All data were corrected for non-specific background measured in control cells.

5.C.2 Inhibitory effects of matrine and oxymatrine on hOCT2-mediated MPP^+ uptake

Significantly increased cellular accumulation of MPP^+ was observed in stably transfected hOCT2-expressing cells (~21 fold) as compared to background control (empty vector) cells (150 ± 17 vs. 7.1 ± 0.4 pmol/mg protein/15 min, respectively). Similarly, quinine completely blocked (>99%) hOCT2-mediated MPP^+ uptake at 200 µM (Figure 5.3). However, neither of these compounds showed significant inhibition at 100 µM. As a result, further kinetic analysis was not performed.

5.C.3 Inhibitory effects of matrine and oxymatrine on hOCT3-mediated MPP^+ uptake

Like hOCT1 and hOCT2, stably transfected hOCT3-expressing cells exhibited greater MPP^+ uptake (189 ± 27 pmol/mg protein/15 min) than control cells (7.1 ± 0.4 pmol/mg protein/15 min), and this active transport was completely blocked (99%) by quinine at 200 µM (Figure 5.4). Since hOCT3 expressed on the apical side of enterocytes would likely be exposed to higher concentrations of these compounds after oral administration, the inhibitory effects on hOCT3 were investigated at increasing concentration levels. While matrine and oxymatrine each failed to produce significant inhibition on hOCT3 transport activity at 100 µM, marked inhibition was observed at elevated concentrations (Figure 5.4). Oxymatrine showed ~26% and ~42% inhibition at 1 and 3 mM, respectively, suggesting an $IC_{50} \geq 3$ mM (Figure 5.4A). Similarly, matrine showed ~34% and ~88% inhibition on hOCT3 at 1 and 6 mM, respectively, suggesting 1 mM < IC_{50} < 6 mM (Figure 5.4B).

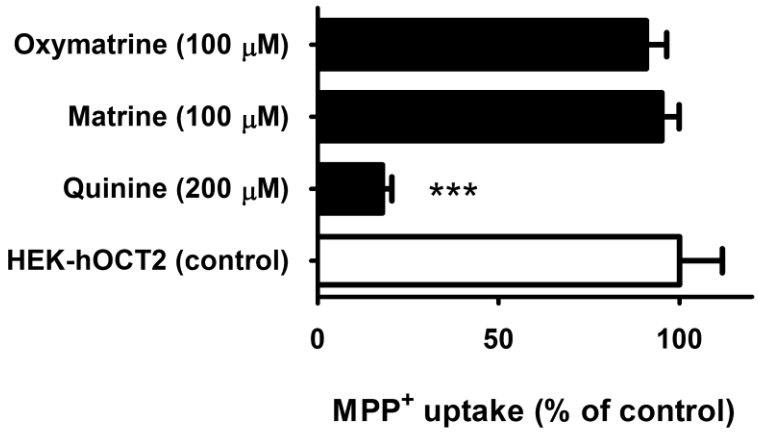

Figure 5.3 Inhibition of hOCT2 by matrine and oxymatrine.

Inhibition of hOCT2-mediated MPP^+ (1 μM) uptake by matrine (100 μM), oxymatrine (100 μM) and quinine (200 μM) was assessed at 15 min. Values are mean ± SD of triplicate samples. Data were corrected for non-specific background measured in control cells.

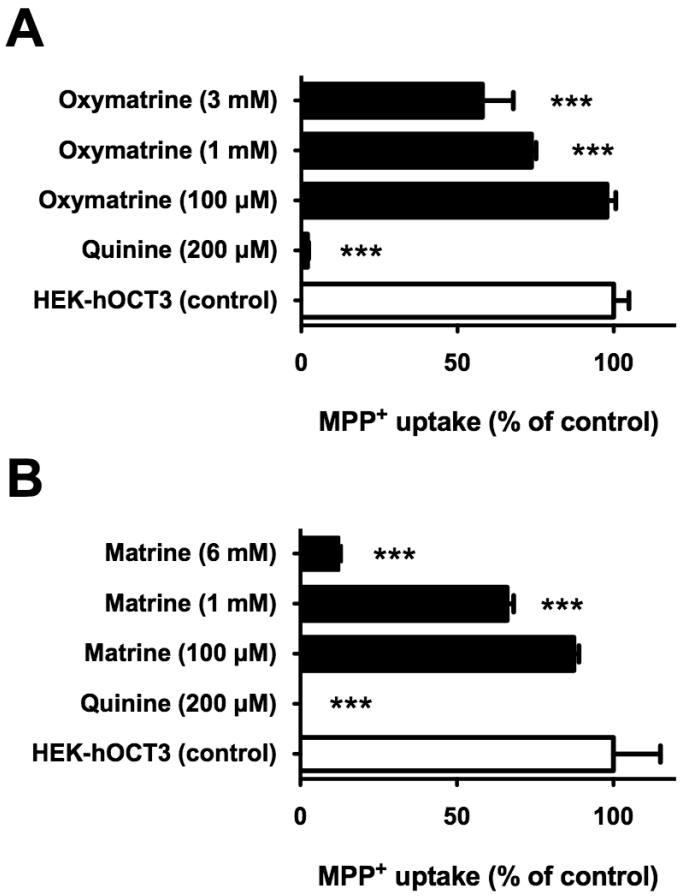

Figure 5.4 Inhibition of hOCT3 by matrine and oxymatrine.

A: Inhibition of hOCT3-mediated MPP^+ (1 µM) uptake by oxymatrine (100 µM, 1 mM and 3 mM) and quinine (200 µM) was assessed at 15 min. B: Inhibition of hOCT3-mediated MPP^+ (1 µM) uptake by matrine (100 µM, 1 mM and 6 mM) and quinine (200 µM) was assessed at 15 min. Data were corrected for non-specific background measured in control cells. Values are mean ± SD of triplicate samples. *** denotes $p < 0.001$ as determined by one-way ANOVA followed by Dunnett's t-test.

5.D DISCUSSION

Herb-drug interactions, which can manifest as impaired drug efficacy and/or enhanced toxicity when patients use natural products and prescribed drugs in combination, have been documented in both pre-clinical and clinical investigations [194]. Increasingly, studies have demonstrated transporter proteins as being the site of drug-drug and botanical-drug interactions [123, 124, 195]. In China, the plant alkaloids matrine and oxymatrine are widely used in clinical therapy due to their broad applications, including the treatment of cancer and viral hepatitis. Therefore, the information on potential DDIs is even more critical for those who suffer from chronic diseases (e.g., HIV and hepatitis C viral infections, cancer) and depend on long-term or even life-time treatment. As OCTs interact with many anti-viral and anti-neoplastic drugs, there is a need to better understand the interaction of OCTs with the botanical alkaloids matrine and oxymatrine.

hOCT1 plays an important role in hepatic and renal secretion and uptake, and inhibition of hOCT1 would potentially impair hepatic metabolism, biliary excretion and renal elimination. A number of antiretroviral drugs, including lamivudine, zalcitabine, pentamidine, and trimethoprim, have been identified as substrates of hOCT1, and oxymatrine and matrine are commonly combined with these drugs during antiviral therapy [163, 196]. In clinical practice, both injectable and oral dosage forms are used. The maximum plasma concentration (C_{max}) was reported as 68 μM after i.v. infusion of 600 mg of oxymatrine [193]. Accordingly, the ratio of C_{max} over IC_{50} (as an indicator of DDI potential) of oxymatrine on hOCT1 was 0.13. While the fraction of plasma protein binding in humans for oxymatrine is unknown, it was reported to be 19% in rats (i.e., 81% exists as the free form) [197]. Assuming similar binding for humans, the DDI index, calculated as unbound C_{max}/IC_{50}, still would be 0.1. Currently, the FDA Guidance for Drug Interaction Studies

suggests that a *DDI index > 0.1 indicates that a* DDI may occur *in vivo* [129]. While hOCT2 is another important transporter involved in renal elimination, the relatively low affinity for matrine and oxymatrine makes it unlikely to be a site for relevant DDIs involving these compounds.

Studies with knockout mice and human tissue have confirmed expression and function of OCT3 in cardiac tissues, although the specific cell type(s) and membrane targeting are still unclear [198, 199]. Regardless, given the plasma levels associated with the clinical use of matrine and oxymatrine, significant DDIs with hOCT3 expressed in the heart are not indicated. In enterocytes, hOCT3 is expressed in the apical membrane and functions as an uptake transporter in the intestinal absorption of cationic drugs. Many *in vivo* studies have demonstrated that inhibition of apical enterocyte uptake transporters resulted in reduced bioavailability of substances handled by these transporters [200]. Both matrine and oxymatrine are water soluble (~100 g/L), therefore, as suggested by the FDA Guidance for Industry regarding the design and analysis of drug interaction studies, the concentration of matrine and oxymatrine in the GI tract after oral administration can be estimated by the ratio of the dose over 250 mL, assuming that patients take their medications with 250 mL of water [129]. According to the oral doses of matrine (400 mg) and oxymatrine (300 mg) reported in clinical studies, the maximum concentration of each could reach 6.5 and 4.5 mM, respectively [192, 201]. Our results showed that matrine and oxymatrine produced 42% and 88% inhibition on hOCT3 transport activity at 3 and 6 mM, respectively, indicating that concentrations of matrine and oxymatrine in the GI tract after oral clinical dosing could be high enough to block hOCT3-mediated intestinal absorption of cationic drugs. Therefore, *in vivo* studies should be conducted to investigate the potential influence of matrine and oxymatrine on the intestinal absorption of co-administered therapeutics that are hOCT3 substrates.

In summary, our findings demonstrated the inhibitory effects of matrine and oxymatrine on hOCTs. Clinically, oxymatrine could interfere with hOCT1-mediated hepatic uptake and renal elimination, and hOCT3-mediated intestinal absorption processes. Matrine only has the potential to block hOCT3 expressed in enterocytes. *In vivo* DDI studies between oxymatrine or matrine and known substrates for hOCT1 and hOCT3 appear necessary in order to establish informed safety guidelines for the development, approval and use of products containing these active alkaloids.

CHAPTER 6

INHIBITION OF HUMAN ORGANIC CATION TRANSPORTERS BY SYNTHETIC CATHINONE ANALOGS ("BATH SALTS")

6.A INTRODUCTION

The abuse of designer drugs 'bath salts' has been an escalating public health crisis in Europe and the United States (US). In 2011, the American Association of Poison Control Center received 6137 calls about exposures to 'bath salts', representing ~20-fold increase from the cases in 2010 (306 calls) [202]. In the United Kingdom, the reports of seizures related to 'bath salt' use increased from less than 10 cases in 2009 to 650 cases in 2010 [203]. The psychoactive components of 'bath salts', including methcathinone, 4-methylmethcathinone (mephedrone), 3,4-methylenedioxymethcathinone (methylone) and 3,4- methylenedioxypyrovalerone (MDPV), are mainly synthetic derivatives of cathinone, a naturally occurring β-ketone analog of amphetamine found in the plant khat (*Catha edulis*). These synthetic cathinones, like other psychostimulants (e.g., amphetamine, methamphetamine, and cocaine), profoundly interact with monoaminergic systems in the central nervous system (CNS). Pharmacological studies have demonstrated that synthetic cathinones increases brain interstitial fluid concentration of some neurotransmitters (e.g. dopamine (DA) and serotonin (5-HT)), via increasing the release and/or inhibiting the uptake of these substances in the CNS, producing various psychoactive effects [204-208]. Evidence of this has been shown *in vivo* with microdialysis studies where mephedrone and methylone rapidly

increased the extracellular levels of DA and serotonin 5-HT in rat brain after subcutaneous (*s.c.*) or intravenous (*i.v.*) administration [204-206]. In addition, long-term serotonergic deficit was observed after repeated mephedrone injection [208]. To better understand the mechanism of action of synthetic cathinones, the interaction of bath salts with monoamine reuptake transporters in the CNS has received considerable interest. Currently, two distinguishable mechanisms of aminergic neurotransmitter clearance in the synapse have been recognized: uptake-1 (high-affinity, low capacity reuptake transporters) and uptake-2 (low-affinity, high capacity reuptake transporters) [91, 92]. Up to now, extensive studies have demonstrated the interaction between synthetic cathinones and uptake-1 transporters, such as dopamine transporter (DAT; SLC6A3), serotonin transporter (SERT; SLC6A4) and norepinephrine transporter (NET; SLC6A2) [206-208]. methcathinone, mephedrone, and methylone have been shown to be non-selective substrates of DAT, SERT and NET, stimulating the transporter-mediated release of monoamine neurotransmitters via reversal of normal transporter flux, while MDPV was demonstrated to be an inhibitor for DAT and NET without any measureable substrate activity [206, 208, 209]. The potential interaction of synthetic cathinones with uptake-2 transporters, including the organic cation transporters (OCTs; SLC22 family), has not been investigated.

OCTs are membrane proteins that interact with a broad variety of cationic and zwitterionic organic molecules [3]. Three OCT subtypes, OCT1 (SLC22A1), OCT2 (SLC22A2) and OCT3 (SLC22A3) are widely expressed in many barrier organs (e.g. liver, kidney and choroid plexus) and *in vivo* mediate the absorption, distribution, and elimination of numerous endogenous and exogenous compounds [3]. Recently, there has been increasing evidence indicating that OCT2/Oct2 and OCT3/Oct3 are widely expressed in different brain regions and actively involved in the CNS aminergic neurotransmitter homeostasis. Firstly, when examined *in vitro* human (h)

OCTs and murine (m) Octs actively transport neurotransmitters such as 5-HT, NE and DA, albeit it with lower affinity (K_m values in higher micromolar range) compared to uptake-1 transporters (K_m values in nanomolar to lower micromolar range) [3, 75, 210-212]. Moreover, *in vivo* intra-hypothalamic perfusion of the OCT inhibitor, decynium-22 (D-22), increased extracellular 5-HT concentrations (2-6.5 fold) in a dose-dependent manner [94]. This increase was comparable to that observed after fluoxetine (an selective serotonin reuptake inhibitor) was administered via the same route [95]. The expression and function of mOct3 in the CNS were significantly increased in SERT knockout mice, indicating that mOct3 may serve as a compensation modulator of neurotransmitters in brain when SERT function is compromised [100, 101]. Furthermore, mOct2 knockout mice displayed reduced tissue concentration of NE and 5-HT in several brain regions (e.g., cortex, hippocampus, and striatum) as compared to wild-type mice [77]. Together, converging lines of evidence lead to the hypothesis that OCTs function as important components of the uptake-2 pathway, and thus may represent an equally important target for psychostimulants such as synthetic cathinone as the uptake-1 pathway.

As low molecular weight compound that are protonated in the physiological environment (pH=7.4), synthetic cathinones have the potential to be substrates and/or inhibitors of OCTs. The aim of the present study was to explore the inhibitory effects of mephedrone, methylone and MDPV on hOCT1-, hOCT2-, and hOCT3-mediated transporter. In addition, since S(-)methcathinone and R(+)methcathinone showed different psychoactive activities [213], the inhibitory effects of each methcathinone enantiomer on hOCT1, hOCT2 and hOCT3 were also investigated. Potent inhibition was further characterized by kinetic investigations to estimate IC_{50} values, which were used to quantitatively evaluate the potential of drug-neurotransmitter

interaction or drug-drug interactions (DDIs) in the CNS and peripheral organs after bath salts consumption.

6.B METHODS

6.B.1 Chemicals

Tritiated 1-methyl-4-phenylpyridinium ([^{3}H]MPP$^+$) was obtained from PerkinElmer Life and Analytical Science (Waltham, MA) and unlabeled MPP$^+$ was purchased from Sigma-Aldrich (Saint Louis, MO). Quinine monohydrochloride dihydrate was obtained from Acros Organics (Fair Lawn, NJ). S(-)methcathinone, R(+)methcathinone, mephedrone, methylone and MDPV were synthesized as previously described [213-216]. The chemical structures of S(-)methcathinone, R(+)methcathinone, mephedrone, methylone and MDPV are shown in Figure 6.1.

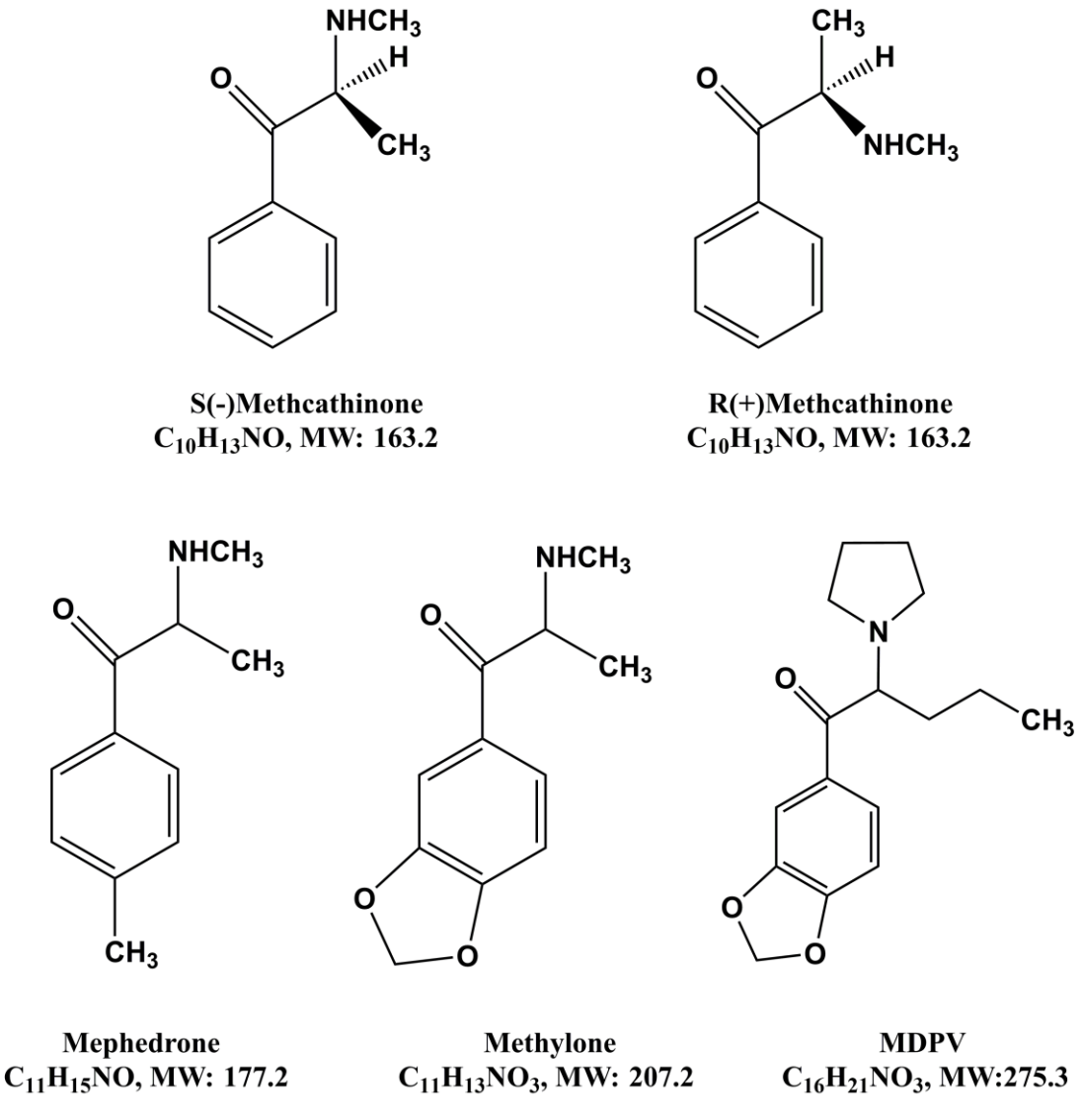

Figure 6.1 Chemical structures of synthetic cathinones.

6.B.2 Tissue culture

Derivation of the human embryonic kidney 293 (HEK) cells stably transfected with hOCT1 (HEK-hOCT1), hOCT2 (HEK-hOCT2), hOCT3 (HEK-hOCT3), as well as the corresponding empty vector transfected cells (background control), has been described previously [14, 148]. The HEK cell lines were maintained in DMEM high glucose media containing 10% of fetal bovine serum and 1% Pen/Strep at 37°C in an atmosphere of 5% CO2. G418 (600 μg/mL) was added to the media for the selection of transfected cells.

6.B.3 Cell accumulation assays

The procedure for cell accumulation assay has been described previously with minor modification [123, 124]. Briefly, 2×10^5 cells/well were seeded in 24-well tissue culture plates in the absence of antibiotics and grown until confluence. Before the cell transport experiment, cells were preincubated in 500 μL transport buffer (Hanks' balanced salt solution containing 10 mM HEPEs, pH 7.4) for 10 min. After equilibration, the transport buffer was replaced with 500 μL of fresh transport buffer containing unlabeled MPP^+ (1 μM) spiked with [^{3}H]MPP^+ (0.25 μCi/mL) in the presence or absence of test compounds. At the end of the incubation, the cells were quickly rinsed three times with ice-cold transport buffer and lysed with 1 M NaOH. The intracellular radioactivity of cell lysate was counted by liquid scintillation and reported as pmol of substrate per milligram total protein. The total protein content of each well was determined by the Bradford method. All uptake data were corrected for background accumulation in corresponding empty vector transfected cells. Kinetic calculations were performed using GraphPad Prism Software version 5.0 (GraphPad Software Inc., San Diego, CA). The half maximal inhibitory concentration (IC_{50}) was calculated using nonlinear regression with the appropriate model. All experiments were repeated at least three times with triplicate wells for each data point.

6.B.4 Statistics

Data in figures and reported raw uptake scores are expressed as mean ± SD, while IC_{50} estimates are mean ± SEM. Statistical differences were analyzed using one-way ANOVA followed by Dunnett's post-hoc t-test (α=0.05).

6.C Results

6.C.1 Inhibitory effects of synthetic cathinones on hOCT1-mediated MPP^+ uptake

Stably transfected HEK-hOCT1 cells demonstrated marked accumulation of MPP^+ (~21 fold) compared to empty vector control cells (43.8 ± 1.0 vs. 2.13 ± 0.2 pmol/mg protein/10 min, respectively; data not shown). The known hOCT1 inhibitor, quinine (200 µM), produce virtually complete inhibition of hOCT1-mediated MPP^+ uptake (>90% inhibition; Figure 6.2). The cell accumulation assay demonstrated that mephedrone, methylone, MDPV, as well as both optical isomers of methcathinone, significantly inhibited hOCT1-mediated MPP^+ transport (>50%) at 100 µM (Figure 6.2). Dose-response studies were performed to estimate the IC_{50} values of synthetic cathinones for hOCT1. Decreased transport activity of hOCT1 was observed in the presence of increasing concentrations of synthetic cathinones (0.01-5000 µM). The IC_{50} values of synthetic cathinones for hOCT1 ranged from 6.5-31.5 µM (Figure 6.3 and Table 6.1). Among five synthetic cathinones, MDPV (IC_{50} = 6.5 ± 1.3 µM) exhibited the lowest IC_{50} for hOCT1, whereas S(-)methcathinone (IC_{50} = 31.5 ± 8.9 µM) showed the highest IC_{50} value for hOCT1. R(+)methcathinone exhibited ~4 fold stronger affinity with hOCT1 than S(-)methcathinone (IC_{50} = 8.4±1.9 µM vs. 31.5 ± 8.9 µM).

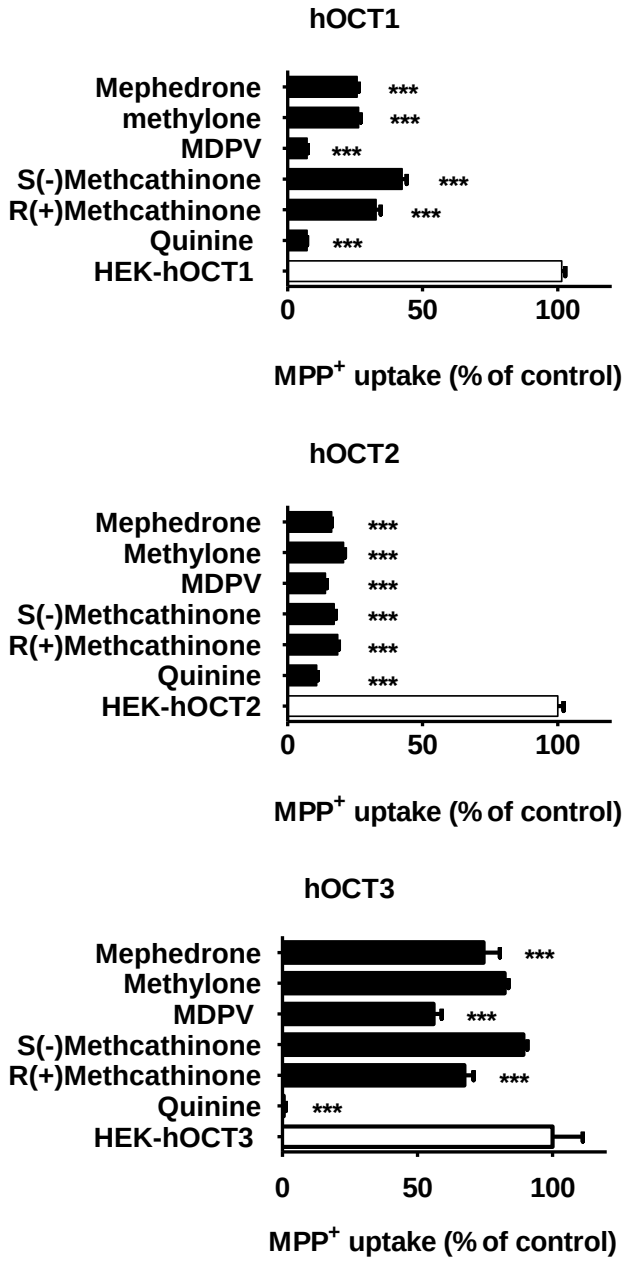

Figure 6.2 Inhibition of hOCT1-, hOCT2 and hOCT3-mediated uptake by synthetic cathinones.

Cellular uptake of [^{3}H]MPP^+ (1 µM, 10 min) was measured in HEK-hOCT1, HEK-hOCT2 and HEK-hOCT3 expressing cells in the absence and presence of synthetic cathinones (100 µM) or quinine (200 µM). All data were corrected for background MPP^+ accumulation measured in corresponding empty vector transfected cells. Values are mean ± S.D. of triplicate values. Significant inhibition denoted by ***$p < 0.001$ as determined by one-way ANOVA followed by Dunnett's t-test.

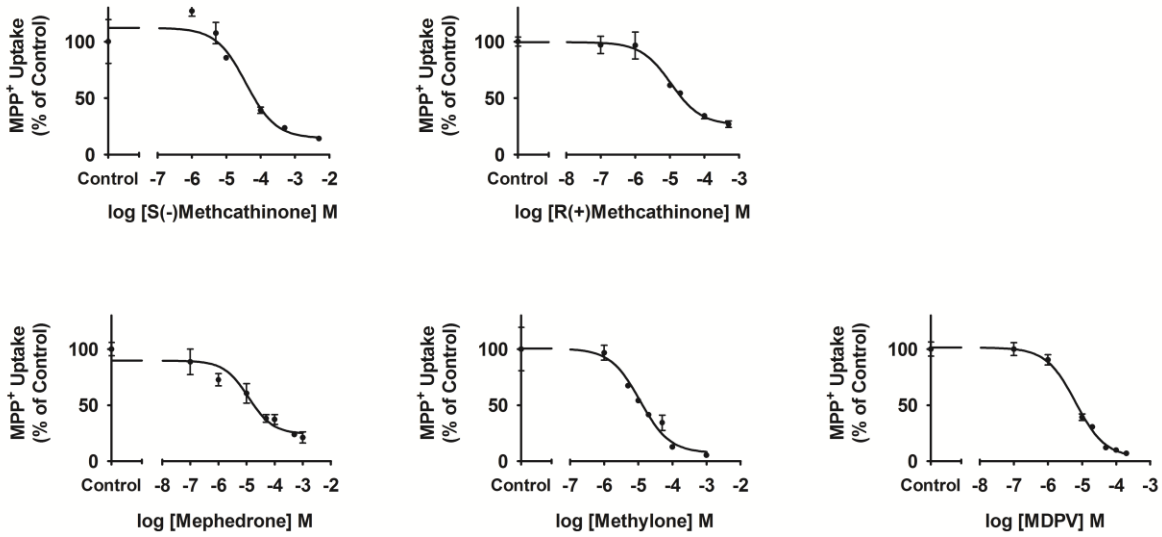

Figure 6.3 Dose–response curves for synthetic cathinones with respect to hOCT1.

One minute uptake of [^{3}H]MPP$^+$ (1 µM) in HEK-hOCT1 cells was measured in the presence of increasing concentrations (10^{-7} to $10^{-2.3}$ M) of test compounds. Data were corrected for non-specific background measured in the corresponding empty vector transfected background control cell. IC_{50} values were determined with nonlinear regression and the "log(inhibitor) vs. response" model. Experiments were repeated three times in triplicate with the mean IC_{50} ± S.E.M. reported in Table 6.1. Graphs shown are from representative experiments with values plotted as mean ± S.D. (n = 3).

6.C.2 Inhibitory effects of synthetic cathinones on hOCT2-mediated MPP^+ uptake

Markedly increased cellular accumulation of MPP^+ was observed in stably transfected HEK-hOCT2 cells (~34 fold) as compared to background control (empty vector) cells (56.7 ± 2.1 vs. 1.5 ± 0.2 pmol/mg protein/10 min, respectively; data not shown). Similarly, quinine completely blocked (>99%) hOCT2-mediated MPP^+ uptake at 200 μM (Figure 6.2). The tested synthetic cathinones (100 μM) produced approximately 80% inhibition on hOCT2-mediated MPP^+ transport (Figure 6.2). Kinetic studies, applying increasing concentrations of test compounds (0.01-5000 μM), were performed to determine the IC_{50} values on hOCT2. S(-)methcathinone demonstrated the lowest IC_{50} value (IC_{50} = 11.9 ± 2.9 μM) for hOCT2, and R(+)methcathinone, mephedrone, methylone, and MDPV showed similar IC_{50} values on hOCT2, ranging from 16.7 to 20.9 μM (Figure 6.4 and Table 6.1).

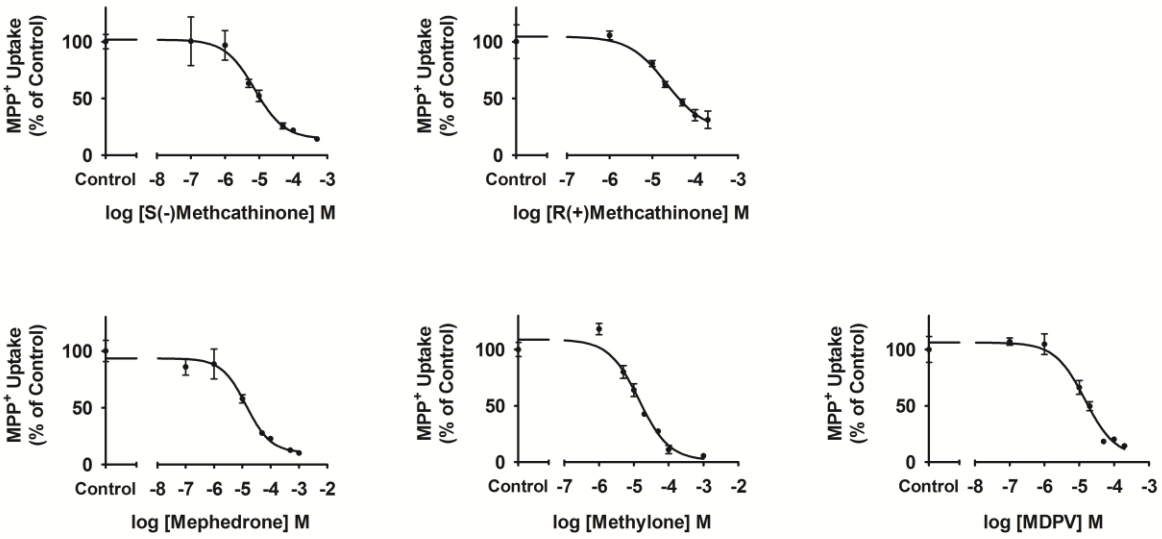

Figure 6.4 Dose–response curves for synthetic cathinones with respect to hOCT2.

One minute uptake of [^{3}H]MPP^+ (1 µM) in HEK-hOCT2 cells was measured in the presence of increasing concentrations (10^{-7} to 10^{-3} M) of test compounds. Data were corrected for non-specific background measured in the corresponding empty vector transfected background control cell. IC_{50} values were determined with nonlinear regression and the "log(inhibitor) vs. response" model. Experiments were repeated three times in triplicate with the mean IC_{50} ± S.E.M. reported in Table 6.1. Graphs shown are from representative experiments with values plotted as mean ± S.D. (n = 3).

6.C.3 Inhibitory effects of synthetic cathinones on hOCT3-mediated MPP^+ uptake

Cellular accumulation of MPP^+ was significantly increased in stably transfected HEK-hOCT3 cells (~21 fold) as compared to background control (empty vector) cells (26.9 ± 2.9 vs. 1.3 ± 0.2 pmol/mg protein/10 min, respectively; data not shown). Inhibition by quinine (200 µM) was complete (>99%; Figure 6.2). R(+)methcathinone, mephedrone and MDPV showed marked inhibitory effects on hOCT3 transport activity at 100 µM, while methylone and S(-)methcathinone failed to produce significant inhibition. Accordingly, further kinetic studies were performed to derive the IC_{50} values for R(+)methcathinone, mephedrone and MDPV (Figure 6.5 and Table 6.1). Estimated IC_{50} values of R(+)methcathinone, mephedrone, and MDPV were 174.0 ± 16.7 µM, 334.7 ± 86.7 µM, 130.5 ± 18.0 µM , respectively.

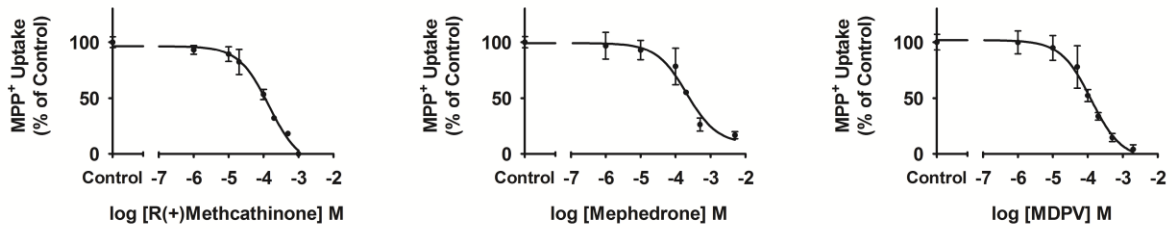

Figure 6.5 Dose–response curves for synthetic cathinones with respect to hOCT3.

One minute uptake of [^{3}H]MPP^+ (1 µM) in HEK-hOCT3 cells was measured in the presence of increasing concentrations (10^{-6} to $10^{-2.3}$ M) of test compounds. Data were corrected for non-specific background measured in the corresponding empty vector transfected background control cell. IC_{50} values were determined with nonlinear regression and the "log(inhibitor) vs. response" model. Experiments were repeated three times in triplicate with the mean IC_{50} ± S.E.M. reported in Table 6.1. Graphs shown are from representative experiments with values plotted as mean ± S.D. (n = 3).

Table 6.1 Estimated IC_{50} (μM) and inhibitory potency of synthetic cathinone for hOCT1, hOCT2 and hOCT3.

Compounds	IC_{50} (μM)			f_u[a] (%)	C[b] (μM)	C_{brain}[c] (μM)	Brain (% inhibition)		Heart (% inhibition)	Liver and kidney (DDI index)[d]		
	hOCT1	hOCT2	hOCT3				hOCT2	hOCT3	hOCT3	hOCT1	hOCT2	hOCT3
Mephedrone	8.6 ± 2.2	18.8 ± 2.7	334.7 ± 86.7	78.4 %	0.7-124.2[f]	0.6-99.4	84%	23%	35%	20.6	9.4	0.5
Methylone	11.5 ± 1.1	20.9 ± 3.4	>> 100	70%	0.3-5.4[f]	0.2-4.3	17%	ND[h]	ND	0.6	0.3	< 0.1
MDPV	6.5 ± 1.3	16.7 ± 1.2	130.5 ± 18.0	?[e]	2.3[f]	0.1-3.3	17%	2%	< 3%	0.5	0.2	< 0.1
S(-)methcathinone	31.5 ± 8.9	11.9 ± 2.9	>> 100	?	3.1[g]	4.5	27%	ND	ND	< 0.1	0.2	< 0.1
R(+)methcathinone	8.4 ± 1.9	20.4 ± 4.5	174.0 ± 16.7	?	3.1[g]	4.5	18%	3%	< 2%	0.3	0.1	< 0.1

Values are reported as mean ± S.E.M.

[a] f_u, fraction unbound in plasma.

[b] Clinical drug concentrations in blood or serum were reported from [217-223].

[c] Brain concentration of mephedrone as reported in [217, 221]. Brain concentrations of methylone, MDPV, S(-)methcathinone and R(+)methcathinone were estimated based on brain to blood concentration ratio.

[d] Drug-drug Interaction index is defined as the unbound concentration of drug divided by the drug IC_{50} for the transporter of interest. A DDI index value > 0.1 is thought to indicate the potential for clinically relevant DDIs

[e] ?, unknown and assume the plasma protein binding is 70%.

[f] blood concentration.

[g] serum concentration.

[h] ND, not determined.

6.D Discussion

The abuse of synthetic cathinones has exhibited a dramatic increase in the US and Europe over the last decade, which brings serious public health concerns. However, there is limited understanding about the mechanism of action of these notorious compounds. Even though numerous studies have demonstrated that synthetic cathinones regulate extracellular concentration of DA and 5-HT via uptake-1 transporters, DAT, SERT, and NET, exerting psychoactive effects [206-208], the influence from other pathways, including those that involve uptake-2 transporters, might be also important. Given the increasing evidence showing the expression of OCTs in astrocytes and cerebellum granule neurons in cerebellum, subfornical organ, dorsal raphe, hypothalamic nuclei, cortex and hippocampus regions in brain [77, 78, 82, 224-226], and their active role in the regulation of neurotransmitter homeostasis, it is necessary to investigate the interaction of synthetic cathinones with hOCTs.

In the present study, all tested synthetic cathinones were found to be potent inhibitors for hOCTs. Specifically, three commonly identified synthetic cathinones, mephedrone, methylone, and MDPV, demonstrated stronger inhibitory effects on hOCT1 and hOCT2 as compared to hOCT3. In addition, methcathinone isomers exerted unique patterns of interaction with hOCTs. The IC_{50} value of S(-)methcathinone for hOCT1 is ~4 fold higher (poorer affinity) than R(+)methcathinone, whereas the IC_{50} value of R(+)methcathinone for hOCT2 is ~2 fold higher (poorer affinity) than S(-)methcathinone. Similar to hOCT2, R(+)methcathinone, rather than S(-)methcathinone, showed significant inhibitory effects on hOCT3, albeit with the poorest affinity (~174 μM).

In order to estimate the inhibitory effects of synthetic cathinones for organic cation transporters in the CNS, it is important to know the brain concentration of these compounds [227].

As the brain concentration of MDPV was reported as 0.1-3.3 μM in postmortem cases [217, 221], the maximum possible inhibition on hOCT2 in the brain would be 17%, while such inhibitory effects on hOCT3 is low (<3%). In addition, the blood concentration of mephedrone and methylone were 0.7-124.2 μM [218, 219, 222] and 0.3-5.4 μM [217, 218], respectively. Even though the brain concentration of the two compounds is not available, as brain to blood concentration ratio of MDPV was 0.8 [228], we assumed that these cathinone derivatives obtained similar partitioning between blood and brain. As the consequence, mephedrone was predicted to produce maximally 84% and 23% inhibition on hOCT2 and hOCT3, respectively, while methylone is less likely to cause significant inhibition of hOCT2 and hOCT3 (~17% and less than 4% on hOCT2 and hOCT3, respectively). Therefore, inhibition of hOCT2 and hOCT3 in the CNS by synthetic cathinones could very well result in increase in extracellular monoamine levels and possibly cause psychoactive effects [77, 95, 208].

In mice, S(-)methcathinone was about 3-5 times more potent than R(+)methcathinone locomotor activity tests and training effects [213, 229]. The discriminative central stimulant effects of these methcathinone optical isomers may be, at least partially, due to their differing affinities for OCTs/Octs. Perhaps indicating a greater role for OCTs as this transporter exhibited stronger interactions than OCT1 or 3 with S(-)methcathinone. The fact that hOCT2 preferentially interacts with S(-)methcathinone might contribute to differing pharmacological effects of these two compounds.

In addition to the psychoactive effect, cardiovascular complications (e.g. sinus tachycardia, palpitations and hypertension) are very common among ‘bath salts’ abusers [230, 231]. The cardiovascular syndromes are often associated with reduced cardiac extraction of NE from the plasma to heart [232-234], which might at least partially, be attributed to OCTs which are also

expressed in capillary and vascular endothelial cells of the heart [15, 199]. Indeed, O-methyl-isoprenaline, the selective hOCT3 inhibitor, abolished concentration difference of NE between the interstitial space and vascular bed in rat heart [235, 236]. In the present study, the IC_{50} values of mephedrone, MDPV and R(+)methcathinone on hOCT3 were 334.7 ± 86.7 µM, 130.5 ± 18.0 µM and 174.0 ± 16.7 µM, respectively. Based on the reported clinical blood concentration of mephedrone (124.2 µM) [218, 219, 222], the plasma protein binding (21.6%) [237] and assuming 55% plasma to blood ratio [237], mephedrone is predicted to inhibit 35% transport activity for hOCT3.

OCTs also play an important role in biliary and renal elimination. hOCT1 and hOCT3 are expressed in the sinusoidal membrane of hepatocytes and represent the first step in the hepatic uptake of many substances, while hOCT2 and hOCT3 are expressed on the basolateral side of proximal tubular cells in the kidney [3]. Clinical studies have demonstrated that impairment of transport function of OCTs might alter the pharmacokinetic properties of other drugs that are substrates for OCTs such as metformin and morphine [105, 166, 238]. The Food and Drug Administration recommends using DDI index (ratio of unbound C_{max} to K_i or IC_{50}) to estimate the drug-drug interaction potency [129], and DDI index > 0.1 indicates the significant DDI potential *in vivo*. As shown in Table 6.1, these compounds demonstrated DDI index greater than 0.1 at least for one hOCT subtype, and mephedrone showed much higher DDI index (>9) on hOCT1 and hOCT2. These results suggested that synthetic cathinones have a great potential to inhibit hOCTs, rendering reduced hOCT1- and hOCT2- mediated renal tubular secretion and biliary elimination. Interaction of hOCT3 was not predicted to result in any potentially significant DDIs. Forensic studies have reported that synthetic cathinone abusers are also likely to simultaneously take heroin, cocaine and morphine [217]. Morphine is an opioid analgesic as well as a major metabolite of

heroin and cocaine [238]. A previous study has demonstrated that morphine was a substrate of hOCT1 and the plasma concentrations of morphine in healthy volunteers were significantly affected by hOCT1 polymorphisms [238]. Therefore, combination use of synthetic cathinones and morphine, heroin or cocaine may increase the plasma concentration of morphine to the lethal range. Indeed, toxicological studies demonstrated that toxicity and rate of fatality were significantly amplified when 'bath salts' were combined with abused drugs [239-241].

In summary, our findings demonstrated that mephedrone, methylone, MDPV, S(-)methcathinone and R(+)methcathinone are inhibitors for hOCT1, hOCT2 and hOCT3. These finding suggest that the psychoactive effects of synthetic cathinones might be due to their inhibitory effects on hOCT2 and hOCT3 that modulate neurotransmitters reuptake in the CNS. In addition, the inhibition of hOCT3 by synthetic cathinone, interferes with NE reuptake in cardiac endothelial cells and could potentially cause cardiovascular complications. Finally, synthetic cathinones showed significant DDI potential on hOCT1 and hOCT2, which might explain the enhanced toxicities when bath salts were combined with other abused drugs such as codeine, morphine and heroin. The role of OCTs in the biological effects of synthetic cathinones as well as elucidating their *in vivo* DDI potential would be important future studies to conduct to provide increased insight in completing the full mechanistic picture.

CHAPTER 7

THERAPEUTIC POTENTIAL OF NOVEL ORGANIC CATION TRANSPORTER (OCT; SLC22 FAMILY) INHIBITORS IN DEPRESSION

7.A INTRODUCTION

Depressive disorder is among the most serious and burdensome psychiatric illnesses in the world. Currently, approximately 17% of the US population suffers from depression and it generates about 60 billion dollars in medical costs annually in the US [242]. Although numerous classes of psychoactive drugs are used in the treatment of depression, undesirable side effects and delayed onset of action are often observed in clinical applications [243, 244]. In addition, current antidepressant treatment fails to produce beneficial effects in nearly 50% of the patient population [243, 245-247].

Depression is often associated with a reduction of monoaminergic neurotransmitters such as serotonin (5-HT) and/or norepinephrine (NE) in the synaptic clefts [92, 246]. Currently, most antidepressants are thought to exert their pharmacological effects via blocking uptake-1, the high affinity, low capacity reuptake system, i.e., serotonin transporter (SERT) and norepinephrine transporter (NET). For example, the most prevalent antidepressants on the market, selective serotonin reuptake inhibitors (SSRIs, e.g., fluoxetine and sertraline) and selective serotonin and norepinephrine reuptake inhibitors (SNRIs, e.g, venlafaxine and duloxetine), target SERT and/or NET. However, there is also a second low-affinity, high capacity clearance pathway for biogenic

amines, uptake-2. Increasing evidence has indicated that organic cation transporter 2 (OCT2) and 3 (OCT3), which are widely expressed in the CNS, interact with dopamine (DA), 5-HT and NE and likely represent an important component of the uptake-2 pathway, playing a role in the regulation of CNS neurotransmitter homeostasis [92]. For example, intra-hypothalamic perfusion of the OCT inhibitor, decynium-22, dose-dependently increased extracellular 5-HT concentrations by approximately 2-6.5 fold [94], which was comparable to the action of fluoxetine (~4 fold) *via* the same route of administration [95]. Furthermore, the expression and function of murine (m)Oct3 in the CNS was significantly increased in SERT knockout mice, indicating that mOct3 may be an important modulator of neurotransmitters in brain when SERT function is compromised [100, 101]. Therefore, OCTs may represent unrecognized targets of known antidepressants and may impact their pharmacological action.

Recently, a series of quinazolines and guanidines were developed as potential novel therapeutic agents for depression in the laboratory of Dr. Dukat [248, 249]. The experimentally determined logP value for KEO-099 was 1.86, suggesting a favorable ability to penetrate the blood-brain barrier [248, 249]. In the murine tail suspension test (TST) model, acute administration of KEO-099 *via* intraperitoneal injection significantly decreased total time immobile relative to the saline group, suggesting a decrease in depression-related behavior in the KEO-099 treatment group [248]. Further studies suggested that these compounds may not produce inhibition of uptake-1, since their binding affinities for SERT and NET were greater than 10 μM (Dr. Dukat laboratory, unpublished data). Quinazolines and guanidines are low molecular weight compounds and, based on their chemical structures, are protonated in the physiological environment. Thus, they might be OCT substrates or inhibitors and potentially possess antidepressant-like activities. To better understand the pharmacological action and mechanism of action of these compounds, we

examined the interaction of quinazolines with human (h)OCT1-3 and mOct1-3, to elucidate if OCTs are contributing to the pharmacological action of these compounds. Median effective dose (ED_{50}) values of lead compounds were characterized for their *in vivo* CNS effects in mice by TST. Finally, a hOCT3 3-D homology model was constructed and docking studies were performed on selected compounds to better understand the interaction between hOCT3 and its substrates or inhibitors.

7.B MATERIALS AND METHODS

7.B.1 Chemicals

Tritiated MPP^+ ($[^3H]MPP^+$) and 5-hydroxytryptamine ($[^3H]$ 5-HT) were purchased from PerkinElmer Life and Analytical Science (Waltham, MA). Unlabeled MPP^+, serotonin hydrochloride and imipramine hydrochloride was obtained from Sigma-Aldrich (Saint Louis, MO). Quinine monohydrochloride dihydrate was purchased from Acros Organics (Fair Lawn, NJ). Saline solution (0.9% sodium chloride) was purchased from Baxter, Inc. (Deerfield, IL). The seven quinazolines (GSW-286, KEO-093, KEO-099, OIA-008, KAI-333, MDA-049 and KAI-302) and six guanidines (KAI-323, MD-354, MDA-057, MDA-058, KAI-325 and KAI-324) were synthesized and provided by Dr. Dukat laboratory. Details of synthetic routes are not provided at this time. The chemical structures and physiochemical properties of quinazolines and guanidines were determined by SYBYL-X version 2.1 (Table 7.1).

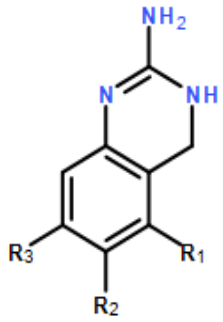

Quinazolines

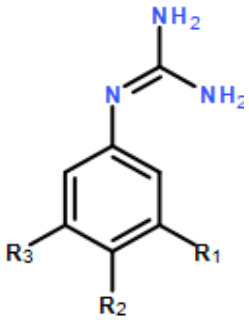

Guanidines

Categories	Compounds	R_1	R_2	R_3	MW	pK_a[a]	cLogP[a]	Rotatable Bonds[a]
Quinazolines	GSW-286	H	H	H	148.2	9.9	0.5	0
	KEO-093	H	H	Cl	182.6	9.1	1.2	0
	KEO-099	H	Cl	H	181.6	9.2	1.2	0
	OIA-008	Cl	H	H	182.6	9.2	1.2	0
	KAI-333	H	F	H	167.2	9.4	-0.3	0
	MDA-049	H	CH_3	H	162.2	9.8	1.0	0
	KAI-302	CH_3	H	H	163.2	9.8	1.0	0
Guanidines	KAI-323	H	H	H	136.2	10.9	-0.1	1
	MD-354	Cl	H	H	170.6	10.2	0.6	1
	MDA-057	H	Cl	H	169.6	10.2	0.6	1
	MDA-058	H	CH_3	H	150.2	10.8	0.4	1
	KAI-325	H	$C(CH)_3$	H	192.3	10.5	1.8	1
	KAI-324	H	$CH_2C_6H_5$	H	226.3	9.5	2.0	3

Table 7.1 Physicochemical properties of quinazolines and guanidines.
[a] Values determined by SYBYL-X version 2.1.

7.B.2 Tissue Culture

Stably transfected human embryonic kidney 293 (HEK) cells expressing hOCT1 (HEK-hOCT1), hOCT2 (HEK-hOCT2) hOCT3 (HEK-hOCT3), mOct1 (HEK-mOct1), mOct2 (HEK-mOct2), or mOct3 (HEK-mOct3), as well as their corresponding empty vector transfected background control cell lines, were maintained at 37ºC with 5% CO_2 in DMEM high glucose media containing 10% serum and 1% Pen/Strep as described previously [14, 148, 250].

7.B.3 Cell accumulation assays

Cells were seeded into 24-well tissue culture plates at a density of 2×10^5 cells/well (without antibiotics) for 48 hours. On the day of the experiment, cells were preincubated in 500 µL transport buffer for 10 min and treated with unlabeled MPP^+ (1 µM) spiked with [^{3}H]MPP^+ (0.25 µCi/mL) or unlabeled 5-HT spiked with [^{3}H]serotonin (0.25 µCi/mL) in the presence of increasing concentrations (0.01 to 200 µM) of unlabeled test compounds for the times indicated. The radioactivity of cell lysate was quantified by liquid scintillation counting and normalized by total protein content in each well. Data were corrected for non-specific background in corresponding empty vector transfected cells. The half maximal inhibitory concentration (IC_{50}) was calculated using nonlinear regression and the "log(inhibitor) vs. response" model using GraphPad Prism Software version 5.0 (GraphPad Software Inc., San Diego, CA). Substrate accumulation was reported as picomoles of substrate per milligram protein. Substrate concentration and accumulation time used for kinetic analysis of hOCT1, hOCT2, hOCT3, mOct1, mOct2 and mOct3 (1 µM for MPP^+ 1 min) were determined previously [3, 107]. The time-course profile for hOCT2-mediated 5-HT accumulation was determined in this study. Experiments were repeated at least three times in triplicate and the results were reported as $IC_{50} \pm$ SEM. Data in figures and reported

raw uptake scores were expressed as mean ± SD. Statistical differences were assessed using one-way ANOVA followed by Dunnett's t-test (α=0.05) for multiple *post-hoc* comparisons.

7.B.4 Mode of inhibition for lead compounds

The mode of inhibition of lead compounds was identified by mixed-model inhibition analysis in stably transfected hOCT2 and hOCT3 expressing cells, respectively. The following equations were used to assess the mode of inhibition:

$$V_{max}^{app} = \frac{V_{max}}{(1 + [I]/(\alpha \times k_i))}$$

$$K_m^{app} = K_m \frac{1 + [I]/k_i}{(1 + [I]/(\alpha \times k_i))}$$

$$Y = \frac{V_{max}^{app} \times [S]}{K_m^{app} + [S]}$$

where V_{max} is the maximum transport velocity in the absence of the inhibitor; K_m is the Michaelis-Menten constant for the substrate; k_i is the inhibition constant estimated from data set under analysis; Y is the substrate uptake rate observed in the experiment; S and I are the concentration of substrate and inhibitor, respectively. The mode of inhibition is determined by the parameter α: if α value is greater than 1, it indicates competitive inhibition. Otherwise, it indicates the mode of inhibition is noncompetitive (α = 1) or uncompetitive (0< α < 1).

In this study, the mode of inhibition experiments were performed under three independent conditions: no inhibitor, plus two different inhibitor concentrations. MPP^+ uptake mediated by hOCT2 and hOCT3 in the presence and absence of selected inhibitors was plotted as a function of substrate concentration. All the data were corrected for background substrate accumulation in

empty vector control cells. Non-linear regression was used to fit the data into the equations shown above using GraphPad Prism Software version 5.0 (GraphPad Software Inc., San Diego, CA). The parameter, α, was used to determine the mode of inhibition for a representative compound.

7.B.5. Mouse behavior assessment

Male wild-type ICR mice (age 8 to 12 weeks) were purchased from Charles River Laboratories. Animals were maintained in temperature (25^{o}C) and humidity-controlled (50–60%) rooms in groups of 4 – 5 with free access to food and water under a 12h/12h light/dark cycle.

The TST were performed following the protocol of Steru et al and Yoshikawa et al with minor modifications [251, 252]. Briefly, mice were acclimated to the laboratory environment for 3 hours before the experiment. Thirty minutes after intraperitoneal injection of saline or drug, the mice were individually suspended 60 cm above the laboratory bench by fixing their tails with adhesive tape to an acrylic bar. In dose-response studies, the wild-type mice received an intraperitoneal injection of a series of increasing doses of test compounds (0.1, 0.3, 1.0, 3.0, 10 and 30 mg/kg). Saline, imipramine (20 mg/kg) and KEO-099 were used as controls. All behavioral experiments were performed blindly. The mice were filmed for 6 min and the recordings were stored for future analysis. Each recording was viewed three times and immobility time was scored (sec), providing a mean score for each animal. Tukey's interquartile range was used to identify outliers in the dataset. Statistical differences were assessed using one-way ANOVA followed by Dunnett's t-test (α=0.05) for multiple post-hoc comparisons.

7.B.6 hOCT3 homology modeling and docking studies

hOCT3 homology models were constructed based on a comprehensive amino acid sequence alignment of hOCT3 with *Piriformospora indica* high affinity phosphate transporter (PiPT, access number A8N031) [253-255]. The crystal structure of PiPT (PDB id 4J05) is currently recommended best template for OCTs [254]. The crystalized PiPT (resolution of 2.9 Å) was in an inward-facing occluded state with a bound phosphate in the membrane buried binding site [253]. The amino acid sequence alignment was performed using Clustal X. The homology model for hOCT3 was built using MODELLER (University of California at San Francisco, San Francisco, CA). MPP^+ and 5 quinazolines (GSW-286, KEO-093, KEO-099, OIA-008 and MDA-049) were docked to the hOCT3 model using GOLD Suite (version 5.2). GOLD's default scoring function was used to score the ligand binding modes, and potential key amino acid residues were identified by analyzing the binding interaction energies. hOCT3 homology modeling and docking studies were done in collaborated with Dr. Dukat laboratory and Kavita Iyer.

7.C Results

7.C.1 Initial screening of quinazolines and guanidines as OCT inhibitors

The inhibitory effects of quinazolines and guanidines were initially screened on three hOCTs and their murine orthologs using [^{3}H]MPP^+ as a prototypical substrate. Stably transfected hOCT1-expressing (HEK-hOCT1) cells showed marked accumulation of MPP^+ (~33 fold) compared to empty vector transfected background control cells (139.8 ± 9.2 vs. 3.5 ± 0.1 pmol/mg protein/10 min, respectively; data not shown). HEK-mOct1 cells exhibited ~38.5 fold accumulation of MPP^+ as compared to empty vector transfected background control cells (100.0 ± 8.2 vs. 2.6 ± 0.5 pmol/mg protein/10 min, respectively; data not shown). The known OCT inhibitor, quinine (200 µM), showed virtually complete inhibition of hOCT1- and mOct1-mediated

MPP^+ uptake (>90% inhibition; Figure 7.1 A and B). The cell accumulation assay demonstrated that all test compounds (100 µM) except KAI-324 significantly inhibited hOCT1 activity (Figure 7.1 A). In HEK-mOct1 cells, KEO-093, KEO-099, OIA-008, KAI-333, KAI-302, KAI-325 and KAI-324, each significantly inhibited mOct1 at 100 µM, while GSW-286, KAI-323, MD-354, MDA-057 and MDA-058 appeared to stimulate mOct1 transport activity and MDA-049 was without effect (Figure 7.1 B).

The inhibitory effect of quinazolines and guanidines on hOCT2- and mOct2-mediated transport were examined next. Cellular accumulation of MPP^+ was significantly increased in stably transfected hOCT2-expressing cells (~23 fold) as compared to background control (empty vector) cells (91.5 ± 5.7 vs. 3.9 ± 0.1 pmol/mg protein/10 min, respectively; data not shown). HEK-mOct2 cells exhibited significantly higher accumulation of MPP^+ (~23.7 fold) as compared to empty vector transfected background control cells (92.5 ± 1.3 vs. 3.9 ± 0.1 pmol/mg protein/10 min, respectively; data not shown). Quinine (200 µM) blocked (>85%) hOCT2- and mOct2-mediated MPP^+ uptake (Figure 7.1 C and D). Similar to hOCT1, significant inhibition of hOCT2-mediated MPP^+ transport was observed for all quinazolines and guanidines at 100 µM (Figure 7.1 C). All compounds except KAI-323 and MD-354 significantly inhibited mOct2-mediated MPP^+ uptake (Figure 7.1 D).

Stably transfected hOCT3-expressing (HEK-hOCT3) cells showed accumulation of MPP^+ ~30 fold greater than empty vector transfected background control cells (80.7 ± 8.1 *vs.* 4.4 ± 0.2 pmol/mg protein/10 min; data not shown). Active transport was completely (95%) blocked by quinine at 200 µM and all quinazolines and guanidines at 100 µM (Figure 7.1 E and F). HEK-mOct3 cells exhibited significantly higher accumulation of MPP^+ (~23.7 fold) as compared to empty vector transfected background control cells (47.0 ± 3.6 vs. 1.2 ± 0.2 pmol/mg protein/10

min, respectively; data not shown). Marked inhibition of mOct3-mediated MPP^+ transport by quinine was observed (Figure 7.1 F). In contrast to hOCT3, while all quinazolines significantly inhibited mOct3-mediated MPP^+ uptake, only two guanidines, KAI-324 and KAI-325, significantly inhibited mOct3-mediated MPP^+ uptake (Figure 7.1 F).

7.C.2 Determination of IC_{50} values for quinazolines and guanidines

Dose-response studies were conducted to estimate the IC_{50} values of quinazolines and guanidines for hOCT1, hOCT2 and hOCT3, as well as their murine orthologs (Figure 7.2, Table 7.2). The IC_{50} values of quinazolines for hOCT1 were in the low micromolar range (1.3 µM to 14.3 µM). The IC_{50} value of unsubstituted quinazoline GSW-286 for hOCT1 was estimated as 14.3 ± 2.2 µM, which is 2-11 fold higher than substituted quinazolines (KEO-093, KEO-099, OIA-008, KAI-333, MDA-049 and KAI-302). In addition, the IC_{50} values of six guanidines for hOCT1 ranged from 0.9 µM to 761.9 µM. The IC_{50} value of unsubstituted guanidine KAI-323 for hOCT1 was estimated as 41.1 ± 14.4 µM, which is 3 fold greater than unsubstituted quinazoline GSW-286. Similar to quinazolines, the IC_{50} values of unsubstituted guanidine KAI-323 for hOCT1 were 3–46 fold higher than some substituted guanidines including MDA-057, MD-354, MDA-058 and KAI-325. However, the IC_{50} value for benzyl substituted guanidine KAI-324 was determined as 761.9 ± 254.7 µM, which was 19 fold greater than that for unsubstituted guanidine KAI-323. Species differences were observed between hOCT1 and mOct1. In general, lower inhibitory effects of quinazolines and guanidines were observed for mOct1 (greater IC_{50} values) as compared to hOCT1 (Table 7.2).

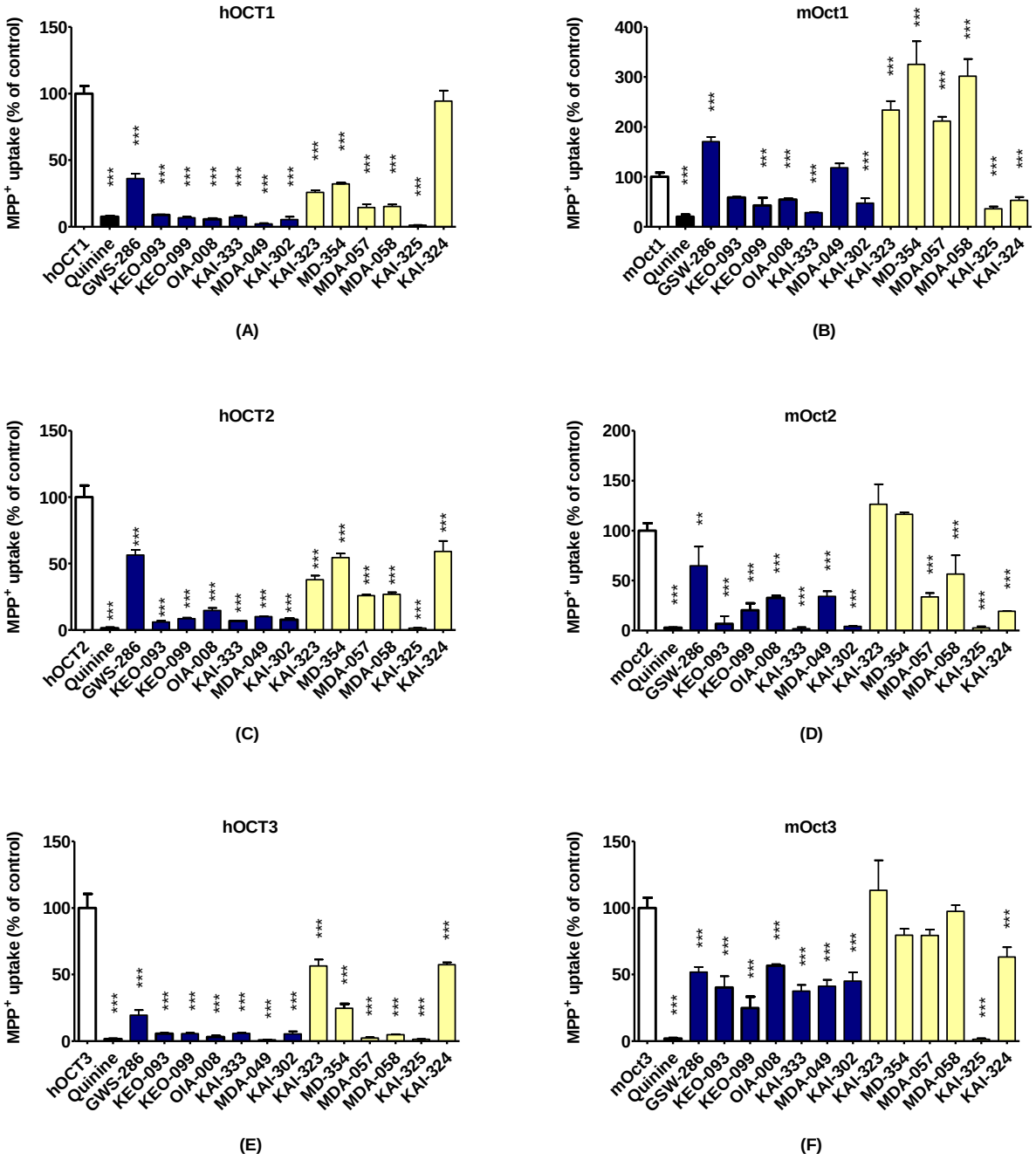

Figure 7.1 Inhibition profiles of quinazolines and guanidines on OCTs.

Inhibition of (A) hOCT1-, (B) mOct1-, (C) hOCT2-, (D) mOct2-, (E) hOCT3- and (F) mOct3-mediated MPP^+ uptake by quinazolines (blue, 100 μM), guanidines (yellow, 100 μM) and quinine (black, 200 μM). The concentration of MPP^+ was 1 μM, incubation time was 10 min, and data shown were corrected for non-specific background. Values are mean ± SD of triplicate values. *** denotes $p < 0.001$ as determined by one-way ANOVA followed by Dunnett's t-test.

The IC_{50} values of substituted quinazolines (KEO-093, KEO-099, OIA-008, KAI-333, MDA-049 and KAI-302) for hOCT2 ranged from 9.0-26.4 µM, which are lower (higher affinity) than that for unsubstituted quinazoline GSW-286 (46.5 ± 0.6 µM). Similarly, chloride, methyl and t-butyl substituted guanidines (MDA-057, MDA-058 and KAI-325) exhibited 1.5-10 fold lower IC_{50} values for hOCT2 than that for unsubstituted guanidine KAI-323 (89.0 ± 12.2 µM). However, benzyl substituted guanidine KAI-324 was not significantly different from unsubstituted guanidine KAI-323. In addition, it was also observed that unsubstituted quinazoline GSW-286 has a lower IC_{50} value for hOCT2 than unsubstituted guanidine KAI-323. The IC_{50} values of the quinazolines and guanidines for hOCT2 were similar to that for mOct2 (Table 7.2). The IC_{50} values of KAI-323 and MD-354 for mOct2 were not determined since they failed to show significant inhibition on mOct2 during the initial screening.

Dose-response studies for hOCT3 and mOct3 indicated that unsubstituted quinazoline GSW-286 exhibited 2-26 fold higher IC_{50} values for hOCT3 than substituted quinazolines KEO-093, KEO-099, OIA-008, KAI-333, MDA-049 and KAI-302. In particular, OIA-008, KAI-333 and KAI-302 demonstrated highest affinity for hOCT3 among all test compounds with IC_{50} values in the nanomolar range. In addition, the IC_{50} value for unsubstituted guanidine KAI-323 was approximately 8 fold greater than that for unsubstituted quinazoline GSW-286 (99.8 ± 2.8 µM vs. 12.2 ± 1.9 µM). Benzyl substituted guanidine KAI-324 exhibited the lowest IC_{50} value for hOCT3 among all test compounds. Species differences were also observed between hOCT3 and mOct3 cells. KEO-093, KEO-099, OIA-008, KAI-333, MDA-049, KAI-302 and KAI-325 demonstrated 3-120 fold lower IC_{50} values for hOCT3 than that for mOct3.

With the notable exception of KAI-324, all other test quinazolines showed preferential affinity for hOCT1 and hOCT3 as compared to hOCT2. In general, chloride, fluoride, methyl and

t-butyl substituted quinazolines and guanidines demonstrated decreased IC_{50} values (higher affinity) for hOCT1, hOCT2 and hOCT3, while benzyl substituted guanidine exhibited a higher IC_{50} values (poorer affinity) for hOCT1 and hOCT3.

Table 7.2 IC_{50} values of test compounds for hOCT1, hOCT2, hOCT3 and their murine orthologs.

	Compounds	IC_{50}[a] (μM)					
		hOCT1	**hOCT2**	**hOCT3**	**mOct1**	**mOct2**	**mOct3**
Quinazolines	GSW-286	14.3 ± 2.2	46.5 ± 0.6	12.2 ± 1.9	ND[b]	31.8 ± 1.3	18.8 ± 2.3
	KEO-093	4.8 ± 0.7	9.0 ± 1.2	5.9 ± 2.3	38.2 ± 9.3	6.2 ± 0.5	15.9 ± 3.1
	KEO-099	3.0 ± 0.5	16.4 ± 2.7	3.9 ± 1.4	40.7 ± 13.7	13.0 ± 0.8	30.3 ± 13.0
	OIA-008	2.3 ± 0.5	13.3 ± 4.0	0.9 ± 0.1	45.2 ± 9.4	16.1 ± 5.5	13.9 ± 1.4
	KAI-333	1.3 ± 0.1	11.9 ± 0.2	0.47 ± 0.01	92.8 ± 1.1	19.2 ± 5.4	19.3 ± 4.3
	MDA-049	8.2 ± 2.2	12.1 ± 0.3	2.0 ± 0.4	ND	15.0 ± 0.5	12.7 ± 2.4
	KAI-302	4.6 ± 0.6	26.4 ± 0.7	0.46 ± 0.02	69.2 ± 2.6	50.7 ± 7.5	56.3 ± 14.6
Guanidines	KAI-323	41.1 ± 14.4	89.0 ± 12.2	99.8 ± 2.8	ND	ND	ND
	MDA-057	10.0 ± 0.6	18.9 ± 0.1	2.8 ± 0.7	ND	14.2 ± 0.4	ND
	MD-354	13.7 ± 0.8	60.5 ± 4.1	7.6 ± 0.7	ND	ND	ND
	MDA-058	10.0 ± 0.2	9.3 ± 4.8	4.6 ± 1.1	ND	22.1 ± 2.4	ND
	KAI-325	0.9 ± 0.2	8.3 ± 3.9	2.2 ± 0.2	18.3 ± 1.0	5.0 ± 1.0	46.0 ± 2.1
	KAI-324	762 ± 255	96.2 ± 8.0	452.5 ± 87.9	82.0 ± 0.9	92.5 ± 4.3	492 ± 128

[a] IC_{50} values were expressed as mean ± SEM from triplicate determinations.

[b] ND, not determined.

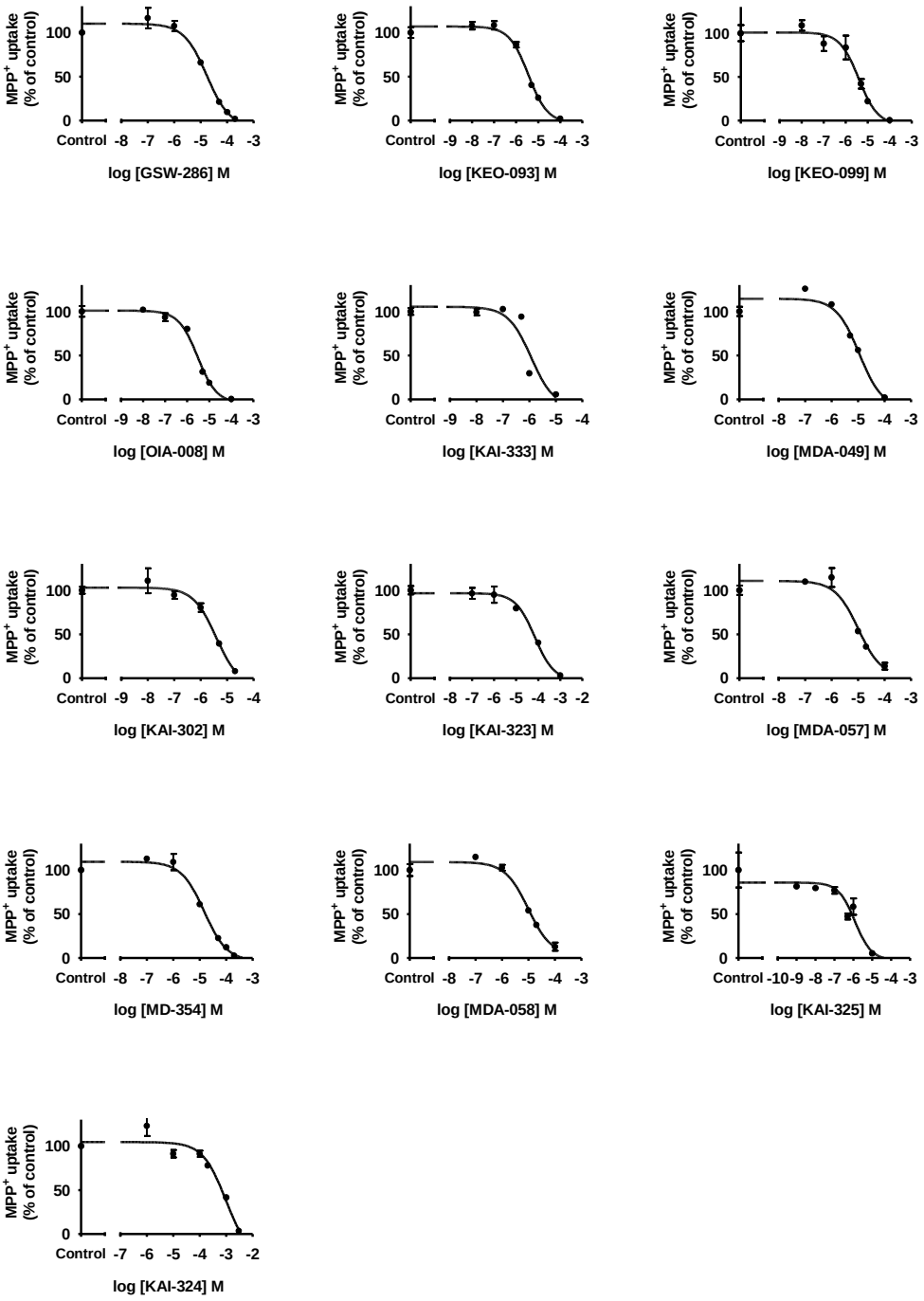

Figure 7.2 (A) Dose-response curves for quinazolines and guanidines on hOCT1.

Representative data showing 1 min uptake of MPP^+ (1 μM) measured in HEK-hOCT1 cells in the presence of increasing concentrations of quinazolines and guanidines (10^{-9} to 10^{-3} M) are shown. Data were corrected for nonspecific background measured in the empty vector control cells and are means ± SD of triplicate values. IC_{50} values were determined with nonlinear regression and the "log(inhibitor) versus response" model using GraphPad Prism software.

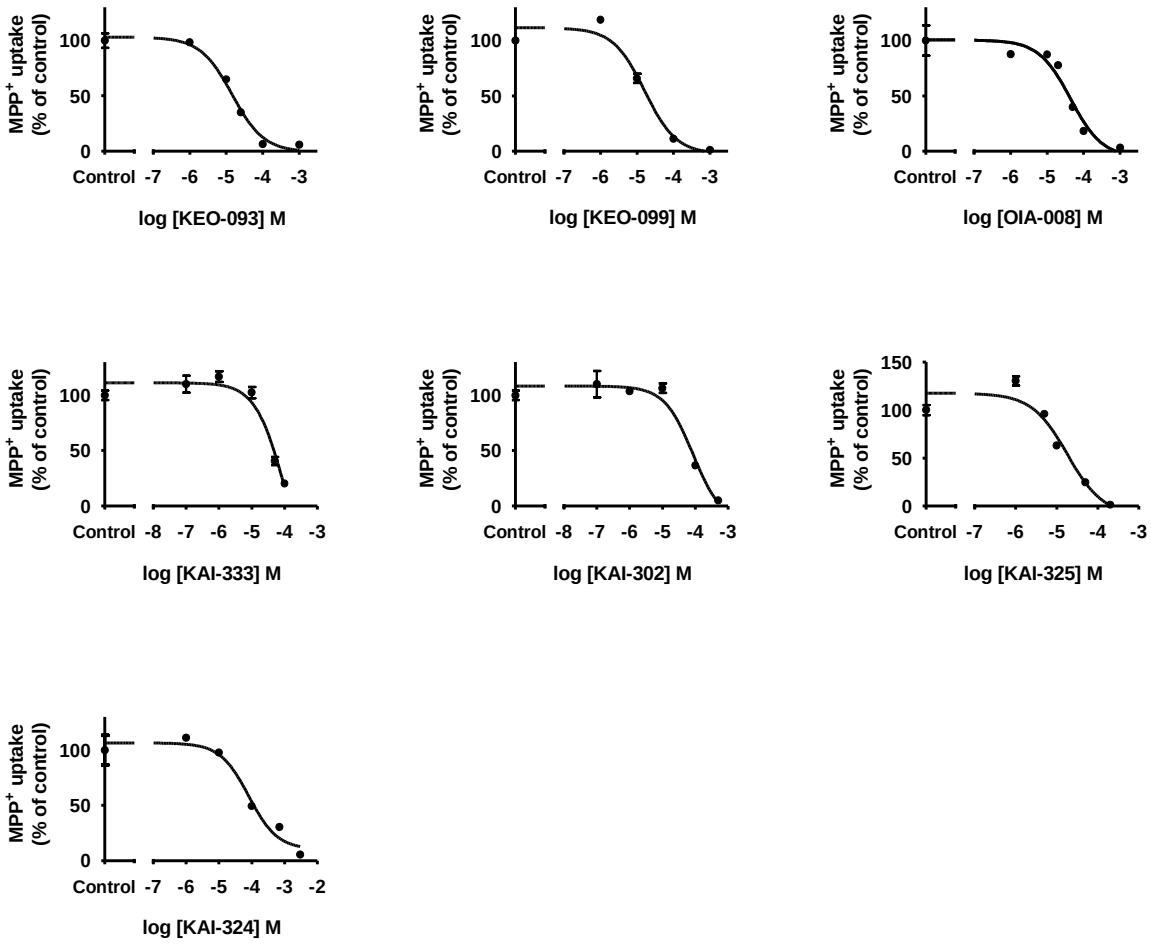

Figure 7.2 (B) Dose-response curves for quinazolines and guanidines on mOct1.

Representative data showing 1 min uptake of MPP^+ (1 μM) measured in HEK-mOct1 cells in the presence of increasing concentrations of quinazolines and guanidines (10^{-7} to $10^{-2.7}$ M) are shown. Data were corrected for nonspecific background measured in the empty vector control cells and are means ± SD of triplicate values. IC_{50} values were determined with nonlinear regression and the "log(inhibitor) versus response" model using GraphPad Prism software.

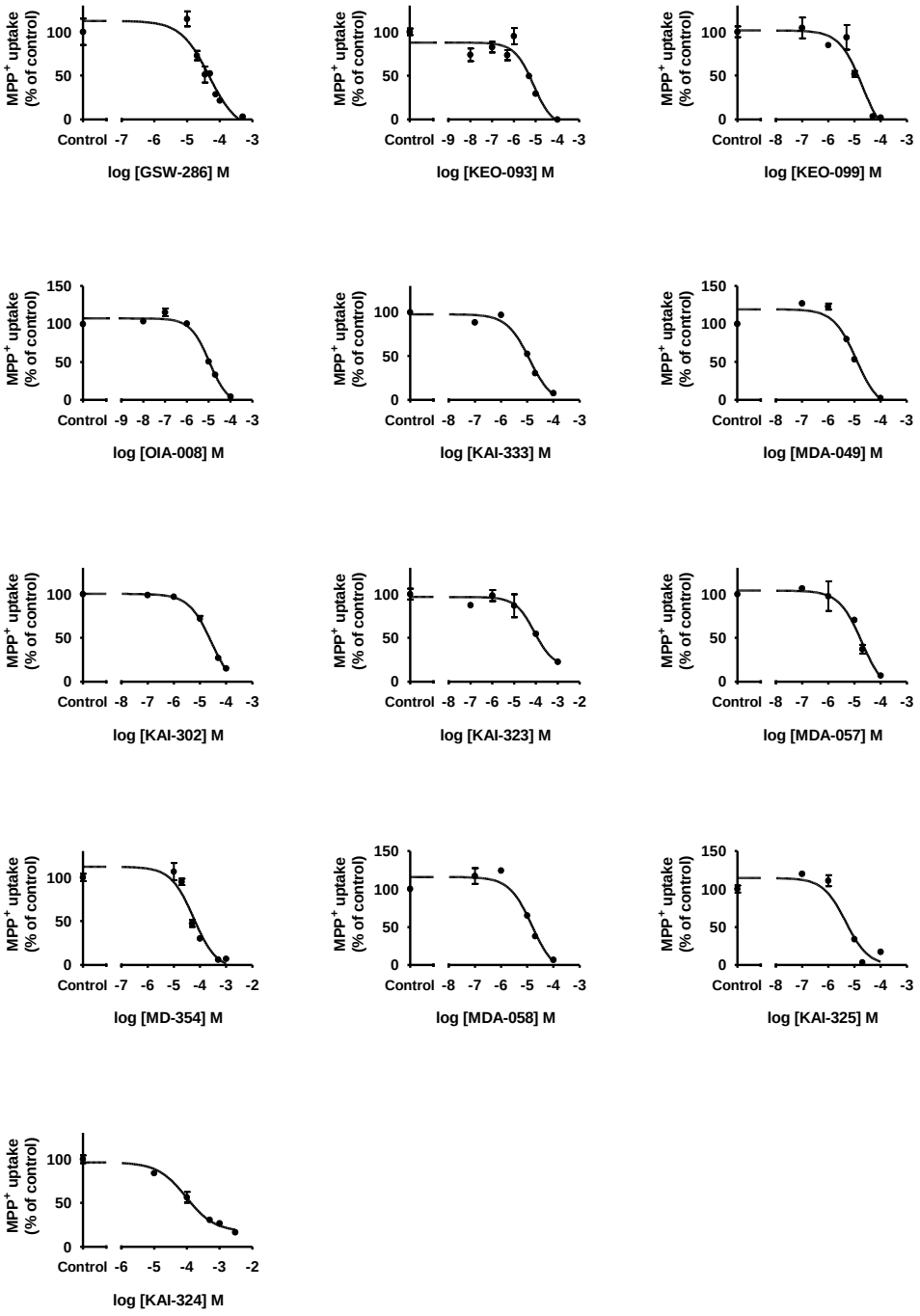

Figure 7.2 (C) Dose-response curves for quinazolines and guanidines on hOCT2.

Representative data showing 1 min uptake of MPP^+ (1 μM) measured in HEK-hOCT2 cells in the presence of increasing concentrations of quinazolines and guanidines (10^{-8} to $10^{-2.3}$ M) are shown. Data were corrected for nonspecific background measured in the empty vector control cells and are means ± SD of triplicate values. IC_{50} values were determined with nonlinear regression and the "log(inhibitor) versus response" model using GraphPad Prism software.

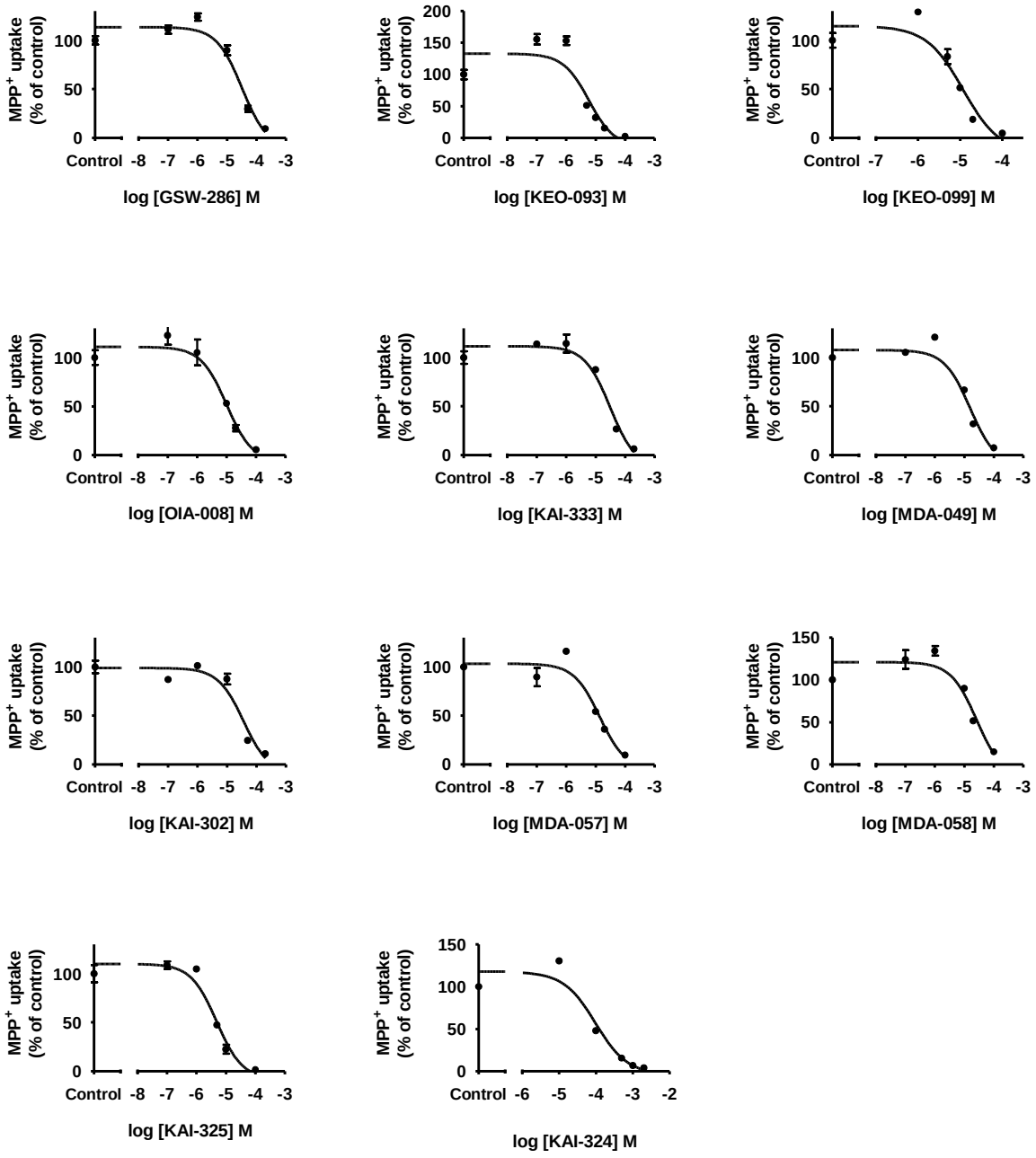

Figure 7.2 (D) Dose-response curves for quinazolines and guanidines on mOct2.

Representative data showing 1 min uptake of MPP^+ (1 μM) measured in HEK-mOct2 cells in the presence of increasing concentrations of quinazolines and guanidines (10^{-7} to $10^{-2.7}$ M) are shown. Data were corrected for nonspecific background measured in the empty vector control cells and are means ± SD of triplicate values. IC_{50} values were determined with nonlinear regression and the "log(inhibitor) versus response" model using GraphPad Prism software.

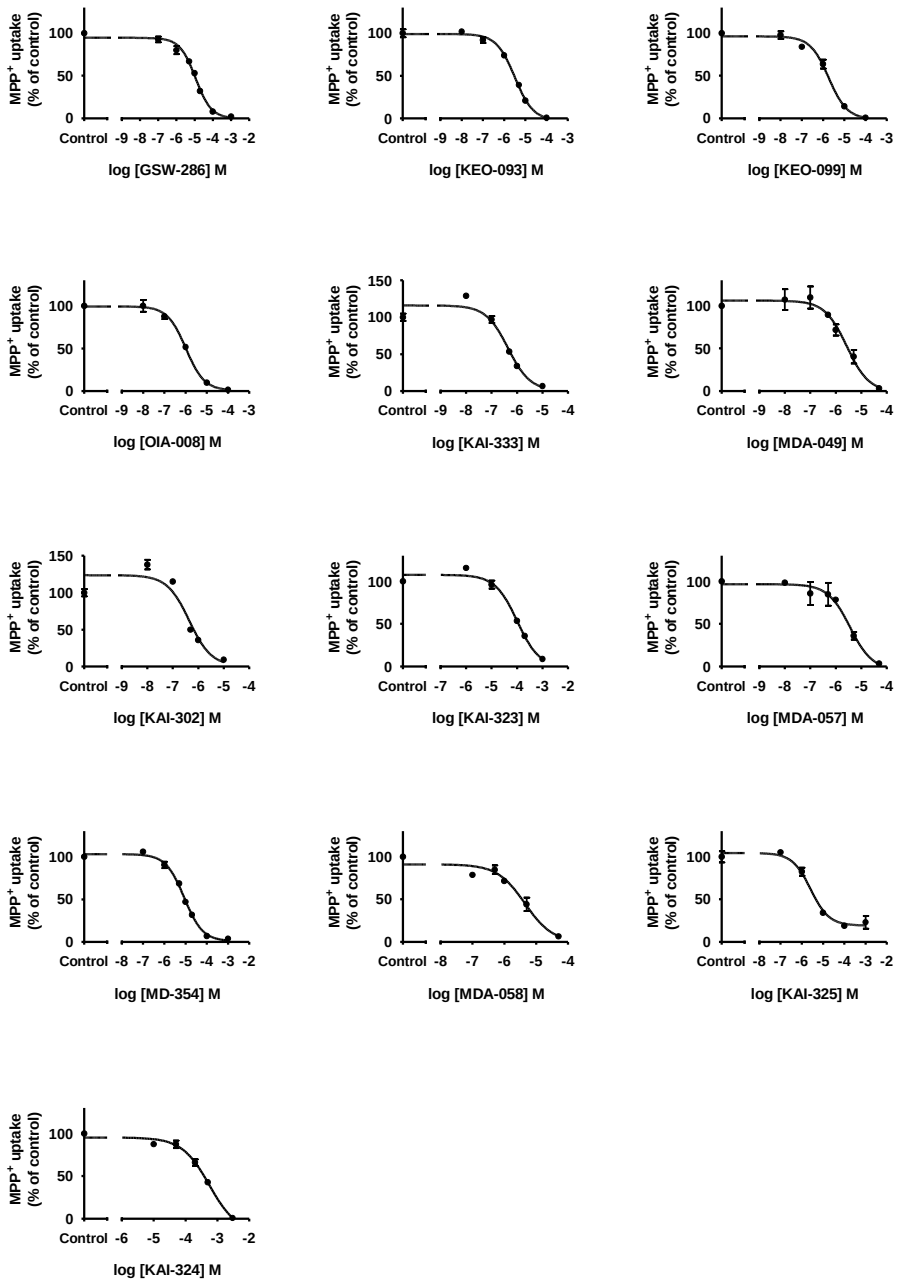

Figure 7.2 (E) Dose-response curves for quinazolines and guanidines on hOCT3.

Representative data showing 1 min uptake of MPP^+ (1 μM) measured in HEK-hOCT3 cells in the presence of increasing concentrations of quinazolines and guanidines (10^{-8} to $10^{-2.7}$ M) are shown. Data were corrected for nonspecific background measured in the empty vector control cells and are means ± SD of triplicate values. IC_{50} values were determined with nonlinear regression and the "log(inhibitor) versus response" model using GraphPad Prism software.

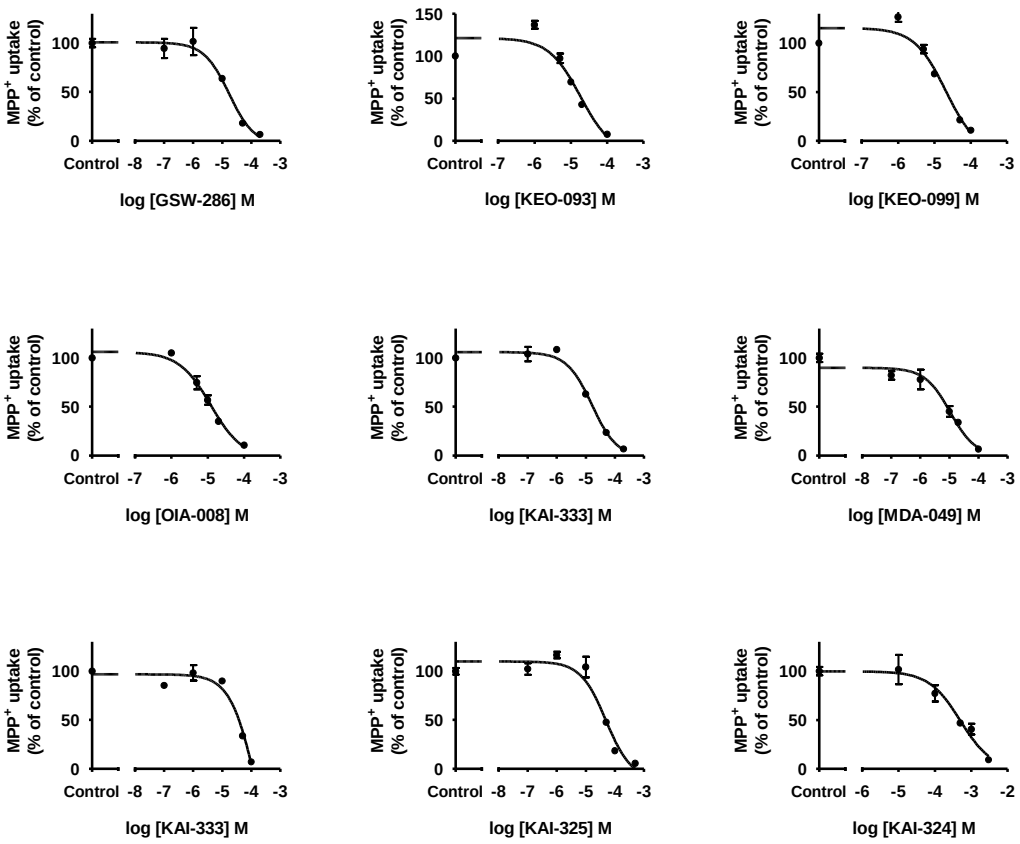

Figure 7.2 (F) Dose-response curves for quinazolines and guanidines on mOct3.

Representative data showing 1 min uptake of MPP^+ (1 μM) measured in HEK-mOct3 cells in the presence of increasing concentrations of quinazolines and guanidines (10^{-7} to $10^{-2.7}$ M) are shown. Data were corrected for nonspecific background measured in the empty vector control cells and are means ± SD of triplicate values. IC_{50} values were determined with nonlinear regression and the "log(inhibitor) versus response" model using GraphPad Prism software.

7.C.3 Inhibition potencies of KEO-099 for hOCT2-mediated 5-HT uptake

The inhibitory effect of KEO-099 on transport activity of hOCT2 was further assessed using 5-HT as the substrate. Time-course studies were performed to assess the initial rate period for hOCT2-mediated 5-HT uptake. The initial phase was defined as the period where uptake rate increased linearly with time. The results demonstrated that hOCT2-mediated uptake was linear for at least the first 5 min (Figure 7.3), therefore a 3 min incubation time was used in all kinetic studies. Dose-response studies were performed to determine the K_m value of 5-HT for hOCT2. Increased 5-HT accumulation in hOCT2-expressing cells was observed in the presence of increasing concentrations of substrate (Figure 7.3). The curve was fit to the Michaelis-Menten equation, and the estimated K_m value for 5-HT on hOCT2 was 227 ± 4 µM.

The inhibitory effect of KEO-099 on monoamine uptake mediated by hOCT2 was then evaluated using [^{3}H]serotonin. Quinine (200 µM) and KEO-099 (100 µM) significantly inhibited hOCT2-meidated 5-HT uptake (Figure 7.4 A). In the presence of increasing concentrations of KEO-099 (0.01-1000 µM), decreased transport activity for hOCT2 was observed (Figure 7.4 B). The IC_{50} value of KEO-099 for hOCT2 was estimated as 0.56 ± 0.08 µM, respectively.

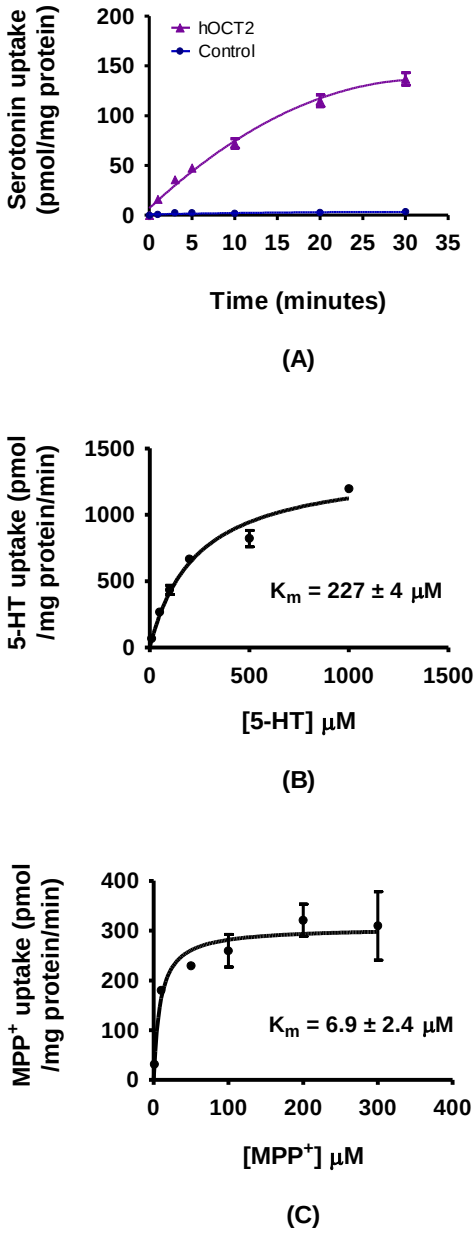

Figure 7.3 hOCT2-mediated 5-HT and MPP^+ uptake.

(A) Time-dependent uptake of 5-HT by hOCT2. Time-dependent experiments were conducted for up to 30 min. The concentration of 5-HT was 1 µM. (B) Michaelis-Menten kinetics of 5-HT transport in hOCT2 cells. The concentration of 5-HT was 1 µM, and the uptake was measured for 3 min at room temperature. (C) Michaelis-Menten kinetics of MPP^+ transport in hOCT2 cells. The concentration of MPP^+ was 1 µM, and the uptake was measured for 1 min at room temperature. Substrate uptake was background corrected by subtracting the non-specific uptake as measured in the HEK-empty vector cells. The Michaelis constant (K_m) value was calculated by nonlinear regression using the Michaelis-Menten model.

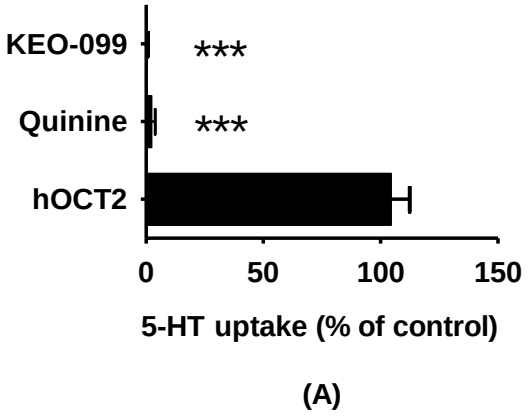

(A)

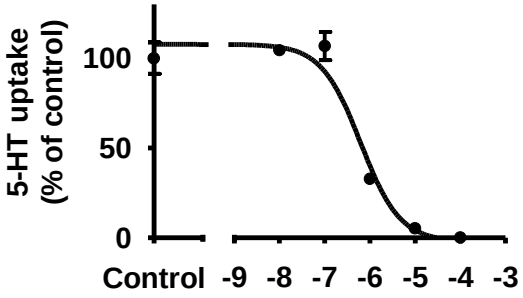

(B)

Figure 7.4 Inhibition of hOCT2-mediated 5-HT uptake by KEO-099.

(A) Inhibition of hOCT2-mediated 5-HT uptake by KEO-099 (100 μM) and quinine (200 μM). The concentration of 5-HT was 1 μM, incubation time was 10 min, and data shown were corrected for non-specific background. *** denotes $p < 0.001$ as determined by one-way ANOVA followed by Dunnett's t-test. (B) Dose-response curve for KEO-099 on hOCT2. Representative data showing 3 min uptake of 5-HT (1 μM) measured in hOCT2 cells in the presence of increasing concentrations of KEO-099 (10^{-8} to 10^{-4} M) are shown. Data were corrected for nonspecific background measured in the empty vector control cells and are means ± SD of triplicate values. IC_{50} values were determined with nonlinear regression and the "log(inhibitor) versus response" model using GraphPad Prism software.

7.C.4 Mode of inhibition for hOCT2 and hOCT3

To properly interpret the inhibition and subsequent modeling and quantitative structure activity relationship (QSAR) study data, the mode of inhibition between OCT substrate and the inhibiting quinazoline and guanidine compounds must be determined. MPP^+ accumulation was linear for at least 1 min and the K_m values were determined as 6.9 µM and 32.1 µM for hOCT2 and hOCT3, which are comparable to the reported values in the literature [3]. Therefore, saturation analysis studies were performed for hOCT2 and hOCT3 in the absence and presence of two different concentrations of representative quinazoline (KEO-099) and guanidine (MDA-057 and KAI-325) compounds. Substrate uptake curves were fit to the equations for mixed-model inhibition, and α values were calculated for each compound. All estimated α values were greater than 1, indicating that KEO-099, MDA-057 and KAI-325 were competitive inhibitors of hOCT2- and hOCT3-mediated transport (Table 7.3).

Table 7.3 Estimated α values from mixed-model inhibition analysis.

Compound	hOCT2	hOCT3
KEO-099	24.6	25.1
MDA-057	34.0	23.0
KAI-325	7.8	17.5
Quinine	6.5	3.9

7.C.5 Mouse behavior studies

Three compounds, KEO-099, GSW-286 and MDA-057, were selected as lead compounds based on *in vitro* data. The ED_{50} value for KEO-099 was determined as 0.23 mg/kg previously [248]. In this study, imipramine (20 mg/kg) significantly decreased the total time spent immobile during 6 min measurement in the TST as compared to the saline group (57.6 ± 7.5 seconds vs 6.9 ± 2.9 seconds, Figure 7.5). The antidepressant-like activity for KEO-099 was confirmed, as KEO-099 (1 mg/kg) significantly reduced the total time spent immobile to 2.8 ± 0.8 seconds. However, unsubstituted quinazoline GSW-286 (0.1 – 30 mg/kg) did not produce a significant decrease in the total time immobile during the TST as compared to the saline group (Figure 7.5). Although the chloride substituted guanidine MDA-057 decreased the total time spent immobile in the TST at 3 mg/kg (57.63 ± 7.52 vs. 24.0 ± 8.5), no statistical differences were observed in the ANOVA test due to the large experimental error. The other doses of MDA-057 did not significantly change the total time spent immobile in the TST (Figure 7.5).

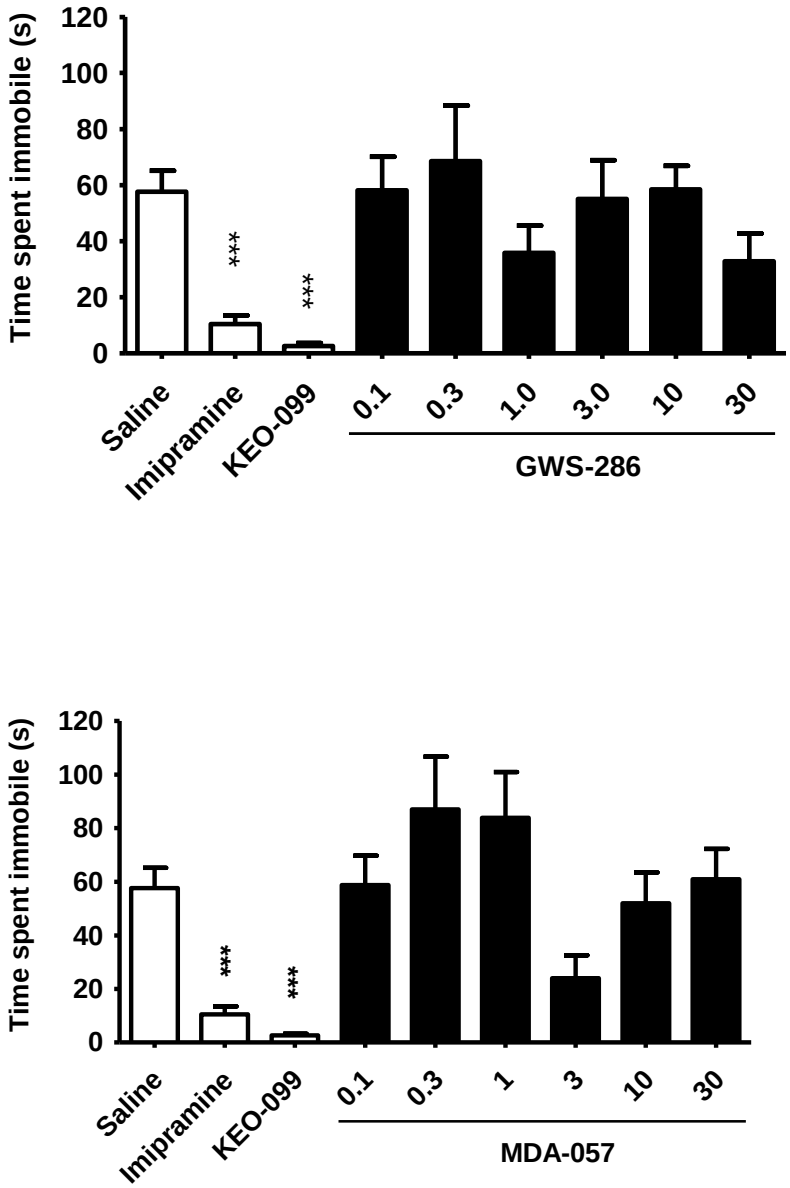

Figure 7.5 Tail suspension test for KEO-099, GSW-286 and MDA-057.

Upper panel: total time spent immobile after administration of imipramine (20 mg/kg), KEO-099 (1 mg/kg) and different doses of GSW-286. Lower panel: total time spent immobile after administration of imipramine (20 mg/kg), KEO-099 (1 mg/kg) and different doses of MDA-057. Effects are reported as mean ± SEM (second) in the mouse TST (n = 8 – 11 mice/treatment). Asterisk (***) denotes a significant difference compared to saline group ($p < 0.05$).

7.C.6 Homology modeling and docking studies for hOCT3

The amino acid sequence of hOCT3 (UniProt: O75751) and the approximate location of the predicted transmembrane domains were obtained from the literature [256, 257]. The amino acid sequence and predicted transmembrane domains of PiPT were obtained from PDB (PDB:4J05, accession number: A8N031). Clustal X was used to align the peptide sequences between hOCT3 and PiPT. A total of 100 homology models of hOCT3 were constructed using MODELLER v9.12 (University of California at San Francisco, San Francisco, CA). The best model was selected and the loops and side chains were refined by MODELLER (Figure 7.6).

The conformation and charge distribution of MPP^+ and quinazolines were optimized with energy minimization using tripos force field with Gasteiger–Hückel charges in SYBYL-X 2.1. MPP^+ docked to hOCT3 through 100 iterations using GOLDSuite 5.2 and GOLD's default scoring function was utilized to select binding modes. The results obtained were analyzed by cluster analysis to find the modes exhibiting similar docking poses, and two plausible binding modes were identified (Figure 7.6). Quinazolines were further docked into the substrate binding site of hOCT3, and the critical amino acid residues that interacted with MPP^+ and quinazolines were identified (Figure 7.7 and Table 7.4). The results suggested that guanidine N-atoms of quinazolines interacted with D478 (TM11) through a salt-bridge interaction, and the guanidine moiety of quinazolines interacted with the aromatic rings of W223 (TM4) and F165 (TM2) through a cation-π interaction. In addition, hydrophobic interactions were observed for the substituted group of quinazolines with the following amino acid residues: KEO-099 and MDA-049 with A362, Y365 and Q366 and OIA-008 and GSW-286 with A362.

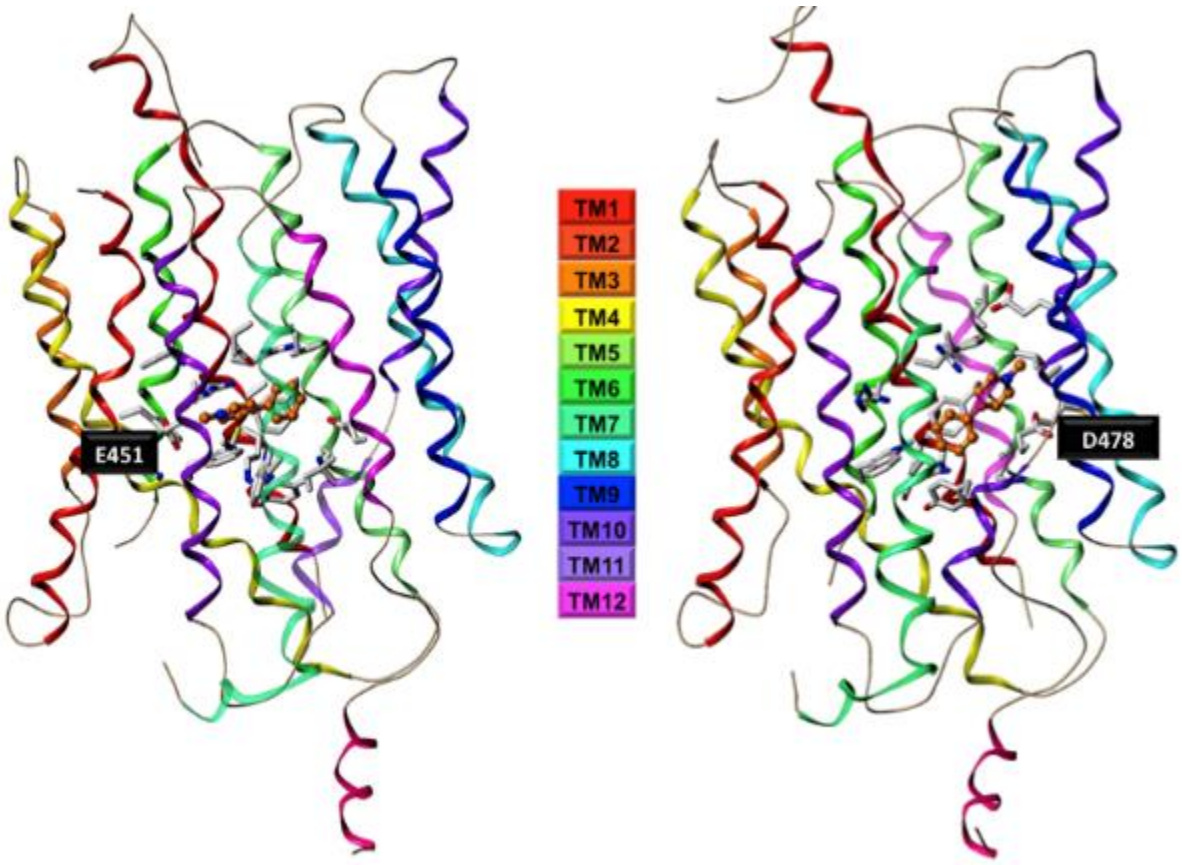

Figure 7.6 The homology models of hOCT3 and two modes of binding for MPP^+.

The homology models of hOCT3 were constructed using the crystal structure of inward-facing conformation of PiPT (PDB number: 4J05). This model was done in collaboration with Dr. Dukat laboratory and Kavita Iyer.

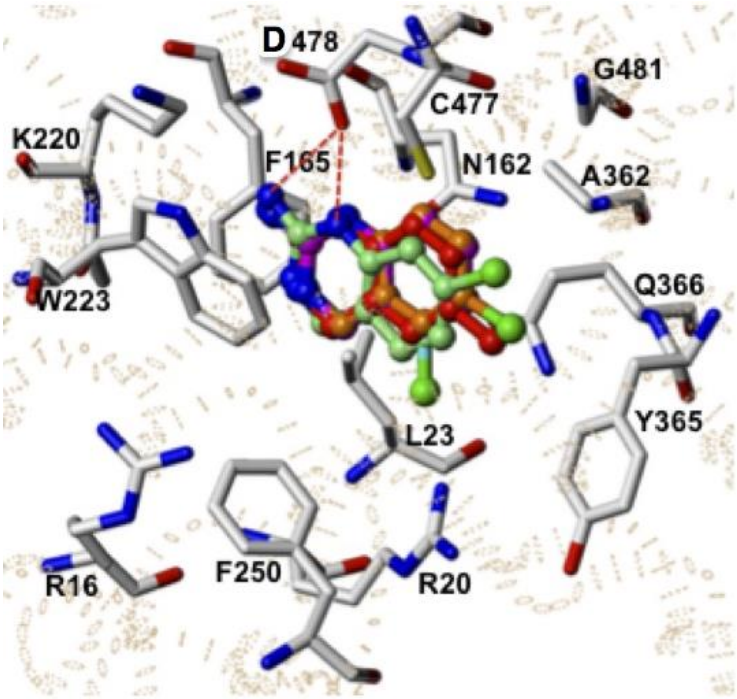

Figure 7.7 Docking the quinazolines into the binding pocket of hOCT3.

Ionic bond interactions are indicated by red dotted lines. Orange: KEO-099; pale green: OIA-008; magenta: GSW-286; cyan: KEO-093; red: MDA-049. This model was done in collaboration with Dr. Dukat laboratory and Kavita Iyer.

Table 7.4 Summary of key amino acid residues identified in docking studies of quinazolines on hOCT3.

Quinazolines	Interactions	Amino acids
GSW-286	Ionic salt-bridge	D478
	Cation-π	F165 and W223
	Hydrophobic	A362
KEO-093	Ionic salt-bridge	D478
	Cation-π	F165 and W223
	Hydrophobic	L23
KEO-099	Ionic salt-bridge	D478
	Cation-π	F165 and W223
	Hydrophobic	A362, Y365and Q366
OIA-008	Ionic salt-bridge	D478
	Cation-π	F165 and W223
	Hydrophobic	A362
MDA-049	Ionic salt-bridge	D478
	Cation-π	F165 and W223
	Hydrophobic	A362, Y365, Q366

7.D DISCUSSION

According to the global burden of disease study 2010, depression is the fourth leading cause of illness-induced disability, and it is predicted that depression will reach second place by 2020 [258]. Although a number of drugs are used clinically in the treatment of depression, approximately one-half of depressed patients failed to find relief using current therapies, especially in mild or moderate cases of depression [243, 245-247]. This may be due to the presence of multiple clearance pathways for monoamine neurotransmitters in brain subject to different modes of regulation. Undesirable side effects, such as weight loss, increased bone fracture risk and gastrointestinal effects, are also often observed in the clinical application of antidepressants [244]. Thus, there is an unmet need to develop antidepressants with a novel mechanism of action and greater efficacy than existing antidepressants. Recently, hOCT2 and hOCT3 have been discovered as key components of uptake-2 and suggested to play an important role in regulating neurotransmitter clearance in brain [91, 92]. In addition, a number of antidepressants currently in use, such as fluoxetine, desipramine and sertraline, are now known to be effective OCT inhibitors *in vitro* [259, 260]. Currently, it remains unclear what, if any, role OCTs may have in their therapeutic action of these compounds, however, together these data suggest OCTs may be viable therapeutic targets in depression. Certainly, at a minimum, an impact on CNS clearance appears likely.

The quinazoline and guanidine compounds examined in this study are a novel series of compounds developed as potential novel therapeutic agents for depression [248]. Although their binding affinities for SERT and NET were greater than 10 μM, a chloride substituted quinazoline demonstrated potent antidepressant-like effects in mice [248]. In

the present study, the interactions of thirteen quinazoline and guanidine compounds with OCTs were studied. The inhibitory effects of the quinazoline and guanidine compounds varied according to the modification of their structures. Overall, hOCT2 was least sensitive to inhibition, with the notable exception of the benzyl substituted guanidine KAI-324 which exhibited 5-8 fold higher affinity for hOCT2 over hOCT1 and 3 (Table 7.2).

Guanidine compounds lack the methylene bridge structure in the quinazoline ring, and have a rotatable bond between the guanidino group and the phenyl group (Table 7.1). Unsubstituted guanidine (KAI-323) had a poor affinity (higher IC_{50} value) for hOCT1-3 as compared to unsubstituted quinazoline (GSW-286), indicating that the flexible open ring structure of guanidine compounds was unfavorable for interaction with hOCT1-3. In addition, substituting R_1-R_3 positions of quinazoline and guanidine compounds with different functional groups changed their inhibitory effects for hOCTs. Chloride and fluoride are electron withdrawing groups, while methyl, t-butyl and benzyl are electron donating groups. However, both electron withdrawing groups (i.e., chloride and fluoride) and electron donating groups (i.e., methyl and t-butyl) increased the affinities of quinazoline and guanidine compounds for hOCT1-3 as compared to the unsubstituted compounds. These results indicated that steric effects, rather than polar effects, impact the affinity of quinazolines and guanidines for hOCTs. It was also observed that R_1 is the most favorable substitution position for quinazoline compounds for hOCT3, as both chloride and methyl substituted quinazolines at R_1 position exhibited 4-6 fold increased inhibitory effects (lower IC_{50} values) for hOCT3 as compared to those for R_2 and R_3 substituted compounds. On the contrary, a large benzyl group (KAI-324) decreased the inhibitory effects of guanidine compounds for hOCT1 and hOCT3, possibly due to the unfavorable

steric effects. Although the affinity of this compound for hOCTs overall is somewhat poor, its *in vitro* profile suggests it to be a hOCT2-selective inhibition and this is being investigated further. Both species similarities and differences were observed between human and mouse OCT orthologs. In general, murine orthologs were less sensitive to inhibition by the test compounds as compared to human (Table 7.2). The IC_{50} values of quinazoline and guanidine compounds for mOct2 were comparable (0.6 to 2.3 fold) to those for hOCT2, whereas relatively weaker inhibitory effects were observed for mOct1 and mOct3 than those for hOCT1 and hOCT3, i.e. there was no trend for mOct2 to be less sensitive to inhibition as compared to mOct1 an dmOct3.

Three lead compounds, KEO-099, GSW-286 and MDA-057 were selected for *in vivo* testing based on *in vitro* inhibitory profiles. KEO-099 is the chloride substituted quinazoline. GSW-286 is the unsubstituted quinazoline, and MDA-057 is the chloride substituted guanidine. The *in vitro* inhibitory effect of KEO-099 *vs.* 5-HT for hOCT2 was ~30 fold stronger (lower IC_{50} value) than that determined using MPP^+, indicating that a nanomolar level of lead compound might provide sufficient inhibition on uptake-2 *in vivo*. KEO-099 exhibited potent antidepressant-like effects in the TST with ED_{50} value determined as low as 0.23 mg/kg [248]. However, unsubstituted quinazoline and chloride substituted guanidine failed to show significant CNS pharmacological effects in the TST (Figure 7.5), suggesting that both substitution groups and the methylene bridge might be important for the pharmacological effects of these compounds. Further pharmacological and pharmacokinetic studies should be performed on KEO-099 as well as other compounds.

To provide hOCT structural information to our data interpretation, we constructed a 3-D homology models for hOCT3 and performed docking studies for MPP^+ and

quinazolines. The protein structures of OCTs are not available due to the difficulties associated with crystallization of membrane proteins. A high-resolution crystal structure of PiPT was used as the template which shared 21% amino acid sequence similarity with hOCT3 [253-255]. As compared with Lactose Permease transporter used previously for OCT homology models, PiPT and OCTs belong to the same major facilitator superfamily and share a higher amino acid sequence similarity [254-256]. A central binding pocket in hOCT3 was chosen for both MPP^+ and quinazolines, since quinazolines demonstrated a competitive mode of inhibition on hOCT3 (Figure 7.7, Table 7.2). The homology modeling studies suggested that hOCT3 interacted with docked compounds through TMDs 1, 2, 4, 7 and 11. A number of potential key amino acid residues in hOCT3 were identified: F165, W223, A362, Y365, Q366 and D478. Whether these residues truly represent transporter-substrate contact points requires further investigation.

In summary, thirteen quinazolines and guanidines were identified as potent inhibitors for hOCTs/mOcts. The inhibitory effects of quinazolines and guanidines with hOCTs/mOcts were compared and lead compounds were selected based on *in vitro* profiles. KEO-099 demonstrated potent antidepressant-like effects in the TST, while GSW-286 and MDA-057 failed to show antidepressant-like activities. This study suggested that novel OCT inhibitors such as quinazolines have the potential to possess antidepressant-like effects even if they did not target SERT or NET. In addition, we performed the homology modeling and docking studies for hOCT3. The mode of inhibition studies showed that representative quinazoline and guanidine compounds competed for the same binding pocket with MPP^+ in hOCT2 and hOCT3. The homology models of hOCT3 were developed, and several amino acid residues were identified by docking studies. This

homology model of hOCT3 could be further used to support 3-D QSAR for designing the next generation of quinazolines and guanidines.

CHAPTER 8

OVERALL CONCLUSIONS AND FUTURE DIRECTIONS

A major function of the polyspecific organic cation OCTs/OATs (SLC22 transporter family) is to exert selection control over the influx of small molecules across cell membranes [2, 3, 6]. Since OCTs/OATs are widely expressed in various peripheral barrier organs, they contribute to the uptake into and secretion from enterocytes, hepatocytes renal proximal tubular cells for a broad variety of endogenous and exogenous compounds [2, 3, 6]. The activity of OCTs/OATs can be altered by a second drug via inhibition, and thus drug-drug interaction may occur during combination therapy when transporter substrates and inhibitors are administered together [191]. In addition, hOCT2/mOct2 and hOCT3/mOct3 are highly expressed in neurons and glial cells in brain, and many monoamine neurotransmitters including serotonin (5-HT), norepinephrine (NE) and dopamine (DA) are their substrates [52, 91, 92]. Thus, OCTs appear to be an important component of uptake-2 and may participate in the regulation of neurotransmitter clearance in the central nervous systems (CNS). In this study, we began to explore the potential role of OCT inhibitors in mood disorders, as well as the roles of OCTs/OATs in drug transporter-mediated drug-drug interaction.

Despite widespread multimorbidity, most clinical therapeutic guidelines are written based on the condition of a single disease and the impact of applying complex multiple drug regimens during polypharmacy is generally not well understood. The potential for transporter mediated drug-drug interactions (DDIs) during combination therapy can be assessed by *in vitro* drug transporter expressing cell models [129]. In chapter 3 to chapter 5, we investigated the inhibitory effects of five different drugs on OCTs and OATs and evaluate their potential in transporter-mediated DDIs. Rhein, a major metabolite of the prodrug diacerein and a major component of the medicinal herb Rheum sp., is used for its beneficial effects in a variety of clinical applications including the treatment of osteoarthritis and diabetic nephropathy [116-119]. In chapter 3, the inhibitory effects of rhein on hOAT1, hOAT3, hOAT4, and mOat1 and mOat3 were examined in heterologous cell lines stably expressing each transporter in isolation. Rhein was shown to potently inhibit hOAT1 and hOAT3, with IC_{50} estimates in the low nanomolar range (IC_{50} = 77.1 ± 5.5 nM and 8.4 ± 2.5 nM, respectively), while poor affinity was observed for hOAT4 (IC_{50} > 100 mM). Marked species differences were observed with hOAT1 and hOAT3 exhibiting 3- and 28-fold higher affinity for rhein as compared to their murine orthologs. The estimated DDI indices (>>0.1) indicated a very strong potential for clinically relevant, rhein perpetrated DDIs mediated by inhibition of hOAT1 (DDI index = 5.0; 83% inhibition) and/or hOAT3 (DDI index = 46; 98% inhibition) transport activity. These results suggested that rhein, from herbal medicines and/or prodrug conversion, may significantly impact the dosing, efficacy and toxicity (i.e., pharmacokinetics and pharmacodynamics) of co-administered hOAT1 and/or hOAT3 drug substrates.

Tuberculosis is a serious and worldwide disease that infect ~9 million people and causes about 1.4 million deaths every year [136]. Moreover, the frequency of comorbidity with HIV and with diabetes is on the rise, increasing the risk of these patients for experiencing DDIs due to polypharmacy [154]. Ethambutol, a first-line antituberculosis drug, is an organic cation at physiological pH, and its major metabolite, EDA, is zwitterionic [145]. In chapter 4, we assessed the effects of ethambutol and 2,2'-(ethylenediimino)dibutyric acid (EDA) on the function of hOCT1, hOCT2, and hOCT3 and that of EDA on hOAT1 and hOAT3. Potent inhibition of hOCT1- and hOCT2-mediated transport by ethambutol was observed, and IC_{50} values of ethambutol were determined as 92.6 ± 10.9 and 253.8 ± 90.8 μM for hOCT1 and hOCT2, respectively. Ethambutol exhibited much weaker inhibition of hOCT3 (IC_{50} = 4.1 ± 1.6 mM); however, significant inhibition (>80%) was observed at physiologically relevant concentrations in the GI tract after oral dosing. EDA failed to exhibit any inhibitory effects that warranted further investigation. DDI analysis indicated a strong potential for ethambutol interaction on hOCT1 expressed in enterocytes and hepatocytes and on hOCT3 in enterocytes, which would alter absorption, distribution, and excretion of coadministered cationic drugs, suggesting that *in vivo* pharmacokinetic studies are necessary to confirm drug safety and efficacy. In particular, TB patients with coexisting HIV or diabetes might experience significant DDIs in situations of coadministration of ethambutol and clinical therapeutics known to be hOCT1/ hOCT3 substrates, such as lamivudine or metformin.

The alkaloids matrine and oxymatrine are widely used in herbal medicine for the treatment of cancer, as well as viral, and cardiac diseases [179-182]. Their physicochemical properties indicated that they are potential inhibitors for hOCTs, leading to drug–drug

interactions. In chapter 5, we assessed the inhibitory effects of matrine and oxymatrine on the function of hOCT1, hOCT2 and hOCT3 using stably transfected transporter-expressing cells. At 100-fold excess, oxymatrine exhibited marked inhibition of hOCT1-mediated substrate uptake, while matrine failed to produce significant inhibition on hOCT1. The IC_{50} value for oxymatrine on hOCT1 was estimated as 513 ± 132 μM. While there was no significant inhibition of hOCT2 or hOCT3 at 100-fold excess, oxymatrine and matrine showed 42% and 88% inhibition of hOCT3-mediated substrate uptake at 3 and 6 mM, respectively. Considering the potential intestinal lumen and reported plasma concentrations of matrine and oxymatrine, these data suggest that drug–drug interactions may occur during hOCT1-mediated hepatic and renal uptake and during hOCT3-mediated intestinal absorption.

In addition, we focused on the potential role of OCTs in CNS action of drugs of abuse. Synthetic cathinones have recently emerged in the US and Europe and grown to be popular drugs of abuse [203, 261]. These drugs have the ability to modulate neurotransmitter levels in brain and possess amphetamine-like properties [204-206]. Serious adverse effects and deaths are often reported in synthetic cathinone users who required medical care [218, 219, 222]. In chapter 6, we explored the inhibitory effects of five synthetic cathinones (mephedrone, methylone, methylenedioxypyrovalerone (MDPV), R(+)methcathinone and S(-)methcathinone) on hOCT1, hOCT2 and hOCT3. All five synthetic cathinones demonstrated marked inhibition of substrate uptake mediated by hOCTs. Generally, the inhibitory potencies of test synthetic cathinones for hOCT1 and hOCT2 were higher (IC_{50}: 6.5-31.5 μM) than those for hOCT3 (IC_{50}: 130.5-334.7 μM). MDPV exhibited the highest potency (lowest IC_{50} values) for hOCT1 (6.5 ± 1.3 μM),

hOCT2 (16.7 ± 1.2 μM) and hOCT3 (130.5 ± 18.0 μM). The optical isomers of methcathinone exhibited different patterns of interaction with hOCTs. S(-)methcathinone demonstrated higher affinity for hOCT2 as compared to R(+)methcathinone, while the inhibitory effect of S(-)methcathinone on hOCT3 was lower than R(+)methcathinone. As hOCT2 and hOCT3 are important components of uptake-2 that modulate neurotransmitter homeostasis in the CNS, these findings suggested that the psychoactive effects of synthetic cathinones for drug abusers might be due to their inhibitory effects on hOCT2 and hOCT3. Moreover, cardiovascular complications caused by synthetic cathinones might also be caused by their inhibitory effects on hOCT3, since hOCT3 participates in the reuptake of NE in cardiac endothelial cells. Finally, the enhanced toxicities of synthetic cathinones when coadministered with other stimulants, such as codeine, morphine and heroin, might be explained by the high DDI potentials mediated by OCTs. Therefore, the role of OCTs in the psychoactive effects/clearance of synthetic cathinones as well as their potential in mediating *in vivo* DDI should be further investigated to elucidate the full mechanistic picture.

The quinazolines and guanidines examined in this work represent a novel series of compounds developed as potential drugs that possess antidepressant-like effects. However, these compounds failed to produce significant inhibition of uptake-1 activity, since their binding affinity for SERT and NET were greater than 10 μM (Dr. Dukat laboratory, unpublished data). Based on their physicochemical properties, we hypothesized that these compounds might be OCT inhibitors and their antidepressant-like activities might involve an uptake-2 mediated mechanism. In chapter 7, we systematically assessed the inhibitory effects of thirteen quinazoline and guanidine compounds on three OCTs in two species,

human and mouse. At 100 μM, all of test compounds, including 7 novel quinazolines and 6 guanidines, showed significant inhibition on three hOCTs. The IC_{50} values for unsubstituted quinazoline GSW-286 was smaller than unsubstituted guanidine KAI-323 (IC_{50} values: 14.3 ± 2.2 μM v.s. 41.1 ± 14.4 μM). This is probably due to the flexible open ring structure of guanidine that decreased the affinity of KAI-323 for hOCTs. In addition, it was also observed that chloride, fluoride, methyl and t-butyl substituted quinazoline and guanidine compounds have lower IC_{50} values (2-46 fold) as compared with their unsubstituted forms, while benzyl substituted guanidine demonstrated higher (~19 and 5 fold) the IC_{50} values for hOCT1 and hOCT3. Since depression is often associated with a decreased level of 5-HT in the CNS, OCT inhibition studies were conducted using radiolabeled 5-HT as the substrate. The IC_{50} value for KEO-099 vs 5-HT for hOCT2 was determined as 0.56 ± 0.08 μM, which is 29 fold higher than that determined using MPP^+. This result suggested that a nanomolar level of KEO-099 might be sufficient to provide significant inhibition on uptake-2 in brain. Based on *in vitro* data, we selected three lead compounds that showed potent inhibition on both human and mouse OCTs to conduct further *in vivo* studies. KEO-099 demonstrated significant antidepressant-like effects during the tail suspension test (TST) with an ED_{50} value estimated as 0.23 mg/kg, while MDA-057 and GSW-286 failed to show significant antidepressant-like effects. This antidepressant-like effects of KEO-099 indicated that this compound is permeable across the blood brain barrier and is likely to exert its psychiatric effects in brain. Finally, the homology modeling of hOCT3 and docking studies were performed based on the knowledge of a competitive mechanism of inhibition of test compounds on hOCT3. In the docking studies, four key amino acid residues in hOCT3 were identified namely E451

(glutamic acid), D478 (aspartic acid), W223 (tryptophan) and F165 (phenylalanine). E451 and D478 interacted with MPP^+ and quinazolines via ionic salt bridge interaction, while W223 and F165 interacted with docking compounds through the cation-π interaction. The present study suggested that novel OCT inhibitors such as quinazolines have the potential to possess antidepressant-like activities, and the hOCT3 homology model could be used as a powerful tool for analyzing and predicting the interaction between hOCT3 and small molecules in future.

In chapter 3 to 5, we evaluated DDI potential of OCT- and OAT-mediated drug-drug interaction for ethambutol, rhein, matrine and oxymatrine. In the future, *in vivo* DDI studies are necessary for these compounds with known substrates for OCTs (e.g. metformin and lamivudine) and OATs (e.g., methotrexate) in order to optimize clinical safety and efficacy in these complex patient populations. In addition, the present study demonstrated that ethambutol, oxymatrine and matrine are inhibitors for OCTs, while rhein is a potent inhibitor for OATs. However, it remains unclear whether these compounds are non-transported inhibitors or actually transporter substrates. This information is key to determining whether OCT- or OAT-mediated active uptake is involved in the hepatic accumulation or renal elimination of these compounds. As a result, a sensitive, robust, and precise bioanalytical method needs to be developed for quantification of these transporter inhibitors in cell lysate to address this issue.

In addition, the role of OCTs in regulating 5-HT, NE and DA clearance in brain should be investigated in the following aspects. Firstly, it is important to characterize the permeability of quinazoline and guanidine compounds across the blood brain barrier (BBB) using appropriate *in vitro* models. The BBB is a highly selective barrier formed by brain

endothelial cells connected by tight junctions that separates the brain interstitial fluid in the CNS from the circulating blood [60]. A perquisite for a good CNS drug candidate is that it has a high permeability across the BBB; otherwise, it is not easy for the drug to reach its target organ. The *in vitro* cell-based BBB models are more cost-effective than animal experiments and have a higher throughput for drug screening. In addition, the permeability profiles of test compounds would support the decisions when prioritizing the lead compounds. Several *in vitro* BBB models have been developed, including steric endothelial cells monoculture models, co-culture models of endothelial cells with glial cells, as well as more sophisticated 3D dynamic co-culture models of BBB [60]. A number of cell lines are available as biological surrogates for BBB, including HMEC-1, HCMEC/D3 and TY08 [60]. Secondly, it is also important to determine the pharmacokinetics and brain distributions of lead compounds *in vivo*. In the present study, the TST was performed following the protocol of Steru et al and Yoshikawa et al [251, 252]. However, the brain distribution of lead compounds at 30 min after i.p. injection was not determined, and it is possible the compounds achieved their C_{max} in brain longer than or shorter than 30 min. Information about the pharmacokinetics and the time-course profiles of the brain distribution of lead compounds would allow us to better characterize the maximum ED_{50} of test compounds in mice. In addition, it would be even more informative if we could determine the extracellular regional concentrations of lead compounds by microdialysis in specific brain regions, such as hippocampus, frontal cortex and amygdala, where mOct2 and mOct3 are richly expressed. This would allow extrapolation of *in vitro* data to *in vivo* level of inhibition on mOct2 and mOct3 in brain. Finally, mOct2 and mOct3 knockout mice could be used as animal models to test the hypothesis that uptake-2 are the

targets for the antidepressant-like effects of guanidine and quinazoline compounds. The antidepressant-like effects of test compounds could be compared between wide-type and mOct2 or mOct3 knockout mice.

As for the synthetic cathinones, it is important to find an appropriate animal model and conduct *in vivo* studies to elucidate the contribution of OCTs in the psychoactive effects of these compounds. This emphasizes the need to understand the potential species differences between human and murine OCTs. The IC_{50} values of synthetic cathinones should be further determined using murine Oct expressing cell lines. After we identify an ideal animal model, the brain extracellular regional distribution of selected synthetic cathinones could be determined by microdialysis studies after intravenous administration. This information is critical for us to estimate the level of inhibition on Oct2 and Oct3 by synthetic cathinones in brain. The psychoactive effects of the synthetic cathinones could also be compared between wild-type and Oct2 knockout animal models. Finally, in order to evaluate OCT-mediated DDIs, it is necessary to conduct *in vivo* DDI studies for synthetic cathinones and known OCT substrate such as morphine.

LIST OF REFERENCES

1. **Sweet D.H., D.S. Miller, and J.B. Pritchard**, *Ventricular choline transport: a role for organic cation transporter 2 expressed in choroid plexus.* 2001. J Biol Chem, 276(45): p. 41611-9.
2. **Wang L. and D.H. Sweet**, *Renal organic anion transporters (SLC22 family): expression, regulation, roles in toxicity, and impact on injury and disease.* 2013. AAPS J, 15(1): p. 53-69.
3. **Koepsell H., K. Lips, and C. Volk**, *Polyspecific organic cation transporters: structure, function, physiological roles, and biopharmaceutical implications.* 2007. Pharm Res, 24(7): p. 1227-51.
4. **Koepsell H.**, *The SLC22 family with transporters of organic cations, anions and zwitterions.* 2013. Mol Aspects Med, 34(2-3): p. 413-35.
5. **Koepsell H.**, *Substrate recognition and translocation by polyspecific organic cation transporters.* 2011. Biol Chem, 392(1-2): p. 95-101.
6. **VanWert A.L., M.R. Gionfriddo, and D.H. Sweet**, *Organic anion transporters: discovery, pharmacology, regulation and roles in pathophysiology.* 2010. Biopharm Drug Dispos, 31(1): p. 1-71.
7. **Sweet D.H., N.A. Wolff, and J.B. Pritchard**, *Expression cloning and characterization of ROAT1. The basolateral organic anion transporter in rat kidney.* 1997. J Biol Chem, 272(48): p. 30088-95.
8. **Grundemann D., V. Gorboulev, S. Gambaryan, et al.**, *Drug excretion mediated by a new prototype of polyspecific transporter.* 1994. Nature, 372(6506): p. 549-52.
9. **Sekine T., N. Watanabe, M. Hosoyamada, et al.**, *Expression cloning and characterization of a novel multispecific organic anion transporter.* 1997. J Biol Chem, 272(30): p. 18526-9.
10. **Gorboulev V., J.C. Ulzheimer, A. Akhoundova, et al.**, *Cloning and characterization of two human polyspecific organic cation transporters.* 1997. DNA Cell Biol, 16(7): p. 871-81.
11. **Wang L., B. Prasad, L. Salphati, et al.**, *Interspecies variability in expression of hepatobiliary transporters across human, dog, monkey, and rat as determined by quantitative proteomics.* 2015. Drug Metab Dispos, 43(3): p. 367-74.
12. **Okuda M., H. Saito, Y. Urakami, et al.**, *cDNA cloning and functional expression of a novel rat kidney organic cation transporter, OCT2.* 1996. Biochem Biophys Res Commun, 224(2): p. 500-7.
13. **Koepsell H., B.M. Schmitt, and V. Gorboulev**, *Organic cation transporters.* 2003. Rev Physiol Biochem Pharmacol, 150: p. 36-90.

14. **Grundemann D., B. Schechinger, G.A. Rappold, et al.**, *Molecular identification of the corticosterone-sensitive extraneuronal catecholamine transporter.* 1998. Nat Neurosci, 1(5): p. 349-51.
15. **Kekuda R., P.D. Prasad, X. Wu, et al.**, *Cloning and functional characterization of a potential-sensitive, polyspecific organic cation transporter (OCT3) most abundantly expressed in placenta.* 1998. J Biol Chem, 273(26): p. 15971-9.
16. **Wu X., W. Huang, M.E. Ganapathy, et al.**, *Structure, function, and regional distribution of the organic cation transporter OCT3 in the kidney.* 2000. Am J Physiol Renal Physiol, 279(3): p. F449-58.
17. **Sata R., H. Ohtani, M. Tsujimoto, et al.**, *Functional analysis of organic cation transporter 3 expressed in human placenta.* 2005. J Pharmacol Exp Ther, 315(2): p. 888-95.
18. **Nies A.T., H. Koepsell, S. Winter, et al.**, *Expression of organic cation transporters OCT1 (SLC22A1) and OCT3 (SLC22A3) is affected by genetic factors and cholestasis in human liver.* 2009. Hepatology, 50(4): p. 1227-40.
19. **Muller J., K.S. Lips, L. Metzner, et al.**, *Drug specificity and intestinal membrane localization of human organic cation transporters (OCT).* 2005. Biochem Pharmacol, 70(12): p. 1851-60.
20. **Lips K.S., C. Volk, B.M. Schmitt, et al.**, *Polyspecific cation transporters mediate luminal release of acetylcholine from bronchial epithelium.* 2005. Am J Respir Cell Mol Biol, 33(1): p. 79-88.
21. **Bahn A., M. Knabe, Y. Hagos, et al.**, *Interaction of the metal chelator 2,3-dimercapto-1-propanesulfonate with the rabbit multispecific organic anion transporter 1 (rbOAT1).* 2002. Mol Pharmacol, 62(5): p. 1128-36.
22. **Cihlar T., D.C. Lin, J.B. Pritchard, et al.**, *The antiviral nucleotide analogs cidofovir and adefovir are novel substrates for human and rat renal organic anion transporter 1.* 1999. Mol Pharmacol, 56(3): p. 570-80.
23. **George R.L., X. Wu, W. Huang, et al.**, *Molecular cloning and functional characterization of a polyspecific organic anion transporter from Caenorhabditis elegans.* 1999. J Pharmacol Exp Ther, 291(2): p. 596-603.
24. **Hagos Y., A. Bahn, A.R. Asif, et al.**, *Cloning of the pig renal organic anion transporter 1 (pOAT1).* 2002. Biochimie, 84(12): p. 1221-4.
25. **Hosoyamada M., T. Sekine, Y. Kanai, et al.**, *Molecular cloning and functional expression of a multispecific organic anion transporter from human kidney.* 1999. Am J Physiol, 276(1 Pt 2): p. F122-8.
26. **Lopez-Nieto C.E., G. You, K.T. Bush, et al.**, *Molecular cloning and characterization of NKT, a gene product related to the organic cation transporter family that is almost exclusively expressed in the kidney.* 1997. J Biol Chem, 272(10): p. 6471-8.
27. **Race J.E., S.M. Grassl, W.J. Williams, et al.**, *Molecular cloning and characterization of two novel human renal organic anion transporters (hOAT1 and hOAT3).* 1999. Biochem Biophys Res Commun, 255(2): p. 508-14.
28. **Wolff N.A., A. Werner, S. Burkhardt, et al.**, *Expression cloning and characterization of a renal organic anion transporter from winter flounder.* 1997. FEBS Lett, 417(3): p. 287-91.
29. **Sweet D.H., D.S. Miller, J.B. Pritchard, et al.**, *Impaired organic anion transport in kidney and choroid plexus of organic anion transporter 3 (Oat3 (Slc22a8)) knockout mice.* 2002. J Biol Chem, 277(30): p. 26934-43.
30. **Monte J.C., M.A. Nagle, S.A. Eraly, et al.**, *Identification of a novel murine organic anion transporter family member, OAT6, expressed in olfactory mucosa.* 2004. Biochem Biophys Res Commun, 323(2): p. 429-36.

31. **Pritchard J.B., D.H. Sweet, D.S. Miller, et al.**, *Mechanism of organic anion transport across the apical membrane of choroid plexus.* 1999. J Biol Chem, 274(47): p. 33382-7.
32. **Sweet D.H., D.S. Miller, and J.B. Pritchard**, *Localization of an organic anion transporter-GFP fusion construct (rROAT1-GFP) in intact proximal tubules.* 1999. Am J Physiol, 276(6 Pt 2): p. F864-73.
33. **Buist S.C. and C.D. Klaassen**, *Rat and mouse differences in gender-predominant expression of organic anion transporter (Oat1-3; Slc22a6-8) mRNA levels.* 2004. Drug Metab Dispos, 32(6): p. 620-5.
34. **Sekine T., S.H. Cha, M. Tsuda, et al.**, *Identification of multispecific organic anion transporter 2 expressed predominantly in the liver.* 1998. FEBS Lett, 429(2): p. 179-82.
35. **Sun W., R.R. Wu, P.D. van Poelje, et al.**, *Isolation of a family of organic anion transporters from human liver and kidney.* 2001. Biochem Biophys Res Commun, 283(2): p. 417-22.
36. **Enomoto A., M. Takeda, M. Shimoda, et al.**, *Interaction of human organic anion transporters 2 and 4 with organic anion transport inhibitors.* 2002. J Pharmacol Exp Ther, 301(3): p. 797-802.
37. **Kusuhara H., T. Sekine, N. Utsunomiya-Tate, et al.**, *Molecular cloning and characterization of a new multispecific organic anion transporter from rat brain.* 1999. J Biol Chem, 274(19): p. 13675-80.
38. **Cha S.H., T. Sekine, J.I. Fukushima, et al.**, *Identification and characterization of human organic anion transporter 3 expressing predominantly in the kidney.* 2001. Mol Pharmacol, 59(5): p. 1277-86.
39. **Zhang X., C.E. Groves, A. Bahn, et al.**, *Relative contribution of OAT and OCT transporters to organic electrolyte transport in rabbit proximal tubule.* 2004. Am J Physiol Renal Physiol, 287(5): p. F999-1010.
40. **Kobayashi Y., N. Ohshiro, A. Tsuchiya, et al.**, *Renal transport of organic compounds mediated by mouse organic anion transporter 3 (mOat3): further substrate specificity of mOat3.* 2004. Drug Metab Dispos, 32(5): p. 479-83.
41. **Kobayashi Y., N. Hirokawa, N. Ohshiro, et al.**, *Differential gene expression of organic anion transporters in male and female rats.* 2002. Biochem Biophys Res Commun, 290(1): p. 482-7.
42. **Hilgendorf C., G. Ahlin, A. Seithel, et al.**, *Expression of thirty-six drug transporter genes in human intestine, liver, kidney, and organotypic cell lines.* 2007. Drug Metab Dispos, 35(8): p. 1333-40.
43. **Hasegawa M., H. Kusuhara, D. Sugiyama, et al.**, *Functional involvement of rat organic anion transporter 3 (rOat3; Slc22a8) in the renal uptake of organic anions.* 2002. J Pharmacol Exp Ther, 300(3): p. 746-53.
44. **Babu E., M. Takeda, S. Narikawa, et al.**, *Role of human organic anion transporter 4 in the transport of ochratoxin A.* 2002. Biochim Biophys Acta, 1590(1-3): p. 64-75.
45. **Cha S.H., T. Sekine, H. Kusuhara, et al.**, *Molecular cloning and characterization of multispecific organic anion transporter 4 expressed in the placenta.* 2000. J Biol Chem, 275(6): p. 4507-12.
46. **Bleasby K., J.C. Castle, C.J. Roberts, et al.**, *Expression profiles of 50 xenobiotic transporter genes in humans and pre-clinical species: a resource for investigations into drug disposition.* 2006. Xenobiotica, 36(10-11): p. 963-88.
47. **Ekaratanawong S., N. Anzai, P. Jutabha, et al.**, *Human organic anion transporter 4 is a renal apical organic anion/dicarboxylate exchanger in the proximal tubules.* 2004. J Pharmacol Sci, 94(3): p. 297-304.

48. **Ugele B., M.V. St-Pierre, M. Pihusch, et al.**, *Characterization and identification of steroid sulfate transporters of human placenta.* 2003. Am J Physiol Endocrinol Metab, 284(2): p. E390-8.
49. **Kusuhara H. and Y. Sugiyama**, *Efflux transport systems for organic anions and cations at the blood-CSF barrier.* 2004. Adv Drug Deliv Rev, 56(12): p. 1741-63.
50. **Strazielle N. and J.F. Ghersi-Egea**, *Choroid plexus in the central nervous system: biology and physiopathology.* 2000. J Neuropathol Exp Neurol, 59(7): p. 561-74.
51. **Dziegielewska K.M., L.A. Hinds, K. Mollgard, et al.**, *Blood-brain, blood-cerebrospinal fluid and cerebrospinal fluid-brain barriers in a marsupial (Macropus eugenii) during development.* 1988. J Physiol, 403: p. 367-88.
52. **Farthing C.A. and D.H. Sweet**, *Expression and function of organic cation and anion transporters (SLC22 family) in the CNS.* 2014. Curr Pharm Des, 20(10): p. 1472-86.
53. **Buist S.C., N.J. Cherrington, S. Choudhuri, et al.**, *Gender-specific and developmental influences on the expression of rat organic anion transporters.* 2002. J Pharmacol Exp Ther, 301(1): p. 145-51.
54. **Nagata Y., H. Kusuhara, H. Endou, et al.**, *Expression and functional characterization of rat organic anion transporter 3 (rOat3) in the choroid plexus.* 2002. Mol Pharmacol, 61(5): p. 982-8.
55. **Sykes D., D.H. Sweet, S. Lowes, et al.**, *Organic anion transport in choroid plexus from wild-type and organic anion transporter 3 (Slc22a8)-null mice.* 2004. Am J Physiol Renal Physiol, 286(5): p. F972-8.
56. **Miller D.S., A.R. Villalobos, and J.B. Pritchard**, *Organic cation transport in rat choroid plexus cells studied by fluorescence microscopy.* 1999. Am J Physiol, 276(4 Pt 1): p. C955-68.
57. **Villalobos A.R., J.T. Parmelee, and J.L. Renfro**, *Choline uptake across the ventricular membrane of neonate rat choroid plexus.* 1999. Am J Physiol, 276(6 Pt 1): p. C1288-96.
58. **Choudhuri S., N.J. Cherrington, N. Li, et al.**, *Constitutive expression of various xenobiotic and endobiotic transporter mRNAs in the choroid plexus of rats.* 2003. Drug Metab Dispos, 31(11): p. 1337-45.
59. **Duan H. and J. Wang**, *Impaired monoamine and organic cation uptake in choroid plexus in mice with targeted disruption of the plasma membrane monoamine transporter (Slc29a4) gene.* 2013. J Biol Chem, 288(5): p. 3535-44.
60. **Pardridge W.M.**, *Drug transport across the blood-brain barrier.* 2012. J Cereb Blood Flow Metab, 32(11): p. 1959-72.
61. **Lin C.J., Y. Tai, M.T. Huang, et al.**, *Cellular localization of the organic cation transporters, OCT1 and OCT2, in brain microvessel endothelial cells and its implication for MPTP transport across the blood-brain barrier and MPTP-induced dopaminergic toxicity in rodents.* 2010. J Neurochem, 114(3): p. 717-27.
62. **Andre P., B. Saubamea, V. Cochois-Guegan, et al.**, *Transport of biogenic amine neurotransmitters at the mouse blood-retina and blood-brain barriers by uptake1 and uptake2.* 2012. J Cereb Blood Flow Metab, 32(11): p. 1989-2001.
63. **Mori S., H. Takanaga, S. Ohtsuki, et al.**, *Rat organic anion transporter 3 (rOAT3) is responsible for brain-to-blood efflux of homovanillic acid at the abluminal membrane of brain capillary endothelial cells.* 2003. J Cereb Blood Flow Metab, 23(4): p. 432-40.
64. **Kikuchi R., H. Kusuhara, D. Sugiyama, et al.**, *Contribution of organic anion transporter 3 (Slc22a8) to the elimination of p-aminohippuric acid and benzylpenicillin across the blood-brain barrier.* 2003. J Pharmacol Exp Ther, 306(1): p. 51-8.

65. **Ohtsuki S., T. Kikkawa, S. Mori, et al.**, *Mouse reduced in osteosclerosis transporter functions as an organic anion transporter 3 and is localized at abluminal membrane of blood-brain barrier.* 2004. J Pharmacol Exp Ther, 309(3): p. 1273-81.
66. **Ohtsuki S., H. Asaba, H. Takanaga, et al.**, *Role of blood-brain barrier organic anion transporter 3 (OAT3) in the efflux of indoxyl sulfate, a uremic toxin: its involvement in neurotransmitter metabolite clearance from the brain.* 2002. J Neurochem, 83(1): p. 57-66.
67. **Wu K.C., Y.H. Lu, Y.H. Peng, et al.**, *Decreased expression of organic cation transporters, Oct1 and Oct2, in brain microvessels and its implication to MPTP-induced dopaminergic toxicity in aged mice.* 2015. J Cereb Blood Flow Metab, 35(1): p. 37-47.
68. **Dickens D., A. Owen, A. Alfirevic, et al.**, *Lamotrigine is a substrate for OCT1 in brain endothelial cells.* 2012. Biochem Pharmacol, 83(6): p. 805-14.
69. **Li R.W., C. Yang, Y.W. Kwan, et al.**, *Involvement of organic cation transporter-3 and plasma membrane monoamine transporter in serotonin uptake in human brain vascular smooth muscle cells.* 2013. Front Pharmacol, 4: p. 14.
70. **Geier E.G., E.C. Chen, A. Webb, et al.**, *Profiling solute carrier transporters in the human blood-brain barrier.* 2013. Clin Pharmacol Ther, 94(6): p. 636-9.
71. **Friedrich A., R.L. George, C.C. Bridges, et al.**, *Transport of choline and its relationship to the expression of the organic cation transporters in a rat brain microvessel endothelial cell line (RBE4).* 2001. Biochim Biophys Acta, 1512(2): p. 299-307.
72. **Okura T., A. Hattori, Y. Takano, et al.**, *Involvement of the pyrilamine transporter, a putative organic cation transporter, in blood-brain barrier transport of oxycodone.* 2008. Drug Metab Dispos, 36(10): p. 2005-13.
73. **Sung J.H., K.H. Yu, J.S. Park, et al.**, *Saturable distribution of tacrine into the striatal extracellular fluid of the rat: evidence of involvement of multiple organic cation transporters in the transport.* 2005. Drug Metab Dispos, 33(3): p. 440-8.
74. **Busch A.E., U. Karbach, D. Miska, et al.**, *Human neurons express the polyspecific cation transporter hOCT2, which translocates monoamine neurotransmitters, amantadine, and memantine.* 1998. Mol Pharmacol, 54(2): p. 342-52.
75. **Duan H. and J. Wang**, *Selective transport of monoamine neurotransmitters by human plasma membrane monoamine transporter and organic cation transporter 3.* 2010. J Pharmacol Exp Ther, 335(3): p. 743-53.
76. **Naganuma F., T. Yoshikawa, T. Nakamura, et al.**, *Predominant role of plasma membrane monoamine transporters in monoamine transport in 1321N1, a human astrocytoma-derived cell line.* 2014. J Neurochem, 129(4): p. 591-601.
77. **Bacq A., L. Balasse, G. Biala, et al.**, *Organic cation transporter 2 controls brain norepinephrine and serotonin clearance and antidepressant response.* 2012. Mol Psychiatry, 17(9): p. 926-39.
78. **Amphoux A., V. Vialou, E. Drescher, et al.**, *Differential pharmacological in vitro properties of organic cation transporters and regional distribution in rat brain.* 2006. Neuropharmacology, 50(8): p. 941-52.
79. **Courousse T., A. Bacq, C. Belzung, et al.**, *Brain organic cation transporter 2 controls response and vulnerability to stress and GSK3beta signaling.* 2014. Mol Psychiatry.
80. **Vialou V., L. Balasse, J. Callebert, et al.**, *Altered aminergic neurotransmission in the brain of organic cation transporter 3-deficient mice.* 2008. J Neurochem, 106(3): p. 1471-82.

81. **Cui M., R. Aras, W.V. Christian, et al.**, *The organic cation transporter-3 is a pivotal modulator of neurodegeneration in the nigrostriatal dopaminergic pathway.* 2009. Proc Natl Acad Sci U S A, 106(19): p. 8043-8.
82. **Wu X., R. Kekuda, W. Huang, et al.**, *Identity of the organic cation transporter OCT3 as the extraneuronal monoamine transporter (uptake2) and evidence for the expression of the transporter in the brain.* 1998. J Biol Chem, 273(49): p. 32776-86.
83. **Gasser P.J., M. Orchinik, I. Raju, et al.**, *Distribution of organic cation transporter 3, a corticosterone-sensitive monoamine transporter, in the rat brain.* 2009. J Comp Neurol, 512(4): p. 529-55.
84. **Marcinkiewcz C.A. and D.P. Devine**, *Modulation of OCT3 expression by stress, and antidepressant-like activity of decynium-22 in an animal model of depression.* 2015. Pharmacol Biochem Behav, 131: p. 33-41.
85. **Hill J.E. and P.J. Gasser**, *Organic cation transporter 3 is densely expressed in the intercalated cell groups of the amygdala: anatomical evidence for a stress hormone-sensitive dopamine clearance system.* 2013. J Chem Neuroanat, 52: p. 36-43.
86. **Nakata T., T. Matsui, K. Kobayashi, et al.**, *Organic cation transporter 2 (SLC22A2), a low-affinity and high-capacity choline transporter, is preferentially enriched on synaptic vesicles in cholinergic neurons.* 2013. Neuroscience, 252: p. 212-21.
87. **Haag C., R. Berkels, D. Grundemann, et al.**, *The localisation of the extraneuronal monoamine transporter (EMT) in rat brain.* 2004. J Neurochem, 88(2): p. 291-7.
88. **Gasser P.J., C.A. Lowry, and M. Orchinik**, *Corticosterone-sensitive monoamine transport in the rat dorsomedial hypothalamus: potential role for organic cation transporter 3 in stress-induced modulation of monoaminergic neurotransmission.* 2006. J Neurosci, 26(34): p. 8758-66.
89. **Vialou V., A. Amphoux, R. Zwart, et al.**, *Organic cation transporter 3 (Slc22a3) is implicated in salt-intake regulation.* 2004. J Neurosci, 24(11): p. 2846-51.
90. **Fakhoury M.**, *Revisiting the Serotonin Hypothesis: Implications for Major Depressive Disorders.* 2015. Mol Neurobiol.
91. **Daws L.C.**, *Unfaithful neurotransmitter transporters: focus on serotonin uptake and implications for antidepressant efficacy.* 2009. Pharmacol Ther, 121(1): p. 89-99.
92. **Daws L.C., W. Koek, and N.C. Mitchell**, *Revisiting serotonin reuptake inhibitors and the therapeutic potential of "uptake-2" in psychiatric disorders.* 2013. ACS Chem Neurosci, 4(1): p. 16-21.
93. **Koepsell H. and H. Endou**, *The SLC22 drug transporter family.* 2004. Pflugers Arch, 447(5): p. 666-76.
94. **Feng N., B. Mo, P.L. Johnson, et al.**, *Local inhibition of organic cation transporters increases extracellular serotonin in the medial hypothalamus.* 2005. Brain Res, 1063(1): p. 69-76.
95. **Maswood S., W. Truitt, M. Hotema, et al.**, *Estrous cycle modulation of extracellular serotonin in mediobasal hypothalamus: role of the serotonin transporter and terminal autoreceptors.* 1999. Brain Res, 831(1-2): p. 146-54.
96. **Rahman S. and M.T. Bardo**, *Environmental enrichment increases amphetamine-induced glutamate neurotransmission in the nucleus accumbens: a neurochemical study.* 2008. Brain Res, 1197: p. 40-6.
97. **Bunin M.A. and R.M. Wightman**, *Quantitative evaluation of 5-hydroxytryptamine (serotonin) neuronal release and uptake: an investigation of extrasynaptic transmission.* 1998. J Neurosci, 18(13): p. 4854-60.

98. **Bunin M.A. and R.M. Wightman**, *Paracrine neurotransmission in the CNS: involvement of 5-HT.* 1999. Trends Neurosci, 22(9): p. 377-82.
99. **Chen J.J., Z. Li, H. Pan, et al.**, *Maintenance of serotonin in the intestinal mucosa and ganglia of mice that lack the high-affinity serotonin transporter: Abnormal intestinal motility and the expression of cation transporters.* 2001. J Neurosci, 21(16): p. 6348-61.
100. **Schmitt A., R. Mossner, A. Gossmann, et al.**, *Organic cation transporter capable of transporting serotonin is up-regulated in serotonin transporter-deficient mice.* 2003. J Neurosci Res, 71(5): p. 701-9.
101. **Baganz N.L., R.E. Horton, A.S. Calderon, et al.**, *Organic cation transporter 3: Keeping the brake on extracellular serotonin in serotonin-transporter-deficient mice.* 2008. Proc Natl Acad Sci U S A, 105(48): p. 18976-81.
102. **Kitaichi K., M. Fukuda, H. Nakayama, et al.**, *Behavioral changes following antisense oligonucleotide-induced reduction of organic cation transporter-3 in mice.* 2005. Neurosci Lett, 382(1-2): p. 195-200.
103. **Horton R.E., D.M. Apple, W.A. Owens, et al.**, *Decynium-22 enhances SSRI-induced antidepressant-like effects in mice: uncovering novel targets to treat depression.* 2013. J Neurosci, 33(25): p. 10534-43.
104. **International Transporter C., K.M. Giacomini, S.M. Huang, et al.**, *Membrane transporters in drug development.* 2010. Nat Rev Drug Discov, 9(3): p. 215-36.
105. **Shu Y., C. Brown, R.A. Castro, et al.**, *Effect of genetic variation in the organic cation transporter 1, OCT1, on metformin pharmacokinetics.* 2008. Clin Pharmacol Ther, 83(2): p. 273-80.
106. **Simonson S.G., A. Raza, P.D. Martin, et al.**, *Rosuvastatin pharmacokinetics in heart transplant recipients administered an antirejection regimen including cyclosporine.* 2004. Clin Pharmacol Ther, 76(2): p. 167-77.
107. **Vanwert A.L., C. Srimaroeng, and D.H. Sweet**, *Organic anion transporter 3 (oat3/slc22a8) interacts with carboxyfluoroquinolones, and deletion increases systemic exposure to ciprofloxacin.* 2008. Mol Pharmacol, 74(1): p. 122-31.
108. **Mulgaonkar A., J. Venitz, D. Grundemann, et al.**, *Human organic cation transporters 1 (SLC22A1), 2 (SLC22A2), and 3 (SLC22A3) as disposition pathways for fluoroquinolone antimicrobials.* 2013. Antimicrob Agents Chemother, 57(6): p. 2705-11.
109. **Muller F., J. Konig, E. Hoier, et al.**, *Role of organic cation transporter OCT2 and multidrug and toxin extrusion proteins MATE1 and MATE2-K for transport and drug interactions of the antiviral lamivudine.* 2013. Biochem Pharmacol, 86(6): p. 808-15.
110. **Li L., M. Tu, X. Yang, et al.**, *The contribution of human OCT1, OCT3, and CYP3A4 to nitidine chloride-induced hepatocellular toxicity.* 2014. Drug Metab Dispos, 42(7): p. 1227-34.
111. **Pan X., L. Wang, D. Grundemann, et al.**, *Interaction of Ethambutol with human organic cation transporters of the SLC22 family indicates potential for drug-drug interactions during antituberculosis therapy.* 2013. Antimicrob Agents Chemother, 57(10): p. 5053-9.
112. **Pan X., L. Wang, D. Grundemann, et al.**, *Inhibition of human organic cation transporters by the alkaloids matrine and oxymatrine.* 2014. Fitoterapia, 92: p. 206-10.
113. **Sun S., K. Wang, H. Lei, et al.**, *Inhibition of organic cation transporter 2 and 3 may be involved in the mechanism of the antidepressant-like action of berberine.* 2014. Prog Neuropsychopharmacol Biol Psychiatry, 49: p. 1-6.
114. **Vallon V., S.A. Eraly, W.R. Wikoff, et al.**, *Organic anion transporter 3 contributes to the regulation of blood pressure.* 2008. J Am Soc Nephrol, 19(9): p. 1732-40.

115. **Ritz E. and R. Dikow**, *Hypertension and antihypertensive treatment of diabetic nephropathy.* 2006. Nat Clin Pract Nephrol, 2(10): p. 562-7.
116. **Goto H., Y. Shimada, K. Tanikawa, et al.**, *Clinical evaluation of the effect of daio (rhei rhizoma) on the progression of diabetic nephropathy with overt proteinuria.* 2003. Am J Chin Med, 31(2): p. 267-75.
117. **Spencer C.M. and M.I. Wilde**, *Diacerein.* 1997. Drugs, 53(1): p. 98-106; discussion 107-8.
118. **Nicolas P., M. Tod, C. Padoin, et al.**, *Clinical pharmacokinetics of diacerein.* 1998. Clin Pharmacokinet, 35(5): p. 347-59.
119. **Magnard O., K. Louchahi, M. Tod, et al.**, *Pharmacokinetics of diacerein in patients with liver cirrhosis.* 1993. Biopharm Drug Dispos, 14(5): p. 401-8.
120. **Ojha A., R. Rathod, and H. Padh**, *Simultaneous HPLC-UV determination of rhein and aceclofenac in human plasma.* 2009. J Chromatogr B Analyt Technol Biomed Life Sci, 877(11-12): p. 1145-8.
121. **Ho E.S., D.C. Lin, D.B. Mendel, et al.**, *Cytotoxicity of antiviral nucleotides adefovir and cidofovir is induced by the expression of human renal organic anion transporter 1.* 2000. J Am Soc Nephrol, 11(3): p. 383-93.
122. **Zhou F., W. Xu, M. Hong, et al.**, *The role of N-linked glycosylation in protein folding, membrane targeting, and substrate binding of human organic anion transporter hOAT4.* 2005. Mol Pharmacol, 67(3): p. 868-76.
123. **Wang L. and D.H. Sweet**, *Potential for food-drug interactions by dietary phenolic acids on human organic anion transporters 1 (SLC22A6), 3 (SLC22A8), and 4 (SLC22A11).* 2012. Biochem Pharmacol, 84(8): p. 1088-95.
124. **Wang L. and D.H. Sweet**, *Competitive inhibition of human organic anion transporters 1 (SLC22A6), 3 (SLC22A8) and 4 (SLC22A11) by major components of the medicinal herb Salvia miltiorrhiza (Danshen).* 2013. Drug Metab Pharmacokinet, 28(3): p. 220-8.
125. **Uwai Y., Y. Ozeki, T. Isaka, et al.**, *Inhibitory effect of caffeic acid on human organic anion transporters hOAT1 and hOAT3: a novel candidate for food-drug interaction.* 2011. Drug Metab Pharmacokinet, 26(5): p. 486-93.
126. **Duan P. and G. You**, *Novobiocin is a potent inhibitor for human organic anion transporters.* 2009. Drug Metab Dispos, 37(6): p. 1203-10.
127. **Bakhiya N., B. Monien, H. Frank, et al.**, *Renal organic anion transporters OAT1 and OAT3 mediate the cellular accumulation of 5-sulfooxymethylfurfural, a reactive, nephrotoxic metabolite of the Maillard product 5-hydroxymethylfurfural.* 2009. Biochem Pharmacol, 78(4): p. 414-9.
128. **Jung K.Y., M. Takeda, D.K. Kim, et al.**, *Characterization of ochratoxin A transport by human organic anion transporters.* 2001. Life Sci, 69(18): p. 2123-35.
129. **U.S. Department of Health and Human Services and Food and Drug Administration.** Guidance for industry: drug interaction studies-study design, data analysis, implications for dosing, and labeling recommendations. Available on: http://www.fda.gov/downloads/Drugs/GuidanceComplianceRegulatoryInformation/Guidances/UCM292362.pdf.
130. **Debord P., K. Louchahi, M. Tod, et al.**, *Influence of renal function on the pharmacokinetics of diacerein after a single oral dose.* 1993. Fundam Clin Pharmacol, 7(8): p. 435-41.
131. **Jiang J.Y., M.W. Yang, W. Qian, et al.**, *Quantitative determination of rhein in human plasma by liquid chromatography-negative electrospray ionization tandem mass/mass*

spectrometry and the application in a pharmacokinetic study. 2012. J Pharm Biomed Anal, 57: p. 19-25.
132. **Zhu W., X.M. Wang, L. Zhang, et al.**, *Pharmacokinetic of rhein in healthy male volunteers following oral and retention enema administration of rhubarb extract: a single dose study.* 2005. Am J Chin Med, 33(6): p. 839-50.
133. **Lee J.H., J.M. Kim, and C. Kim**, *Pharmacokinetic analysis of rhein in Rheum undulatum L.* 2003. J Ethnopharmacol, 84(1): p. 5-9.
134. **Lee S.H., Y.S. Kim, S.J. Lee, et al.**, *The protective effect of Salvia miltiorrhiza in an animal model of early experimentally induced diabetic nephropathy.* 2011. J Ethnopharmacol, 137(3): p. 1409-14.
135. **Kang E.S., G.T. Lee, B.S. Kim, et al.**, *Lithospermic acid B ameliorates the development of diabetic nephropathy in OLETF rats.* 2008. Eur J Pharmacol, 579(1-3): p. 418-25.
136. **WHO**, 2012, WHO global tuberculosis report 2012. Available on: http://apps.who.int/iris/bitstream/10665/75938/1/9789241564502_eng.pdf.
137. *Treatment Guidelines for The Medical Letter.2012.Drugs for tuberculosis. Treat. Guidel. Med. Lett.* 201210: p. 29-36.
138. **Sivakumaran P., A.C. Harrison, J. Marschner, et al.**, *Ocular toxicity from ethambutol: a review of four cases and recommended precautions.* 1998. N Z Med J, 111(1077): p. 428-30.
139. **Postlethwaite A.E., A.G. Bartel, and W.N. Kelley**, *Hyperuricemia due to ethambutol.* 1972. N Engl J Med, 286(14): p. 761-2.
140. **Khanna B.K.K., J.**, *Hyperuricemic effect of ethambutol and pyrazinamide administered concomitantly.* 1991. Ind. J. Tuberc, 38: p. 21–24.
141. **Peloquin C.A., A.E. Bulpitt, G.S. Jaresko, et al.**, *Pharmacokinetics of ethambutol under fasting conditions, with food, and with antacids.* 1999. Antimicrob Agents Chemother, 43(3): p. 568-72.
142. **Hall R.G., 2nd, M.A. Swancutt, C. Meek, et al.**, *Ethambutol pharmacokinetic variability is linked to body mass in overweight, obese, and extremely obese people.* 2012. Antimicrob Agents Chemother, 56(3): p. 1502-7.
143. **Zhu M., W.J. Burman, J.R. Starke, et al.**, *Pharmacokinetics of ethambutol in children and adults with tuberculosis.* 2004. Int J Tuberc Lung Dis, 8(11): p. 1360-7.
144. **Jonsson S., A. Davidse, J. Wilkins, et al.**, *Population pharmacokinetics of ethambutol in South African tuberculosis patients.* 2011. Antimicrob Agents Chemother, 55(9): p. 4230-7.
145. **Buyske D.A., E. Peets, and W. Sterling**, *Pharmacological and biochemical studies on ethambutol in laboratory animals.* 1966. Ann N Y Acad Sci, 135(2): p. 711-25.
146. **Hartkoorn R.C., B. Chandler, A. Owen, et al.**, *Differential drug susceptibility of intracellular and extracellular tuberculosis, and the impact of P-glycoprotein.* 2007. Tuberculosis (Edinb), 87(3): p. 248-55.
147. **Cha S.H., H.P. Kim, N.H. Jung, et al.**, *Down-regulation of organic anion transporter 2 mRNA expression by nitric oxide in primary cultured rat hepatocytes.* 2002. IUBMB Life, 54(3): p. 129-35.
148. **Grundemann D., C. Hahne, R. Berkels, et al.**, *Agmatine is efficiently transported by non-neuronal monoamine transporters extraneuronal monoamine transporter (EMT) and organic cation transporter 2 (OCT2).* 2003. J Pharmacol Exp Ther, 304(2): p. 810-7.
149. **Holdiness M.R.**, *Clinical pharmacokinetics of the antituberculosis drugs.* 1984. Clin Pharmacokinet, 9(6): p. 511-44.

150. **Ito K., T. Iwatsubo, S. Kanamitsu, et al.**, *Prediction of pharmacokinetic alterations caused by drug-drug interactions: metabolic interaction in the liver.* 1998. Pharmacol Rev, 50(3): p. 387-412.
151. **Riccardi G., M.R. Pasca, and S. Buroni**, *Mycobacterium tuberculosis: drug resistance and future perspectives.* 2009. Future Microbiol, 4(5): p. 597-614.
152. **UK Health Protection Agency.** 2012, Tuberculosis in the UK: 2012 report. Available on: http://www.hpa.org.uk/webc/HPAwebFile/HPAweb_C/1317134913404.
153. **Faurholt-Jepsen D., N. Range, G. PrayGod, et al.**, *The role of diabetes on the clinical manifestations of pulmonary tuberculosis.* 2012. Trop Med Int Health, 17(7): p. 877-83.
154. **Pawlowski A., M. Jansson, M. Skold, et al.**, *Tuberculosis and HIV co-infection.* 2012. PLoS Pathog, 8(2): p. e1002464.
155. **Garcia-Martin F., F. Mampaso, G. de Arriba, et al.**, *Acute interstitial nephritis induced by ethambutol.* 1991. Nephron, 59(4): p. 679-80.
156. **Collier J., A.M. Joekes, P.E. Philalithis, et al.**, *Two cases of ethambutol nephrotoxicity.* 1976. Br Med J, 2(6044): p. 1105-6.
157. **Stone W.J., J.A. Waldron, J.H. Dixon, Jr., et al.**, *Acute diffuse interstitial nephritis related to chemotherapy of tuberculosis.* 1976. Antimicrob Agents Chemother, 10(1): p. 164-72.
158. **Mustak H., G. Rogers, and C. Cook**, *Ethambutol induced toxic optic neuropathy in HIV positive patients.* 2013. Int J Ophthalmol, 6(4): p. 542-5.
159. **Enomoto A., H. Kimura, A. Chairoungdua, et al.**, *Molecular identification of a renal urate anion exchanger that regulates blood urate levels.* 2002. Nature, 417(6887): p. 447-52.
160. **Vavricka S.R., J. Van Montfoort, H.R. Ha, et al.**, *Interactions of rifamycin SV and rifampicin with organic anion uptake systems of human liver.* 2002. Hepatology, 36(1): p. 164-72.
161. **Schuetz E.G., A.H. Schinkel, M.V. Relling, et al.**, *P-glycoprotein: a major determinant of rifampicin-inducible expression of cytochrome P4503A in mice and humans.* 1996. Proc Natl Acad Sci U S A, 93(9): p. 4001-5.
162. **Moss D.M., W.S. Kwan, N.J. Liptrott, et al.**, *Raltegravir is a substrate for SLC22A6: a putative mechanism for the interaction between raltegravir and tenofovir.* 2011. Antimicrob Agents Chemother, 55(2): p. 879-87.
163. **Jung N., C. Lehmann, A. Rubbert, et al.**, *Relevance of the organic cation transporters 1 and 2 for antiretroviral drug therapy in human immunodeficiency virus infection.* 2008. Drug Metab Dispos, 36(8): p. 1616-23.
164. **Kimura N., M. Okuda, and K. Inui**, *Metformin transport by renal basolateral organic cation transporter hOCT2.* 2005. Pharm Res, 22(2): p. 255-9.
165. **Nies A.T., U. Hofmann, C. Resch, et al.**, *Proton pump inhibitors inhibit metformin uptake by organic cation transporters (OCTs).* 2011. PLoS One, 6(7): p. e22163.
166. **Shu Y., S.A. Sheardown, C. Brown, et al.**, *Effect of genetic variation in the organic cation transporter 1 (OCT1) on metformin action.* 2007. J Clin Invest, 117(5): p. 1422-31.
167. **Jung N., C. Lehmann, A. Rubbert, et al.**, *Organic cation transporters OCT1 and OCT2 determine the accumulation of lamivudine in CD4 cells of HIV-infected patients.* 2013. Infection, 41(2): p. 379-85.
168. **Pan B.F., D.H. Sweet, J.B. Pritchard, et al.**, *A transfected cell model for the renal toxin transporter, rOCT2.* 1999. Toxicol Sci, 47(2): p. 181-6.
169. **Ciarimboli G., T. Ludwig, D. Lang, et al.**, *Cisplatin nephrotoxicity is critically mediated via the human organic cation transporter 2.* 2005. Am J Pathol, 167(6): p. 1477-84.

170. **Yokoo S., A. Yonezawa, S. Masuda, et al.**, *Differential contribution of organic cation transporters, OCT2 and MATE1, in platinum agent-induced nephrotoxicity.* 2007. Biochem Pharmacol, 74(3): p. 477-87.
171. **Yokoo S., S. Masuda, A. Yonezawa, et al.**, *Significance of organic cation transporter 3 (SLC22A3) expression for the cytotoxic effect of oxaliplatin in colorectal cancer.* 2008. Drug Metab Dispos, 36(11): p. 2299-306.
172. **Dobyan D.C., J. Levi, C. Jacobs, et al.**, *Mechanism of cis-platinum nephrotoxicity: II. Morphologic observations.* 1980. J Pharmacol Exp Ther, 213(3): p. 551-6.
173. **Goldstein R.S. and G.H. Mayor**, *Minireview. The nephrotoxicity of cisplatin.* 1983. Life Sci, 32(7): p. 685-90.
174. **Goldstein R.S., B. Noordewier, J.T. Bond, et al.**, *cis-Dichlorodiammineplatinum nephrotoxicity: time course and dose response of renal functional impairment.* 1981. Toxicol Appl Pharmacol, 60(2): p. 163-75.
175. **Daley-Yates P.T. and D.C. McBrien**, *The mechanism of renal clearance of cisplatin (cis-dichlorodiammine platinum ii) and its modification by furosemide and probenecid.* 1982. Biochem Pharmacol, 31(13): p. 2243-6.
176. **Klein J., Y. Bentur, D. Cheung, et al.**, *Renal handling of cisplatin: interactions with organic anions and cations in the dog.* 1991. Clin Invest Med, 14(5): p. 388-94.
177. **Nelson J.A., G. Santos, and B.H. Herbert**, *Mechanisms for the renal secretion of cisplatin.* 1984. Cancer Treat Rep, 68(6): p. 849-53.
178. **Osman N.M. and C.L. Litterst**, *Effect of probenecid and N'-methylnicotinamide on renal handling of cis-dichlorodiammineplatinum-II in rats.* 1983. Cancer Lett, 19(1): p. 107-11.
179. **Wang H.H.C., J.T.**, *Antitrichomonal activity of matrine, an active substance from Sophora flavescens.* 1994. Phytotherapy Research, 8(1): p. 70-73.
180. **Zhang L., H. Y, L. Wang, et al.**, *Several compounds from Chinese traditional and herbal medicine as immunomodulators.* 1995. Phytotherapy Research, 9(3): p. 315-322.
181. **Wang S., G. Wang, X. Li, et al.**, *Simultaneous determination of oxymatrine and its active metabolite matrine in dog plasma by liquid chromatography-mass spectrometry and its application to pharmacokinetic studies.* 2005. J Chromatogr B Analyt Technol Biomed Life Sci, 817(2): p. 319-25.
182. **Wang Y., Y. Ma, X. Li, et al.**, *Simultaneous determination and pharmacokinetic study of oxymatrine and matrine in beagle dog plasma after oral administration of Kushen formula granule, oxymatrine and matrine by LC-MS/MS.* 2007. Biomed Chromatogr, 21(8): p. 876-82.
183. **Lao Y.**, *[Clinical study of matrine injection on preventing liver function damage of anti-tumor drugs during chemotherapy of breast cancer].* 2005. Zhong Yao Cai, 28(8): p. 735-7.
184. **Long Y., X.T. Lin, K.L. Zeng, et al.**, *Efficacy of intramuscular matrine in the treatment of chronic hepatitis B.* 2004. Hepatobiliary Pancreat Dis Int, 3(1): p. 69-72.
185. **Liu Y.H., Y.F. Liu, and X.X. Guo**, *Current studies on anti-endotoxic chemical components of traditional Chinese medicine in China.* 2001. Acta Pharmacol Sin, 22(12): p. 1071-7.
186. **Cao Y.G., S. Jing, L. Li, et al.**, *Antiarrhythmic effects and ionic mechanisms of oxymatrine from Sophora flavescens.* 2010. Phytother Res, 24(12): p. 1844-9.
187. **Du S. and Y. Deng**, *Studies on the encapsulation of oxymatrine into liposomes by ethanol injection and pH gradient method.* 2006. Drug Dev Ind Pharm, 32(7): p. 791-7.
188. **Hu Q., G. Hu, T. Zhou, et al.**, *Determination of dissociation constants of anthrocycline by capillary zone electrophoresis with amperometric detection.* 2003. J Pharm Biomed Anal, 31(4): p. 679-84.

189. **Takeda M., S. Khamdang, S. Narikawa, et al.**, *Human organic anion transporters and human organic cation transporters mediate renal antiviral transport.* 2002. J Pharmacol Exp Ther, 300(3): p. 918-24.
190. **Wang D.S., J.W. Jonker, Y. Kato, et al.**, *Involvement of organic cation transporter 1 in hepatic and intestinal distribution of metformin.* 2002. J Pharmacol Exp Ther, 302(2): p. 510-5.
191. **Nies A.T. and M. Schwab**, *Organic cation transporter pharmacogenomics and drug-drug interaction.* 2010. Expert Rev Clin Pharmacol, 3(6): p. 707-11.
192. **Zhang X.L., H.R. Xu, W.L. Chen, et al.**, *Matrine determination and pharmacokinetics in human plasma using LC/MS/MS.* 2009. J Chromatogr B Analyt Technol Biomed Life Sci, 877(27): p. 3253-6.
193. **Wu X.L., T.J. Hang, J.P. Shen, et al.**, *Determination and pharmacokinetic study of oxymatrine and its metabolite matrine in human plasma by liquid chromatography tandem mass spectrometry.* 2006. J Pharm Biomed Anal, 41(3): p. 918-24.
194. **Kennedy D.A. and D. Seely**, *Clinically based evidence of drug-herb interactions: a systematic review.* 2010. Expert Opin Drug Saf, 9(1): p. 79-124.
195. **de Lima Toccafondo Vieira M. and S.M. Huang**, *Botanical-drug interactions: a scientific perspective.* 2012. Planta Med, 78(13): p. 1400-15.
196. **Ma Z.J., Q. Li, J.B. Wang, et al.**, *Combining Oxymatrine or Matrine with Lamivudine Increased Its Antireplication Effect against the Hepatitis B Virus In Vitro.* 2013. Evid Based Complement Alternat Med, 2013: p. 186573.
197. **Wang J. and e. al.**, *Pharmacokinetics of Matrine in Rats.* 1996. Acta Universitatis Medicinalis Secondae Shanghai, 16(4): p. 250-253.
198. **Zwart R., S. Verhaagh, M. Buitelaar, et al.**, *Impaired activity of the extraneuronal monoamine transporter system known as uptake-2 in Orct3/Slc22a3-deficient mice.* 2001. Mol Cell Biol, 21(13): p. 4188-96.
199. **Solbach T.F., M. Grube, M.F. Fromm, et al.**, *Organic cation transporter 3: expression in failing and nonfailing human heart and functional characterization.* 2011. J Cardiovasc Pharmacol, 58(4): p. 409-17.
200. **Kalliokoski A. and M. Niemi**, *Impact of OATP transporters on pharmacokinetics.* 2009. Br J Pharmacol, 158(3): p. 693-705.
201. **Zhang X. and e. al**, *Effect of Oxymatrine on chronic hepatitis B: an analysis of 312 cases.* 2005. Shijie Huaren Xiaohua Zazhi, 13(3): p. 317-320.
202. **A.A.o.P.C. Centers**, Bath Salts Data. Available on: https://aapcc.s3.amazonaws.com/files/library/Bath_Salts_Web_Data_through_Nov2013.pdf.
203. **European monitoring Center for Drugs and Drug Addiction.** 2012, Synthetic cathinones. Available on: http://www.emcdda.europa.eu/publications/drug-profiles/synthetic-cathinones.
204. **Kehr J., F. Ichinose, S. Yoshitake, et al.**, *Mephedrone, compared with MDMA (ecstasy) and amphetamine, rapidly increases both dopamine and 5-HT levels in nucleus accumbens of awake rats.* 2011. Br J Pharmacol, 164(8): p. 1949-58.
205. **Wright M.J., Jr., D. Angrish, S.M. Aarde, et al.**, *Effect of ambient temperature on the thermoregulatory and locomotor stimulant effects of 4-methylmethcathinone in Wistar and Sprague-Dawley rats.* 2012. PLoS One, 7(8): p. e44652.
206. **Baumann M.H., M.A. Ayestas, Jr., J.S. Partilla, et al.**, *The designer methcathinone analogs, mephedrone and methylone, are substrates for monoamine transporters in brain tissue.* 2012. Neuropsychopharmacology, 37(5): p. 1192-203.

207. **Cameron K.N., R. Kolanos, E. Solis, Jr., et al.**, *Bath salts components mephedrone and methylenedioxypyrovalerone (MDPV) act synergistically at the human dopamine transporter.* 2013. Br J Pharmacol, 168(7): p. 1750-7.
208. **Hadlock G.C., K.M. Webb, L.M. McFadden, et al.**, *4-Methylmethcathinone (mephedrone): neuropharmacological effects of a designer stimulant of abuse.* 2011. J Pharmacol Exp Ther, 339(2): p. 530-6.
209. **Sitte H.H. and M. Freissmuth**, *The reverse operation of Na(+)/Cl(-)-coupled neurotransmitter transporters--why amphetamines take two to tango.* 2010. J Neurochem, 112(2): p. 340-55.
210. **Gether U., P.H. Andersen, O.M. Larsson, et al.**, *Neurotransmitter transporters: molecular function of important drug targets.* 2006. Trends Pharmacol Sci, 27(7): p. 375-83.
211. **Larsen M.B., M.S. Sonders, O.V. Mortensen, et al.**, *Dopamine transport by the serotonin transporter: a mechanistically distinct mode of substrate translocation.* 2011. J Neurosci, 31(17): p. 6605-15.
212. **Ramamoorthy S., A.L. Bauman, K.R. Moore, et al.**, *Antidepressant- and cocaine-sensitive human serotonin transporter: molecular cloning, expression, and chromosomal localization.* 1993. Proc Natl Acad Sci U S A, 90(6): p. 2542-6.
213. **Glennon R.A., R. Young, B.R. Martin, et al.**, *Methcathione ("cat"): an enantiomeric potency comparison.* 1995. Pharmacol Biochem Behav, 50(4): p. 601-6.
214. **Glennon R.A., M. Yousif, N. Naiman, et al.**, *Methcathinone: a new and potent amphetamine-like agent.* 1987. Pharmacol Biochem Behav, 26(3): p. 547-51.
215. **J. d.D.S.S.**, *A homolog of ephedrine.* 1929. Bull Soc Chim Fr, 45: p. 284–286.
216. **Köppe H.L., G.; Holstein, W.; Zile, L.**, *1-(3′,4′-Methylenedioxy-phenyl-2-pyrrlidino-alkanones-(1).* 1969. US Patent 3,478,050, (11): p. 1969.
217. **Marinetti L.J. and H.M. Antonides**, *Analysis of synthetic cathinones commonly found in bath salts in human performance and postmortem toxicology: method development, drug distribution and interpretation of results.* 2013. J Anal Toxicol, 37(3): p. 135-46.
218. **Cawrse B.M., B. Levine, R.A. Jufer, et al.**, *Distribution of methylone in four postmortem cases.* 2012. J Anal Toxicol, 36(6): p. 434-9.
219. **Rojek S., M. Klys, M. Maciow-Glab, et al.**, *Cathinones derivatives-related deaths as exemplified by two fatal cases involving methcathinone with 4-methylmethcathinone and 4-methylethcathinone.* 2014. Drug Test Anal, 6(7-8): p. 770-7.
220. **Belhadj-Tahar H. and N. Sadeg**, *Methcathinone: a new postindustrial drug.* 2005. Forensic Sci Int, 153(1): p. 99-101.
221. **Wyman J.F., E.S. Lavins, D. Engelhart, et al.**, *Postmortem tissue distribution of MDPV following lethal intoxication by "bath salts".* 2013. J Anal Toxicol, 37(3): p. 182-5.
222. **Torrance H. and G. Cooper**, *The detection of mephedrone (4-methylmethcathinone) in 4 fatalities in Scotland.* 2010. Forensic Sci Int, 202(1-3): p. e62-3.
223. **Pedersen A.J., L.A. Reitzel, S.S. Johansen, et al.**, *In vitro metabolism studies on mephedrone and analysis of forensic cases.* 2013. Drug Test Anal, 5(6): p. 430-8.
224. **Yoshikawa T., F. Naganuma, T. Iida, et al.**, *Molecular mechanism of histamine clearance by primary human astrocytes.* 2013. Glia, 61(6): p. 905-16.
225. **Perdan-Pirkmajer K., S. Pirkmajer, K. Cerne, et al.**, *Molecular and kinetic characterization of histamine transport into adult rat cultured astrocytes.* 2012. Neurochem Int, 61(3): p. 415-22.

226. **Shang T., A.V. Uihlein, J. Van Asten, et al.**, *1-Methyl-4-phenylpyridinium accumulates in cerebellar granule neurons via organic cation transporter 3.* 2003. J Neurochem, 85(2): p. 358-67.
227. **Liu X., O. Vilenski, J. Kwan, et al.**, *Unbound brain concentration determines receptor occupancy: a correlation of drug concentration and brain serotonin and dopamine reuptake transporter occupancy for eighteen compounds in rats.* 2009. Drug Metab Dispos, 37(7): p. 1548-56.
228. **Simmler L.D., T.A. Buser, M. Donzelli, et al.**, *Pharmacological characterization of designer cathinones in vitro.* 2013. Br J Pharmacol, 168(2): p. 458-70.
229. **Young R. and R.A. Glennon**, *Discriminative stimulus effects of S(-)-methcathinone (CAT): a potent stimulant drug of abuse.* 1998. Psychopharmacology (Berl), 140(3): p. 250-6.
230. **Prosser J.M. and L.S. Nelson**, *The toxicology of bath salts: a review of synthetic cathinones.* 2012. J Med Toxicol, 8(1): p. 33-42.
231. **Zawilska J.B. and J. Wojcieszak**, *Designer cathinones--an emerging class of novel recreational drugs.* 2013. Forensic Sci Int, 231(1-3): p. 42-53.
232. **Rumantir M.S., D.M. Kaye, G.L. Jennings, et al.**, *Phenotypic evidence of faulty neuronal norepinephrine reuptake in essential hypertension.* 2000. Hypertension, 36(5): p. 824-9.
233. **Esler M.D., G. Wallin, P.K. Dorward, et al.**, *Effects of desipramine on sympathetic nerve firing and norepinephrine spillover to plasma in humans.* 1991. Am J Physiol, 260(4 Pt 2): p. R817-23.
234. **Esler M., G. Jennings, G. Lambert, et al.**, *Overflow of catecholamine neurotransmitters to the circulation: source, fate, and functions.* 1990. Physiol Rev, 70(4): p. 963-85.
235. **Obst O.O., M.C. Linssen, G.J. Van der Vusse, et al.**, *Interstitial noradrenaline concentration of rat hearts as influenced by cellular catecholamine uptake mechanisms.* 1996. Mol Cell Biochem, 163-164: p. 173-80.
236. **Hayer-Zillgen M., M. Bruss, and H. Bonisch**, *Expression and pharmacological profile of the human organic cation transporters hOCT1, hOCT2 and hOCT3.* 2002. Br J Pharmacol, 136(6): p. 829-36.
237. **Martinez-Clemente J., R. Lopez-Arnau, M. Carbo, et al.**, *Mephedrone pharmacokinetics after intravenous and oral administration in rats: relation to pharmacodynamics.* 2013. Psychopharmacology (Berl), 229(2): p. 295-306.
238. **Tzvetkov M.V., J.N. dos Santos Pereira, I. Meineke, et al.**, *Morphine is a substrate of the organic cation transporter OCT1 and polymorphisms in OCT1 gene affect morphine pharmacokinetics after codeine administration.* 2013. Biochem Pharmacol, 86(5): p. 666-78.
239. **Carhart-Harris R.L., L.A. King, and D.J. Nutt**, *A web-based survey on mephedrone.* 2011. Drug Alcohol Depend, 118(1): p. 19-22.
240. **Schifano F., J. Corkery, and A.H. Ghodse**, *Suspected and confirmed fatalities associated with mephedrone (4-methylmethcathinone, "meow meow") in the United Kingdom.* 2012. J Clin Psychopharmacol, 32(5): p. 710-4.
241. **Dickson A.J., S.P. Vorce, B. Levine, et al.**, *Multiple-drug toxicity caused by the coadministration of 4-methylmethcathinone (mephedrone) and heroin.* 2010. J Anal Toxicol, 34(3): p. 162-8.
242. **NIMH**. NIMH depression statistics. Available on: http://www.nimh.nih.gov/statistics/index.shtml.
243. **Leadholm A.K., A.J. Rothschild, W.A. Nolen, et al.**, *The treatment of psychotic depression: is there consensus among guidelines and psychiatrists?* 2013. J Affect Disord, 145(2): p. 214-20.

244. **Anderson I.M., I.N. Ferrier, R.C. Baldwin, et al.**, *Evidence-based guidelines for treating depressive disorders with antidepressants: a revision of the 2000 British Association for Psychopharmacology guidelines.* 2008. J Psychopharmacol, 22(4): p. 343-96.
245. **Vervisch K., M. D'Hooghe, K.W. Tornroos, et al.**, *A new approach towards 1-phenyl and 1-benzyl substituted 2-(aminomethyl)cyclopropanecarboxamides as novel derivatives of the antidepressant Milnacipran.* 2009. Org Biomol Chem, 7(16): p. 3271-9.
246. **Little A.**, *Treatment-resistant depression.* 2009. Am Fam Physician, 80(2): p. 167-72.
247. **Al-Harbi K.S.**, *Treatment-resistant depression: therapeutic trends, challenges, and future directions.* 2012. Patient Prefer Adherence, 6: p. 369-88.
248. **Dukat M., K. Alix, J. Worsham, et al.**, *2-Amino-6-chloro-3,4-dihydroquinazoline: A novel 5-HT3 receptor antagonist with antidepressant character.* 2013. Bioorg Med Chem Lett, 23(21): p. 5945-8.
249. **Rahman A.A., M.K. Daoud, M. Dukat, et al.**, *Conformationally-restricted analogues and partition coefficients of the 5-HT3 serotonin receptor ligands meta-chlorophenylbiguanide (mCPBG) and meta-chlorophenylguanidine (mCPG).* 2003. Bioorg Med Chem Lett, 13(6): p. 1119-23.
250. **Schlatter E., P. Klassen, V. Massmann, et al.**, *Mouse organic cation transporter 1 determines properties and regulation of basolateral organic cation transport in renal proximal tubules.* 2014. Pflugers Arch, 466(8): p. 1581-9.
251. **Steru L., R. Chermat, B. Thierry, et al.**, *The tail suspension test: a new method for screening antidepressants in mice.* 1985. Psychopharmacology (Berl), 85(3): p. 367-70.
252. **Yoshikawa T., A. Watanabe, Y. Ishitsuka, et al.**, *Identification of multiple genetic loci linked to the propensity for "behavioral despair" in mice.* 2002. Genome Res, 12(3): p. 357-66.
253. **Pedersen B.P., H. Kumar, A.B. Waight, et al.**, *Crystal structure of a eukaryotic phosphate transporter.* 2013. Nature, 496(7446): p. 533-6.
254. **Schlessinger A., S.W. Yee, A. Sali, et al.**, *SLC classification: an update.* 2013. Clin Pharmacol Ther, 94(1): p. 19-23.
255. **Schlessinger A., N. Khuri, K.M. Giacomini, et al.**, *Molecular modeling and ligand docking for solute carrier (SLC) transporters.* 2013. Curr Top Med Chem, 13(7): p. 843-56.
256. **Popp C., V. Gorboulev, T.D. Muller, et al.**, *Amino acids critical for substrate affinity of rat organic cation transporter 1 line the substrate binding region in a model derived from the tertiary structure of lactose permease.* 2005. Mol Pharmacol, 67(5): p. 1600-11.
257. **Sweet D.H. and J.B. Pritchard**, *The molecular biology of renal organic anion and organic cation transporters.* 1999. Cell Biochem Biophys, 31(1): p. 89-118.
258. ***Institute for Health Metrics and Evaluation.*** *2013, The global burden of disease: generating evidence, guiding policy.*
259. **Haenisch B., E. Drescher, L. Thiemer, et al.**, *Interaction of antidepressant and antipsychotic drugs with the human organic cation transporters hOCT1, hOCT2 and hOCT3.* 2012. Naunyn Schmiedebergs Arch Pharmacol, 385(10): p. 1017-23.
260. **Zhu H.J., D.I. Appel, D. Grundemann, et al.**, *Evaluation of organic cation transporter 3 (SLC22A3) inhibition as a potential mechanism of antidepressant action.* 2012. Pharmacol Res, 65(4): p. 491-6.
261. **American Association of Poison Control Centers**. 2011, Bath Salts Data Available on: https://aapcc.s3.amazonaws.com/files/library/Bath_Salts_Web_Data_through_Nov2013.pdf.

VITA

Xiaolei Pan received her Bachelor of Science in Pharmacy in 2009 and a Master of Science in Pharmaceutics in 2011 from Shenyang Pharmaceutical University, Shenyang, China. She joined Drug Transporter Research Group at Department of Pharmaceutics, Virginia Commonwealth University in 2011.

During her PhD graduate education, Xiaolei has published three manuscripts and three abstracts. She has presented her research at Annual Meetings of the American Association of Pharmaceutical Scientists (AAPS) in 2013 and 2014, and AAPS Workshop on Drug Transporters in ADME: From the Bench to the Bedside in 2013, in addition to the poster presentations within School of Pharmacy. In addition, she finished an internship at Pfizer from June 2014 to August 2014.

She received an AAPS Pharmaceuticals in Global Health Student Travelship in 2013. Additionally, she has also received VCU School of Pharmacy Jyotsna and Mavji Thacker Award in 2012 and John Wood Award in 2015 for academic excellence at Department of Pharmaceutics. She was also a finalist for the 2015 Dean's Award in School of Pharmacy.

PUBLICATIONS

1. Xiaolei Pan, Li Wang, Dirk Gründemann, and Douglas H. Sweet. Interaction of ethambutol with human organic cation transporters (SLC22 Family) indicates potential for drug-drug interactions during antituberculosis therapy. Antimicrobial Agents and Chemotherapy 2013; 57: 5053-5059.
2. Li Wang, Xiaolei Pan[*], and Douglas H. Sweet. The anthraquinone drug rhein potently interferes with organic anion transporter-mediated renal elimination. Biochemical Pharmacology 2013; 86: 991-996 ([*]co-first author).
3. Xiaolei Pan, Li Wang, Dirk Gründemann, and Douglas H. Sweet. Inhibition of human organic cation transporters by the alkaloids matrine and oxymatrine. Fitoterapia 2013; 92: 206-210.

ABSTRACTS

1. Xiaolei Pan and Douglas H. Sweet. Potent Inhibition of Human Organic Cation Transporters 1, 2, and 3 by Synthetic Cathinones. AAPS Annual Meeting and Exposition, San Diego, CA. November 2014.
2. Xiaolei Pan and Douglas H. Sweet. Potential for Drug-Drug Interactions on Human Organic Solute Carriers (SLC22 Family) During Antituberculosis Therapy. AAPS Annual Meeting and Exposition, San Antonio, TX. November 2013.
3. Xiaolei Pan and Douglas H. Sweet. Inhibition Potencies of Ethambutol and its Carboxyl Metabolite on Five Human Organic Cation/Anion Transporters from the SLC22 Transporter Family. AAPS Workshop on Drug Transporters in ADME: From the Bench to the Bedside. Bethesda, MD, March 2013.